SAFETY ASSESSMENT FRAMEWORK FOR EVALUATING STABILITY IN STANDING IN THE FLOW BELOW A WEIR OR LOW HEAD DAM

A Thesis Submitted to the

College of Graduate and Postdoctoral Studies

In Partial Fulfillment of the Requirements

for the Degree of Master of Science in the

Department of Civil, Geological, and Environmental Engineering

University of Saskatchewan

Saskatoon.

By

Mohammad Mohibul Hasan

PERMISSION TO USE

In presenting this thesis in partial fulfilment of the requirements for a Postgraduate degree from the University of Saskatchewan, I agree that the Libraries of this University may make it freely available for inspection. I further agree that permission for copying of this thesis in any manner, in whole or in part, for scholarly purposes may be granted by the professors who supervised my thesis work or, in their absence, by the Head of the Department or the Dean of the College in which my thesis work was done. It is understood that any copying or publication or use of this thesis or parts thereof for financial gain shall not be allowed without my written permission. It is also understood that due recognition shall be given to me and to the University of Saskatchewan in any scholarly use which may be made of any material in my thesis.

Requests for permission to copy or to make other use of material in this thesis in whole or part should be addressed to:

Head of the Department of Civil, Geological, and Environmental Engineering
University of Saskatchewan
57 Campus Drive
Saskatoon, Saskatchewan
Canada, S7N 5A9

OR

Dean
College of Graduate and Postdoctoral Studies
University of Saskatchewan
116 Thorvaldson Building, 110 Science Place
Saskatoon, Saskatchewan
Canada, S7N 5C9.

ABSTRACT

Three hundred two fatalities have been reported at dams in Canada among three hundred sixty-seven safety incidents, and approximately thirty-one percent of the incidents have been at low head dams or weirs. Many of these fatalities occurred due to the misjudging of flow conditions below the weir or dam. Overflow structures such as low head dams and weirs often result in the formation of submerged hydraulic jumps immediately downstream. People who are kayaking, swimming, and fishing around the sites often consider submerged hydraulic jumps as safe because the water surface looks reasonably calm. However, the submerged hydraulic jump has a large roller that produces a countercurrent surface velocity. If a person falls into the flow below the weir, this strong backward flow in the roller can be life-threatening. For this reason, the submerged hydraulic jump is known as a "drowning machine." However, it is not only the presence of a roller that makes the flow dangerous; it is the magnitude of the forces acting on a human body and the flow velocities due to the presence of the roller that might make it impossible for a person to stand in the flow.

In this study, a force-based framework was developed to evaluate the stability of a person who is trying to stand within the recirculating flow of a submerged hydraulic jump. The framework was then applied to assess the flows for which it would be impossible to stand below the structure at the Wolf River Sea Lamprey Barrier on the Wolf River in Ontario, Canada. At this barrier, submerged hydraulic jump conditions exist over a large range of flows.

The framework is used to assess the stability of a person based on the net moment generated by forces about two points of balance. To calculate the net moment, methodologies for calculating forces such as the person's weight, buoyancy, and drag and respective moment arms for those forces were developed. For this work, dimensionless relationships were generated for variation of the frontal area and submerged volume of a person with flow depth, which is necessary for calculating the drag forces and buoyancy. For these work, two-dimensional and three-dimensional male and female body models were created. The change of the center of buoyancy with flow depth was also estimated to find the moment due to buoyancy for a particular flow depth. A method of predicting the velocity profiles below the weir as a part of the drag force calculations on the bodies was also developed.

Velocity profiles predicted for the flow below the Wolf River Barrier were compared to the velocity profiles measured in experiments in a scale model of the barrier by Mazurek *et al*. (2008). The proposed method for predicting velocity profiles showed good agreement with the experimental data.

The framework was then applied to assess the maximum safe discharges for standing below the Wolf River Barrier. By analyzing velocity profiles at different downstream locations for six flow rates, it was concluded that the maximum safe discharge is between 15 and 17 m^3/s.

ACKNOWLEDGMENTS

All praises are due to the almighty Allah, and I am thankful to Allah for granting me the patience, ability, knowledge, and strength to pursue my M.Sc. degree successfully.

I am very grateful to my supervisor, Dr. Kerry A. Mazurek, and want to acknowledge her constant support and guidance in completing my M.Sc. at the University of Saskatchewan. I also thank my advisory committee members, Dr. Warren Helgason, Dr. David Sumner, and Dr. Hossein Azinfar, for their valuable comments, reviews, and suggestions for improving my research.

Thanks to Tracy McArthur, the former departmental assistant of the Hydrotechnical Laboratory, and my lab colleagues for creating an excellent working environment in the laboratory.

Special thanks to my parents, my elder brother, my sister-in-law, and my friends for providing me with continuous mental support, love, and inspiration from a distance. None of this would be possible without you.

Also, thanks to my loving wife, Jannatul Taslima, for her patience and continuous support during this challenging journey.

DEDICATION

This thesis work is dedicated to all the frontline workers who are risking their own lives to save the world from the COVID 19 pandemic.

TABLE OF CONTENTS

LIST OF TABLES

LIST OF FIGURES

LIST OF NOTATIONS

A_{F2D}	frontal area of 2D model
A_{F3D}	frontal area of 3D model
A_n	projected area of the human body normal to the flow
A_{ni}	projected area of the human body for a particular interval of a velocity profile
b	length scale, the distance from the boundary (bed) where U=0.5 U_m
b_r	distance from the water surface to the point where U=0.75 U_s
B	width of rectangular channel
C_d	coefficient of drag
C_L	coefficient of head loss
D_{flow}	depth of flow in flood condition
F_1	Froude number at section 1
F_B	buoyancy
F_D	drag force on the body
F_{Di}	drag force in a particular interval of a velocity profile
F_{DB}	drag force due to backward flow
F_{DF}	drag force due to forward flow
g	gravitational acceleration
h	head on the weir
H	height of a person
H_{DB}	moment arm for F_{DB}
H_{DF}	moment arm for F_{DF}

L	length scale, longitudinal distance from the start of the jump to point where $U_m/U_1 = 0.5$
L_B	moment arm representing horizontal distance from the heel to center of buoyancy
L_{cr}	length of countercurrent region
L_{foot}	length of a person's foot
L_m	length in the model
L_p	length in the prototype
L_{sj}	length of submerged hydraulic jump
L_W	moment arm representing horizontal distance from the heel to center of mass
M	human body's mass
M_P	moment around the point of balance
N	natural number (1,2,3 … … …)
P	weir height
q	flow discharge per unit width
Q	flow discharge
R	correlation coefficient
S	submergence
t	tailwater depth as measured from the weir crest
U	velocity at a point along the flow depth Y
U_o	velocity of flow upstream of the weir
U_1	forward velocity at section 1
U_i	average velocity of flow at a particular interval of a velocity profile
U_m	maximum velocity of the flow along the bed at any X'

U_s	local reverse surface velocity at particular X'
v^*	the maximum reverse velocity through the jump
V_{flow}	average forward flow velocity in flood condition
W	human weight
X	horizontal distance from the upstream face of weir, horizontal axis
X'	horizontal distance from section 1
X_j	horizontal distance from weir crest to section 1
$\overline{X_u}$	horizontal distance travelled by the upper nappe from the weir crest to where the upper nappe crosses the level of the crest
X_w	horizontal distance from weir crest to where upper nappe touches the downstream water surface
Y	vertical distance from bottom of the weir, vertical axis
Y_1	depth of the forward flow formed just downstream of the point of nappe impingement
Y_2	subcritical sequent depth
Y_s	vertical distance from the water surface at downstream
Y_u	vertical distance from the weir crest
$\overline{Y_u}$	vertical distance from the crest to the energy grade line just upstream of the weir
Y_w	vertical distance from weir crest to where upper nappe touches the downstream water surface
y_d	depth downstream of the weir as measured from bed level
y_t	tailwater depth
$\bar{y}_i$	vertical axis coordinate of the center of a particular interval in a velocity profile

Y depth of flow at a particular X'

$\bar{Y}$ H_{DF} for forward drag force and H_{DB} for backward drag force

z_o bed elevation at section O, upstream of the weir

z_1 bed elevation at section 1, downstream of the weir

γ_w specific weight of water

λ parameter to check submerged flow regimes below a weir

λ_s volume of submerged portion of body

ρ_w density of water

LIST OF ABBREVIATIONS

ADV	Micro-Acoustic Doppler Velocimeter
ASCE	American Society of Civil Engineers
BMI	Body Mass Index
CFD	Computational Fluid Dynamics
DFO	Fisheries and Oceans Canada
OPG	Ontario Power Generation
PWQMN	Provincial (Stream) Water Quality Monitoring Network
SHJ	Submerged Hydraulic Jump
WHO	World Health Organization
WSC	Water Survey of Canada

CHAPTER 1: INTRODUCTION

1.1 Background

Overflow structures such as weirs and low head dams are used for different purposes, such as measuring the discharge in rivers and streams, maintaining navigable depth upstream in rivers, and or flood control. As a result, there are countless such hydraulic structures around the world. Water sports enthusiasts often treat these overflow structures as a threat. Non-technical literature related to outdoor activities notes serious personal injuries and drowning at these structures (Elverum and Smalley 2012). For example, between 1976 and 1996, 17 fatalities occurred at Dock Street Dam in Harrisburg, Pennsylvania (Kern *et al*. 2015). Kern *et al.* (2015) report that there have been 430 fatalities at 222 low head dam locations throughout the U.S. before 2015. Bennett (2018) developed the Ontario Power Generation International Public Safety Database and recorded safety incidents at dam sites in Canada since 1843. As of November 19, 2021, 367 safety incidents at dam sites have been recorded, including 302 fatalities, and approximately 31% of the recorded incidents have been at low head dams or weirs[1]. Sixty percent of the safety incidents occurred in Ontario, which has many dams and the highest population among Canadian provinces (Bennett 2018). Leutheusser (1988) and Leutheusser and Birk (1991) also report multiple incidents in Ontario. The Association of State Dam Safety Officials (2019) in the United States mentioned in their Public Safety Incident Report for 2019 that there were 56 deaths and 19 injuries at dams throughout the U.S. in that year, and many of those incidents were caused by recirculating flow downstream of overflow structures. In many of these incidents people were kayaking, swimming, and fishing around the sites.

Among various types of weirs, the rectangular sharp-crested weir is one of the most common. It is widely used in channels and laboratories to measure flow (Lakshmana Rao 1975; Azimi *et al*. 2016). In addition, the characteristics of flow below other types of weirs are not substantially dissimilar (Zachoval *et al*. 2013). Flow over these weirs, that is not impacted by the downstream depth or "tailwater" conditions (called "free-flow" over the weir) is reasonably well-

[1]Personal communication with Tony Bennett, Ontario Power Generation (2021)

understood. What is less understood is the flow pattern that forms below weirs. For a rigid, flat downstream bed, it has been seen that there are several flow patterns that form below weirs (Leutheusser 1988; Rajaratnam and Muralidhar 1969, Wu and Rajaratnam 1996; Azimi *et al.* 2016).

One of these flow patterns is the submerged hydraulic jump. The submerged hydraulic jump has a large roller that produces a countercurrent velocity, which is often called a "hydraulic" or a "drowning-machine" (Borland-Coogan and Filmspace 1980, Leutheusser and Birk 1991). If a person falls into the flow below the weir, this strong backward flow in the roller can be life-threatening; the flow below a weir is referred to as a submerged hydraulic jump.

A few studies have been carried out to develop possible methods to eliminate this deadly roller below the low head dams (Leutheusser and Birk 1991, Freeman and Garcia 1996, Mazurek *et al*. 2008 and Olsen *et al.* 2013). Some studies have provided a better understanding of the flow characteristics and have focused on determining the countercurrent velocities. Notable studies were by Leutheusser (1988), Ohtsu and Yasuda (1991), Leutheusser and Birk (1991), Hotchkiss and Comstock (1992), Leutheusser and Fan (2001), and Mossa *et al.* (2004). Research has also been conducted on the presence of rollers in a submerged hydraulic jump (Leutheusser and Birk 1991, Hotchkiss and Comstock 1992, and Leutheusser and Fan 2001).

However, it is not only the presence of a roller that makes the flow dangerous. It is the magnitude of the forces acting on a human body that might make it impossible for a person to stand within the flow or swim out of it. Hence, an analysis of the forces acting on a body within the flow is important to conduct. In this study, a force-based framework will be developed to evaluate human stability in standing below a weir (or low head dam) where a recirculating flow exists. Then, the framework will be applied to assess the stability of a person in standing below the Wolf River Sea Lamprey Barrier located on the Wolf River in Northern Ontario. This weir (or a low head dam) has been a structure of concern for Fisheries and Oceans Canada with respect to drowning (Mazurek *et al.* 2008) and is of a height (0.9 m) where a person could potentially stand within the flow.

1.2 Study Objectives

The objectives of this study are the following:

i) To develop a force-based framework to evaluate the stability of a person trying to stand within recirculating flow of a submerged hydraulic jump; and
ii) To apply the framework to assess the stability of a person in standing just downstream of a weir or a low head dam where it is known that submerged hydraulic jump conditions sometimes exist.

1.3 Scope of the Study

The scope of this study includes developing a framework to assess the ability of a person stand within a submerged hydraulic jump created below a weir or low head dam. The study will use flow depth and velocity data produced in laboratory experiments by Mazurek *et al.* (2008) in physical scale models of the Wolf River Sea Lamprey Barrier to help assess the validity of the proposed framework. No data were collected from the Wolf River site for this study; however, the study uses stage-discharge relationships developed by Mazurek *et al.* (2008) from data collected at the site from September 14, 2004, to August 17, 2005, by Fisheries and Oceans Canada (DFO).

1.4 Organization of the Thesis Document

This thesis contains five chapters, including this introductory chapter. Chapter 2 provides a literature review of the flow patterns below a weir and features of submerged hydraulic jumps. It also includes a review of previous works that analyze human stability in different flow conditions. Next, Chapter 3 explains the research work methodology and describes the data collection and the framework to analyze human stability. In Chapter 4, the developed framework is applied to the Wolf River Sea Lamprey Barrier and the results are discussed. Finally, Chapter 5 presents the conclusions of the research work and recommendations for future work.

CHAPTER 2: LITERATURE REVIEW

2.1 Introduction

This chapter includes a literature review and first focusses on the flow regimes that can form below a weir. Since the submerged hydraulic jump is an important flow pattern with respect to drowning that forms below a weir or low head dam, the review also describes the characteristics of the submerged hydraulic jump, including the details of the roller formed near the water surface and the forward and backward velocity profiles. In addition, this chapter describes various methods that might be used to assess the dangers that countercurrent rollers pose to human stability in a flow.

2.2 Flow Regimes Below a Weir with a Rigid Bed Downstream

One of the main factors determining the flow regime below a weir is the tailwater depth, y_t (Wu and Rajaratnam 1996, Azimi *et al.* 2016). Figure 2.1 shows the different flow regimes that form with varying tailwater. In Fig. 2.1, the flow that falls over the weir is called a nappe. The upper and lower layers of the nappe are called upper and lower nappe, respectively, and have well-defined characteristics created by the weir's crest. At very low tailwater depths (Case A), a swept-out hydraulic jump occurs when the flow over-spilling the weir has enough momentum to push the hydraulic jump that would normally form below the weir further downstream. An increase in tailwater depth causes the hydraulic jump to move towards the weir to form eventually a free hydraulic jump or “optimum jump” (Case B). A free hydraulic jump is one that is not submerged by the tailwater; the momentum of the flow upstream of the jump is equal to the momentum of the flow on the downstream side of the jump (Blalock and Sturm 1981). Case B is sensitive to the tailwater depth and a small decrease in tailwater depth can turn it into a swept-out jump (Case A). Alternatively, a small increase in tailwater depth can turn Case B into Case C, where the tailwater pushes the hydraulic jump towards the face of the weir and creates a submerged hydraulic jump. A certain tailwater depth is required to cause a jump to form by equal momentum upstream and downstream of the jump, but a deeper tailwater depth is present than required in a submerged hydraulic jump (Hager 1992). Case C is called the plunging jet regime by Leutheusser and Birk

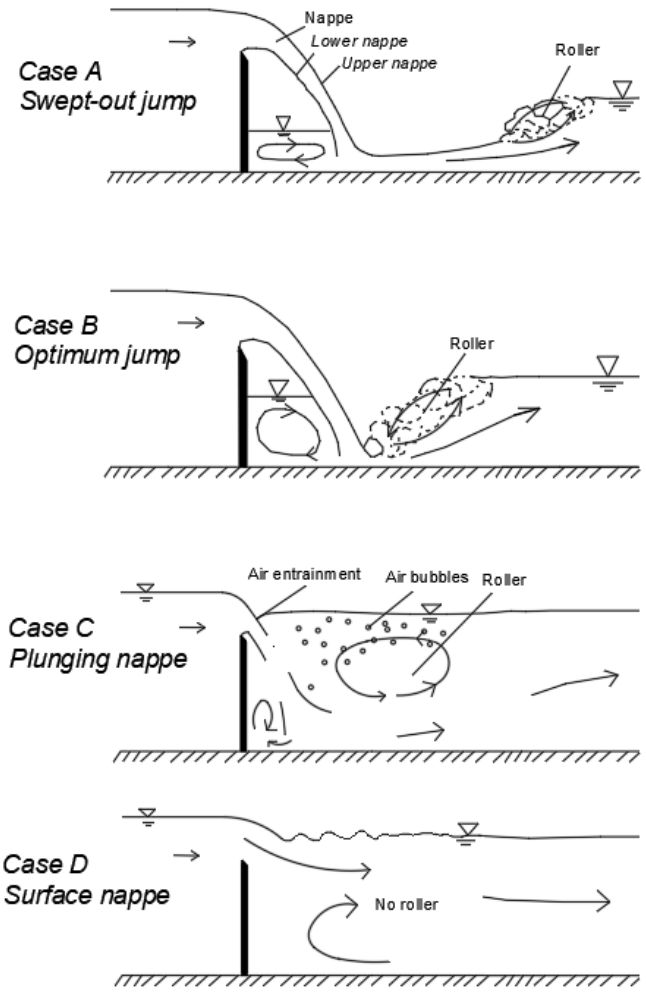

Figure 2.1. Flow patterns below a rectangular sharp-crested weir for rigid bed conditions (adapted from Leutheusser and Birk (1991)).

(1991) or the impinging jet regime by Wu and Rajaratnam (1996). With further increases in tailwater depth, where the tailwater depth nears that of the upstream water level, the plunging nappe will flip to flow along the water surface as a surface jet (Case D). In this case, the nappe flow over the weir remains at the surface of the water and the hydraulic jump disappears (and there is no roller). This is also called a "surface nappe" (Leutheusser and Birk 1991). Others have classified the surface jet further as a breaking wave, surface wave, or surface jet (Wu and Rajaratnam 1996).

Case A can be a hazardous flow if the velocity of water from the location where the plunging nappe flow over the weir impinges on the bed of the channel to the start of the hydraulic jump is high enough to create a problem for a person standing. There is also the backwards velocity

that forms on the water surface because of the roller of the jump, although the jump does not form just downstream of the weir. However, a free hydraulic jump has a very turbulent water surface, and it is obvious that the flow is hazardous and should not be entered. Similarly, in Case B, a hydraulic jump with a roller, forms just below the weir, which can entrap a body near the weir, but it is an obviously hazardous flow.

For the submerged hydraulic jump of Case C, the plunging flow over the weir flows along the bottom of the channel and forms a roller above it. The roller forms strong backwards flow velocities towards the plunging nappe over the weir. A person that gets trapped in the water would be pushed towards the weir by the backwards flow in the roller then down towards the bed by the plunging flow over the weir to the channel bed. This flow pattern is extremely difficult to escape. Further, once the hydraulic jump is submerged, the water surface looks calm and no longer visibly hazardous. A person who misjudges the flow for Case C to be safe can easily get trapped.

A person in a flow moving as Case D would simply be pushed away from the weir. These surface jet-type cases do not represent a drowning hazard at the weir.

The transition between the impinging jet regime (Case C) and the surface jet (Case D) is impacted by hysteresis (Fan 1993, Wu and Rajaratnam 1996). This means that the change from the impinging jet regime to the surface jet occurs at a different (higher) tailwater depth when the tailwater depth is increasing as compared to the depth when the tailwater depth is decreasing (a lower depth). Wu and Rajaratnam (1996) defined two curves as the upper and lower transition states, where the transitions occur for increasing and decreasing tailwater depths, respectively (shown in Figure 2.2). For Figure 2.2, t/h is plotted against the parameter $\lambda = g(h-t)^{0.5}/(q/y_t)$. As shown in Figure 2.3, the variable t is the tailwater depth as measured from the weir crest, h is the upstream depth of water as measured from the weir crest (measured at a location before the flow starts to contract over the weir), g is gravitational acceleration, q is the volumetric flow per unit width, P is the weir height, and y_t is the tailwater depth as measured from the bed of the channel. In the surface flow regimes, $\sqrt{2}\lambda$ is the ratio of velocity of surface flow to the mean velocity of flow in the downstream channel.

Therefore, in Figure 2.2, the two curves define the lower and upper transition stages. Above upper transition curve, the flow is in the surface flow regime and below lower transition curve, the

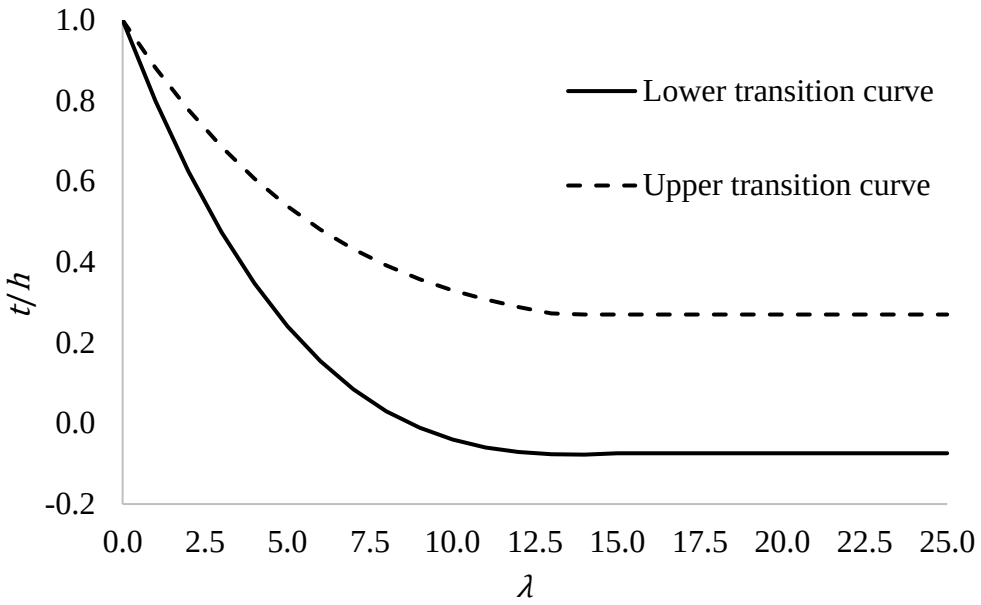

Figure 2.2. Boundaries of impinging jet and surface flow regimes (adapted from Wu and Rajaratnam (1996)).

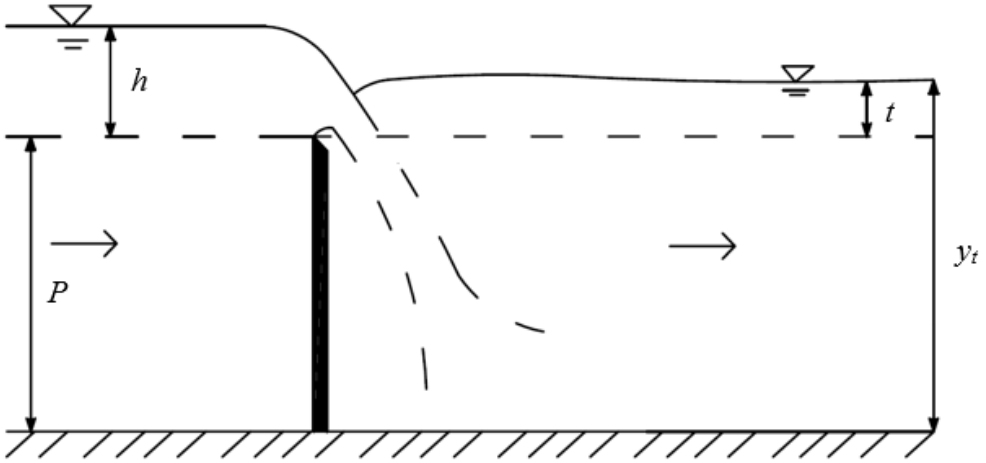

Figure 2.3. Definition sketch for flow over a weir.

flow is in the impinging jet regime. In between two curves, flow is defined as the transition regime. In this transition region, the impinging jet regime and surface flow regime can be switched from one to another by an external disturbance. If the tailwater is gradually increased, the impinging jet will hold up to curve 2, and if the tailwater depth is gradually decreased, the submerged flow regime will hold down to curve 1 (Wu and Rajaratnam 1996). Azimi *et al.* (2016) updated and defined some of the boundaries between regimes.

2.3 Characteristics of Submerged Hydraulic Jumps

Submerged hydraulic jumps at overflow structures are hazardous due to the upstream directed (*i.e.,* backward) current (Fan 1993). Although studies on the characteristics of submerged hydraulic jumps below overflow structures (*e.g.,* weirs) are limited (Hotchkiss and Comstock 1992; Fan 1993; Leutheusser and Fan 2001), jumps below overflow structures are thought to be similar to those below gates, which is a more studied flow (Rao and Rajaratnam 1963; Rajaratnam 1965a,b,c; Long *et al.* 1990; Wu 1994).

2.3.1 Roller

The flow below a weir with a submerged hydraulic jump is thought to have five regions of behavior (see Fig. 2.4): the nappe region; the deceleration region; the countercurrent region; the recovered region; and the aeration region (Fan 1993). In the nappe region, the flow accelerates very rapidly over the weir crest and then moves downward into the tailwater at an angle as an obliquely impinging jet, and entrains air in the process (Fan 1993, Wu and Rajaratnam 1996). The deceleration region is the continuation of the nappe flow, as the flow moves along the channel bed and expands towards the free surface of the flow as it moves away from the weir (Fan 1993). The behavior of the flow along the bed is thought to be similar to a wall jet (Long *et al.* 1990; Wu and Rajaratnam 1995). The countercurrent region is located above the deceleration region with an upstream-directed flow near the water surface. As for free hydraulic jumps (Case B), at low values of submergence of a jump, the countercurrent region looks violent with a large amount of air entrainment. Submergence is defined as the ratio of the excess tailwater above that required to form a jump to the tailwater depth required to form a jump (Rajaratnam 1967). At higher tailwater depths and therefore at higher submergences, the water surface of a submerged hydraulic jump looks calm, but the flow remains directed upstream. Past the countercurrent region (roller), the recovered region has a downstream-directed flow through the entire flow depth. The velocity profile starts to recover the form typical of an open channel flow. The aeration region is located upstream of the nappe, and there is no net flow out of it (Fan 1993). The roller or standing vortex of the submerged hydraulic jump, is made up of the countercurrent region and the deceleration regions of the flow.

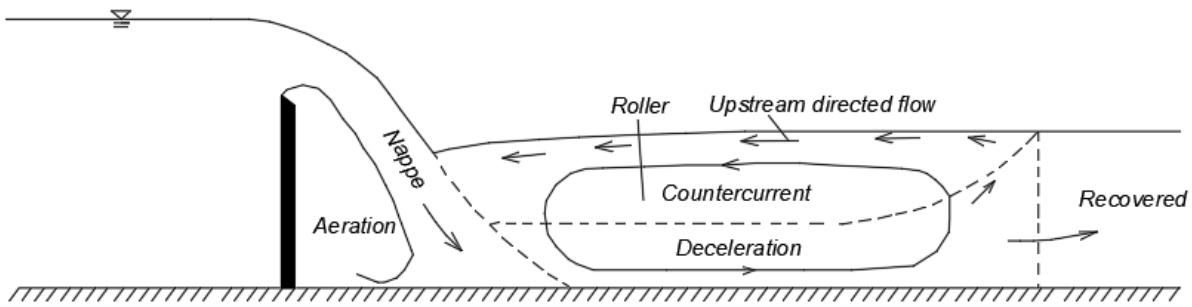

Figure 2.4. Flow regions in the flow with submerged hydraulic jump below a weir (adapted from Fan (1993)).

For an overflow structure such as a weir, the length of the roller is defined as the horizontal distance along the direction of flow between the points where the falling nappe first touches the water surface and where the upstream directed flow velocity becomes zero at the end of the roller (Fan 1993). Fan (1993) found the length of the countercurrent region (L_{cr}) can be made dimensionless by the subcritical sequent depth (Y_2) of the nappe flow along the bed, and has a linear relationship with submergence (S) as

$$\frac{L_{cr}}{Y_2} = 5.46 + 6.67S. \tag{2.1}$$

The submergence S is defined as

$$S = \frac{y_t - Y_2}{Y_2}. \tag{2.2}$$

For overflow structures, the length of the countercurrent region (L_{cr}) for a submerged hydraulic jump is typically about 5 to 6 times the tailwater depth (y_t) (Fan 1993).

For the length of the submerged jump formed below a gate, taken to be the horizontal distance along the direction of flow from the point where the jump occurs to the point where the free surface levels off downstream of the jump, Rajaratnam (1967) also found a linear relationship between the length of a submerged hydraulic jump (L_{sj}) in terms of Y_2 with submergence,

$$\frac{L_{sj}}{Y_2} = 6.1 + 4.9S\ . \tag{2.3}$$

2.3.2 Velocity Distribution

The velocity distribution through the depth of flow below a weir in submerged hydraulic jumps varies with horizontal distance away from the weir. The high velocity of the nappe region is turned to flow along the bed and then decelerates and expands with distance away from the weir to eventually fill the entire flow depth. Velocities are near parallel to the bed in this forward flow region. Above the flow along the bed is the roller, which has a backwards surface velocity. This means that there is a transition between forward and backward flow, and therefore a shear layer, at some depth within the jump (*i.e.*, there is a position above the bed where there is no velocity). The maximum portion of the depth of flow through a roller that has a backwards flow is about $^1/_3$ to $^1/_2$ of the flow depth (Fan 1993).

The velocity profile within a submerged hydraulic jump formed below overflow structures is not well studied, but there is research on velocity profiles in submerged hydraulic jumps formed below underflow structures (sluice gates) (Wu 1994, Wu and Rajaratnam 1995). Since the velocity profiles are likely similar between the two cases, Wu's (1994) results are discussed here. The submerged hydraulic jump has almost the same longitudinal forward velocity distribution as the free-jump and classical wall jet, although some differences are found in the upper part of the velocity profile due to differences in the reverse flow (Wu 1994). Wu (1994) expressed the longitudinal forward velocity profile in dimensionless form. Wu (1994) used the maximum forward velocity through the depth of flow at a particular longitudinal distance along the bed as a scale for the velocities, and the distance up from the bed where the local forward velocity is equal to half of the maximum value, and velocity gradient in the vertical direction is negative, as the length scale. Wu (1994) noticed that the velocity scale decay with distance along the bed can be wall-jet-like or free-jump-like, depending on the submergence of the jump. If the submergence $S < 12F_1^{-1.3}$, where here F_1 is Froude number for the flow under a gate or underflow structure, the decay of the velocity scale will be free-jump-like rather than wall-jet-like.

Wu (1994) also presented a dimensionless velocity profile to describe the velocities in the reverse flow of the roller. He used the local backwards velocity at the water surface (U_s) as the velocity scale and the distance from the water surface to the point where local backwards velocity

is 75% of the backwards surface velocity as the length scale (b_r). The length scale b_r can be taken as $0.2y_t$ for simplicity (Wu 1994). The velocity profile will be shown in more detail in Chapter 3.

For an underflow gate, Wu (1994) developed an expression for the variation of maximum reverse surface velocity v^* seen along the length of a submerged hydraulic jump in terms of jet velocity and Froude number at the inflow to the jump and jump submergence. Wu (1994) also developed a relationship between U_s and v^*, which is presented in Chapter 3. For an overflow structure, from experimental data Fan (1993) plotted the maximum countercurrent surface velocity, v^*, as a function of submergence (S), subcritical sequent depth (Y_2), and Froude number (F_1) of the inflow to the submerged jump (Fig. 2.5). Wu's (1994) research can predict the maximum reverse surface velocity v^* for supercritical Froude number (F_1) from 2.12 to 8.48, whereas Fan's (1993) findings are for a range of Froude number (F_1) of 3.0 to 5.5 (see Fig. 2.5). Fan (1993) gave only the maximum surface velocity that occurs along the length of the jump, not the surface velocity at a particular location along the jump.

2.4 Defining Hazardous Conditions for the Flow at a Weir

One can define what flow pattern might occur at a weir site for a particular set of flow conditions. It is thought that the submerged hydraulic jump is the flow pattern that is hazardous. However, the jump may be very shallow, or velocities may be slow. Thus, there must be some criteria for deciding whether the flow presents a hazard to a person within it. Leutheusser and Birk (1991), Hotchkiss and Comstock (1992), Leutheusser and Fan (2001), and Olsen *et al*. (2013) defined the flow below the weir as dangerous when a forced vortex having a significant upstream directed (countercurrent) free-surface velocity is noticed.

Fan (1993) tried to understand how hazardous a submerged flow below a weir can be by comparing the maximum countercurrent velocity with human swimming capability. If the flow was in the submerged jump flow regime, he estimated the backwards surface velocity for a given set of flow conditions based on his equations developed from experiments with hydraulic jumps of varied submergence formed below a weir (Fig. 2.5). He compared this backwards velocity to the typical swimming speed of an "ordinary person", which he took as 0.25 to 0.87 m/s for poor to good swimmers, respectively. Leutheusser and Birk (1991) took the maximum human swimming speed to be about 2 m/s, based on the average velocities of Olympic swimmers. No

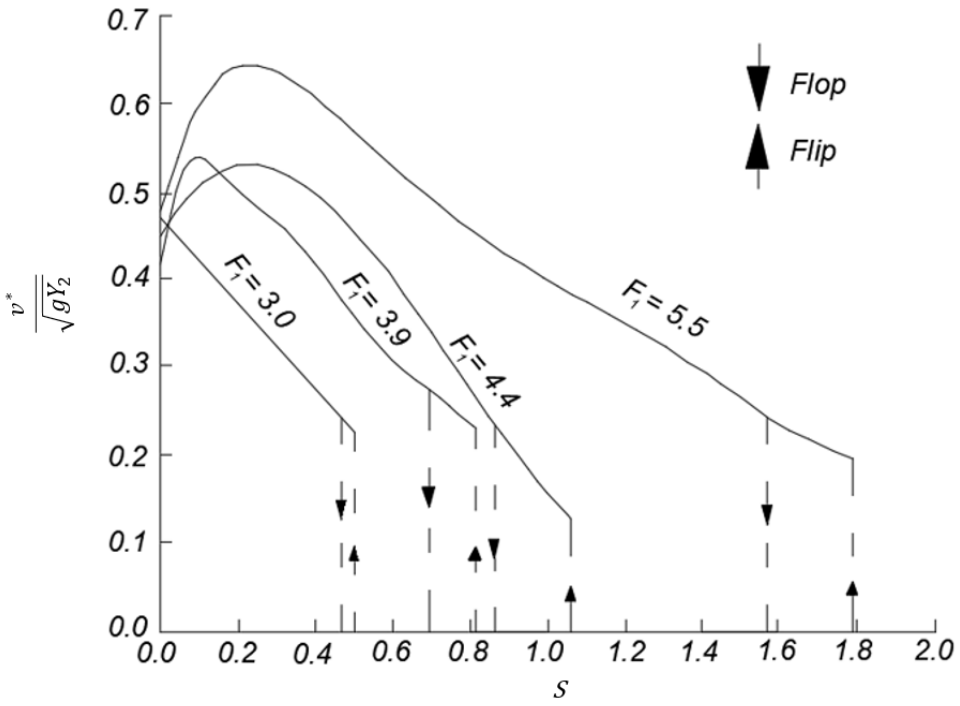

Figure 2.5. Maximum countercurrent surface velocity (v^*) in a submerged hydraulic jump below a weir is a function of submergence (S), subcritical sequent depth (Y_2) and supercritical Froude number (F_1) of the hydraulic jump (adapted from Fan (1993)).

features of the person (*e.g.*, height, weight) were specified. From swimming speed studies, McArdle *et al*. (2007) reported the maximum velocity of an untrained swimmer to be about 0.35 m/s.

Olsen *et al.* (2013) used the computational fluid dynamics (CFD) software Flow-3D to aid in analyzing the risk of entrapment below a weir. For the analysis, Olsen *et al.* (2013) used a dimensionless velocity factor, which represented the minimum surface velocity for the jump, as a proxy for the strength of the roller. A negative value of this velocity factor indicates the presence of the roller below the weir. To distinguish between different states of flow, Olsen *et al.* (2013) related this velocity factor to $\frac{(P+h)-y_t}{P}$, where *P* is the height of weir. The latter term he called the "risk factor". From a plot of the velocity factor *vs.* the risk factor, he divided the risk factor into different ranges. For low head dams, the "dangerous zone" (which he considered was the formation of the roller) occurred in a range of risk factors from 0.343 and 0.708. Lower than this range, the flow pattern would be a flipped nappe (surface jet), and higher than this range, there would be a

swept-out hydraulic jump. Both flow patterns were considered less hazardous with respect to drowning (Olsen *et al.* 2013).

There are no force-based analyses in the literature for evaluating drowning risk for a submerged jump formed below a weir. However, there are analyses based on velocity and depth for flows of only forward velocities (*e.g.*, a river flow over a flooded street) that might be considered in developing a force-based analysis for the drowning risk within a submerged hydraulic jump. Examples include Abt *et al*. (1989), Takahashi *et al*. (1992), Lind *et al*. (2004), Jonkman *et al.* (2005), Jonkman (2007), Jonkman *et al*. (2008) and Cox *et al.* (2010).

Abt *et al.* (1989) introduced the "Product Number" to define the hazard of a forward flow; it is a product of flow depth and average velocity (depth × average velocity = $D_{flow}V_{flow}$ (m^2s^{-1})). For a flood flow, Lind *et al.* (2004), Jonkman *et al.* (2005) and Jonkman *et al.* (2008) suggested that above a value of the depth-velocity product of about 0.6 m^2/s, a person would be unable to stand in a flood flow. Based on the work of Abt *et al.* (1989), the Ontario Ministry of Natural Resources (OMNR) (1988) suggested a more conservative guideline. OMNR (1988) suggests that if a flood flow depth is higher than 0.8 m, it will not be easy to stand in a flow due to buoyancy. It also suggested that for flow velocities greater than 1.7 m/s, a person will be knocked over by a flood flow. However, Abt *et al.* (1989) had tested velocities up to 3.05 m/s and did not suggest such conservative guidelines. The United States Bureau of Reclamation (1988) also gave similar guidelines in the form of separate plots for adults and children that give the degree of danger with respect to losing stability in standing for a given velocity for different flood flow depths.

Jonkman *et al.* (2005) suggested that the depth-velocity product of a flood flow has a physical relationship with moment instability and represented depth-velocity product as a function of human mass. For example, according to their relationship, a person of 100 kg weight would be unsafe in a flood flow if the depth-velocity product of a flood flow is more than 1.1 m^2/s.

Cox *et al.* (2010) classified the hazards for human stability based on the product number of the flow and a factor based on the person's height and mass (Height×Mass = *HM* (m·kg)). Cox *et al.* (2010) combined the data from many studies (Foster and Cox 1973, Abt *et al.* 1989, Takahashi *et al.* 1992, Karvonen *et al.* 2000, Yee 2003, Jonkman *et al.* 2008) and classified humans according to their *HM* and flood flows according to the depth-velocity product. Humans were sorted into three groups: infants or small children (*HM* ≤ 25), children (*HM* 25 to 50), and

adults (*HM* > 50). Cox *et al.* (2010) also defined five flow states: safe, low hazard, moderate hazard, significant hazard, and extreme hazard. According to Cox *et al.* (2010), every flow creates an extreme hazard for infants and small children. In the case of children (*HM* 25 to 50), an extreme hazard was found when the flow $D_{flow}V_{flow} \geq 0.6$ m^2s^{-1}. Adults (*HM* > 50) face an extreme hazard when the flow $D_{flow}V_{flow} \geq 1.2$ m^2s^{-1}. Cox *et al.* (2010) also suggested maximum safe flow depths for children and adults, which were 0.5 m for children regardless of velocity, and 1.2 m for adults if the velocity is less than 0.5 m/s.

Studies show there are two mechanisms of human instability in horizontal, forward flows (flood flows): sliding and toppling (Takahashi *et al.* 1992, Shu *et al.* 2016 and Chen *et al.* 2019). Sliding is frictional instability, which usually occurs during a high-speed, shallow depth flow. Toppling is moment instability, which occurs in deeper flows. Takahashi *et al.* (1992) examined the stability of adults for different directional uniform flows (flood flows) and found that the drag force coefficient for an adult in straight flow exposure varies in between 0.6 and 1.1 when the feet remain together. Jonkman *et al.* (2008) pointed out that it is difficult to consider the total reaction of a body as postural adaptation of a person to the flow is a complex and unorthodox process. Xia *et al.* (2014) derived a mechanics-based formula for a forward-only flow (moment around point of balance) for calculating incipient velocity of a human body and compared the formula with experimental data from previous studies (Abt *et al.* 1989, Karvonen *et al.* 2000). Later, Chen *et al.* (2019) did further improvement of Xia *et al.* (2014)'s work, considering postural adjustment of human body in uniform flow (flood flow). Xia *et al.* (2014) calculated the buoyancy force based on the physical structure of a typical Chinese person, whereas Chen *et al*. (2019) considered the typical American or European human physiques.

None of the research mentioned in this literature review has tried to define the submerged hydraulic jump's hazardous level by calculating the forces acting on the human body considering the actual submerged hydraulic jump velocity profile below a weir. Using human models and the velocity profiles of submerged hydraulic jumps can help to develop a force-based method to understand the weir's hazard.

CHAPTER 3. METHODOLOGY

3.1 Introduction

This chapter presents the methodology followed in this study. The discussion first sets out how different forces act on a human body in a forward flow and how the forces create moments which may cause toppling. Then, the additional forces that act in submerged jump flow conditions are included. Next, to determine whether hazardous flow conditions exist below a weir, a framework for analysis is established. The framework includes the assessment of the velocity profile through a submerged hydraulic jump formed below a weir, determining the relevant characteristics of a human body needed to find the forces acting on that body, and then assessing those forces and the resulting moment arms and moments. At the end of the chapter, details of the Wolf River Barrier site and the associated laboratory model by Mazurek *et al.* (2008) are presented.

3.2 Forces Acting on a Human Body in a Flow

There has been little research to evaluate the forces that act on a human body entrapped in a submerged hydraulic jump formed below a weir. The focus of research on human stability in water flows has been for floods and flows over roadways (Abt *et al.* 1989, Takahashi *et al.* 1992, Lind *et al.* 2004, Jonkman *et al.* 2008, Xia *et al.* 2014, Chen *et al.* 2019).

In addition to his or her weight, a person in a flow is subjected to drag, buoyancy, hydrostatic downstream and upstream pressure forces, and surface friction below his or her feet. A human body could rotate or topple if the moment created about their toe or heel is higher than the resisting moment. The countercurrent velocity in a submerged hydraulic jump can introduce an additional moment over that seen in forward-only flows.

Human stability in a uniform flow (*i.e.,* a flow with a depth that does not change with distance along the channel and moves with a constant velocity through the depth of flow) can be evaluated with the help of Figure 3.1. Abt *et al.* (1989) considered a standing human as a monolith; the center of mass and center of buoyancy for that monolith falls along the same line of action. The point of balance was only taken at the heel by Abt *et al.* (1989) assuming that the person is

looking upstream. For this case, taking a clockwise moment as positive, a person remains stable when the moment around the point of balance, M_p, is zero or negative. Abt *et al.* (1989) and Jonkman *et al.* (2005) describe this moment balance as

$$M_P = \left(F_D \frac{D_{flow}}{2}\right) - (W - F_B)L_w \leq 0\,, \tag{3.1}$$

where $W = Mg$ is the weight of the body, M is the body's mass, g is gravitational acceleration, F_B is the buoyant force on the body, F_D is the drag force on the body; L_w is the horizontal distance from the center of mass of the body to the point of balance; and D_{flow} is the depth of the flow. The drag force is

$$F_D = C_d A_n \frac{\rho_w V_{flow}{}^2}{2}\,, \tag{3.2}$$

where C_d is the coefficient of drag, A_n is the projected area of the human body normal to the flow, ρ_w is the density of water, and V_{flow} is the average forward flow velocity. The buoyancy force on the body is estimated as

$$F_B = \lambda_s \gamma_w\,, \tag{3.3}$$

where λ_s is the submerged volume of the body and $\gamma_w = g\rho_w$ is the specific weight of water.

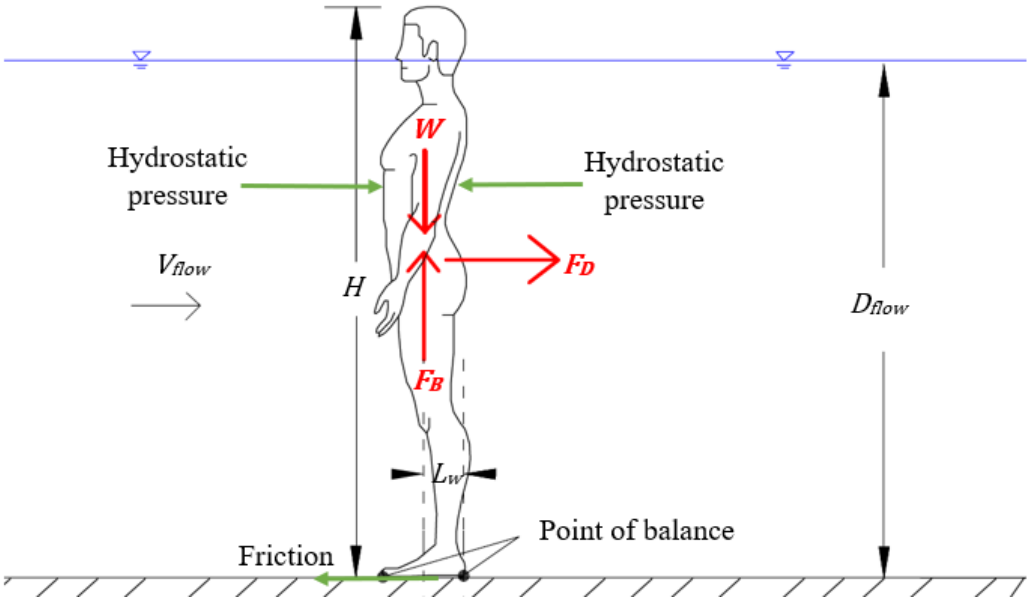

Figure 3.1. Forces acting on a human body under uniform (forward) flow conditions.

As the flow under the weir is a mixed form of submerged plane obliquely turbulent impinging jet and a submerged hydraulic jump, more forces act on a body standing within the flow as compared to the case of a flooded river or street (Figure 3.2). Four major forces create moments around the point of balance (heel or toe), with a clockwise moment considered positive: the person's weight (W), buoyancy (F_B), and the drag forces due to the backward (F_{DB}) and forward (F_{DF}) flows within the jump. There are also the hydrostatic pressure forces at the front and back of the body to consider. However, the thickness of a human is not large as compared to the length of the roller in a submerged jump, so flow depths on the front and back of the body are similar, although the depths through a roller are increasing with distances along the channel. Therefore, the pressure forces generated by the difference in water levels on the front and back of the body will be neglected in this study.

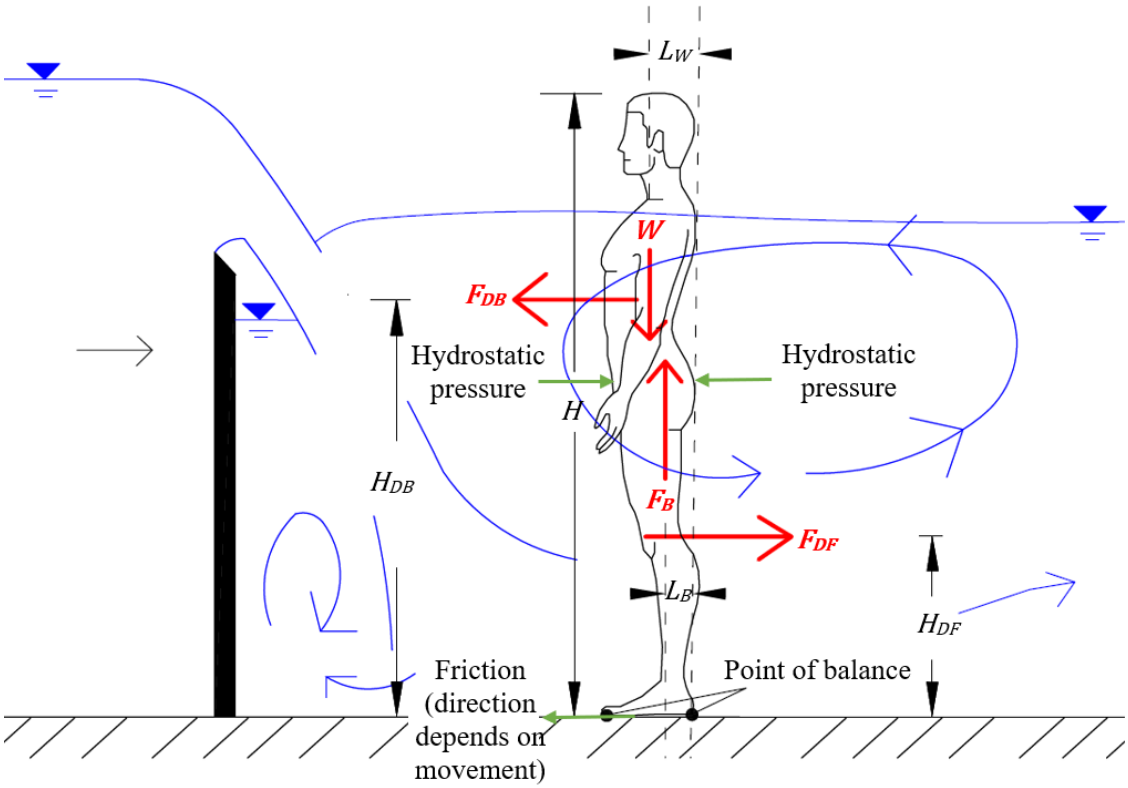

Figure 3.2. Forces acting on a human body under submerged flow condition below the weir.

Because in a submerged hydraulic jump a considerable amount of flow is upstream directed, the point of balance in considering stability of a person standing in the flow can be the toe or heel. Here it is assumed that the person is facing upstream, which is the case that provides a conservative estimate of toppling moment (shown in later sections). If the moment due to the

backward flow is higher than the moment due to the forward flow, the point of balance will be at the toe, otherwise it will be at the heel. Moment arms for the forward and backward flow do not depend on the decision of the point of balance, as these are assumed to be horizontal forces and the moment arms will be vertical distances from the channel bed. However, the choice of the point of balance does impact the moment arms for the weight and buoyancy forces, as these are vertical forces, and their moment arms will be horizontal distances.

Moreover, the moment arms for the body's weight and buoyancy are not the same. The human body does not have uniform density (Clauser *et al*. 1969, Sendroy and Collison 1966), which shifts the location of the center of mass from the centroid of the body. Also, here it is assumed that the person is not fully submerged, and the buoyancy force then acts at the centroid of the submerged volume. Since human bodies have an irregular cross-section with height, the centroid of the submerged volume is not likely in the same horizontal position as the centroid of the overall volume of the body.

A person will be stable standing in a submerged hydraulic jump if the moment created by the balancing force, the person's weight, is higher than the combined moment created by the unbalancing force, which is buoyancy. The forward and backward drag forces can be respectively stabilizing or destabilizing depending on the situation. For a person standing facing the weir and for a point of balance at the heel, a person will remain stable in a submerged hydraulic jump if

$$M_P = F_{DF}H_{DF} - F_{DB}H_{DB} + F_B L_B - W L_W \leq 0 \tag{3.4}$$

where again M_p is the moment about the point of balance and F_{DF} and F_{DB} are drag forces due to forward and backward flows, respectively. Here, H_{DF} and H_{DB} are the moment arms for F_{DF} and F_{DB}, respectively (as measured from the bottom of the foot), and L_B and L_W are moment arms representing horizontal distances from the heel, respectively, for the buoyancy force and weight.

On the other hand, when the point of balance is at the toe, for a person standing facing the weir, a person will remain stable in a submerged hydraulic jump if

$$M_P = F_{DF}H_{DF} - F_{DB}H_{DB} - F_B\left(L_{foot} - L_B\right) + W\left(L_{foot} - L_W\right) \geq 0 \tag{3.5}$$

where L_{foot} is the length of the person's foot.

3.3 Framework for Determining Whether a Flow is Hazardous

The framework for defining whether a flow is hazardous with respect to the stability of a person standing in that flow below a weir where a submerged hydraulic jump has formed consists of three major tasks: (1) determining the forces acting on the person; (2) determining the location of application of those forces; and (3) computing the moments about the point of balance to decide whether the person is stable or unstable.

3.3.1 Forces

As noted above, there are four forces acting on the person to consider: weight, buoyancy, and the drag forces due to the forward and backward velocities through the jump.

3.3.1.1 Estimating the Weight of a Body

For this work, the height of the person will be used as the basis for estimating the person's weight, volume, and frontal area. In determining a typical person's weight based on their height, the BMI (Body Mass Index) is used. BMI is a person's weight in kilograms divided by the square of height in meters; this parameter is often used to characterize a person's weight in the health sciences field (*e.g.*, Janssen *et al.* 2005, Evans *et al.* 2006, Davies *et al*. 2020). If a person's height is known, BMI values will give typical values of weight. A person is underweight for BMI < 18.5, of normal weight for 18.5 < BMI < 25, over-weight if 25 < BMI < 30, and obese if BMI > 30 (National Heart, Lung, and Blood Institute and National Institute of Diabetes and Digestive and Kidney Disease 1998, WHO 2000). Shields *et al.* (2011) reported average Canadian male and female heights, weights, and BMI's based on the 2008 Canadian Community Health Survey. For the analysis herein, the average BMI's of Canadian adult males and females of 26.4 and 25.4 and average heights 175.8 cm and 162.1 cm, respectively, will be used for analysis (Shields *et al.* 2011). However, this framework can also easily be used for a person of other weights and heights.

3.3.1.2 Buoyancy Force

As noted above (see Eqn. 3.3), the submerged volume of the person and the specific weight of water are required to determine buoyancy force acting on that person. The specific weight of the water depends on temperature. The station (station ID: 01009400102) located near Wolf River is currently inactive (active from 1973 to 1975), but the Wolf River watershed is similar to the Thunder Bay region. Water quality data from The Provincial (Stream) Water Quality Monitoring Network (PWQMN) for 2019, where measurements of water temperature of the watershed near Thunder Bay, reported water temperatures ranged from -0.5˚C to 30.2˚C (Government of Ontario 2021). In this study, it is assumed here that the temperature of the water is 5˚C.

For a person of a certain height, to estimate their submerged volume for a particular flow depth, relationships were developed to give their submerged volumes with flow depth for males and females. To develop these relationships, three-dimensional (3D) male and female models were built in SketchUp Pro 2021 (Fig. 3.3). To make sure that the proportions of the model body were correct, Contini's (1972) information on the length and width of body parts relative to the person's height were used for both "standard" males and females. These standards are seen in Figures 3.4a and 3.5a. It was confirmed that Contini's (1972) sketches are to scale.

Outlines of the frontal areas of these bodies were sketched in AutoCAD 2018 for a male of 175.8 cm height and a female of 162.1 cm (the average heights for Canadians indicated above). Body part lengths in the frontal area outline were compared to the dimensions of the typical American given Contini's (1972) standards (see Table 3.1). Then, the frontal area of each three-dimensional body model was then compared to the frontal area found from the 2018 AutoCAD body outlines. The three-dimensional model male had a 2.43% higher area than the 2D AutoCAD model. This percent difference was calculated by

$$\text{Percent difference} = \frac{A_{F3D} - A_{F2D}}{A_{F2D}} * 100\%, \tag{3.6}$$

where A_{F3D} is the frontal area of 3D model and A_{F2D} is the frontal area of 2D model.

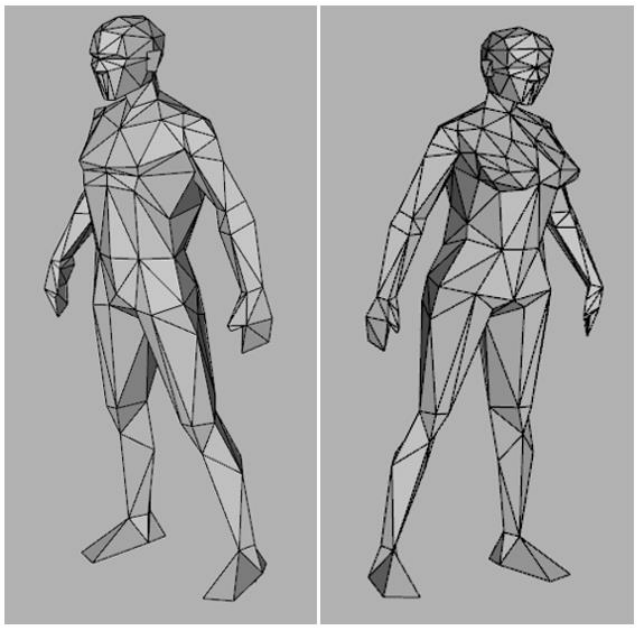

(a) (b)

Figure 3.3. Three-dimensional models created in SketchUp Pro 2021 for a (a) male and (b) female.

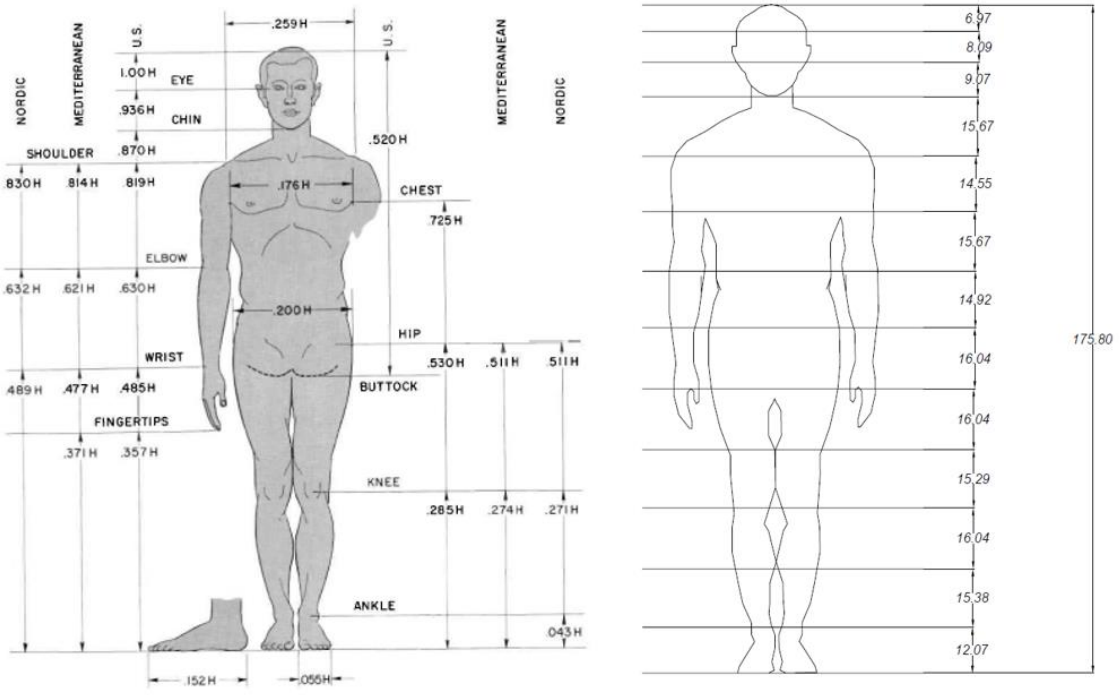

(a) (b)

Figure 3.4.(a) Standard dimensions of an American male as a proportion of his height *H* (adapted from Contini (1972); (b) two-dimensional sketch of male produced in AutoCAD 2018 which maintains Contini's (1972) ratios for a male of 175.80 cm (all dimensions in part b are in cm).

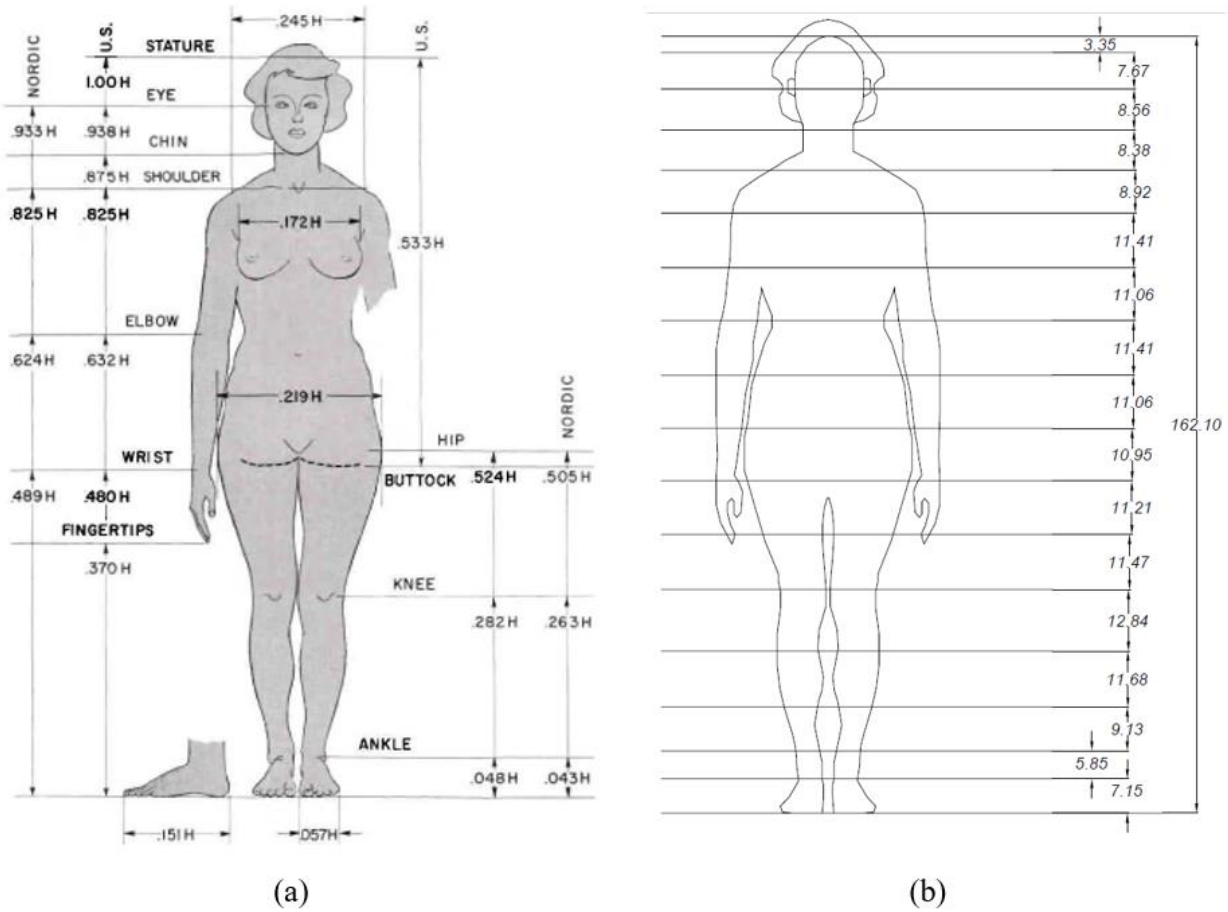

Figure 3.5. (a) Standard dimensions of an American female as a proportion of her height *H* (adapted from Contini (1972); (b) two-dimensional sketch of female produced in AutoCAD 2018 which maintains Contini's (1972) ratios for a female of 162.10 cm (all dimensions in part b are in cm).

Table 3.1. Body part length comparison between Contini (1972) and the dimensions of the two-dimensional body produced in AutoCAD 2018 for both male and females of heights H.

Body measurements	American Male	2D model Male	Percent difference[1] (%)	American Female	2D model Female	Percent difference[2] (%)
Foot to ankle	$0.043H$	$0.043H$	0	$0.043H$	$0.047H$	9.3
Foot to knee	$0.285H$	$0.286H$	0.35	$0.282H$	$0.276H$	-2.12
Foot to hip	$0.530H$	$0.510H$	-3.77	$0.524H$	$0.485H$	-7.44
Foot to chest	$0.725H$	$0.740H$	2.07	$0.725H$	$0.725H$	0
Foot to shoulder	$0.819H$	$0.814H$	-0.61	$0.825H$	$0.821H$	-0.48
Foot to chin	$0.870H$	$0.863H$	-0.80	$0.875H$	$0.869H$	-0.69
Foot to eye	$0.936H$	$0.932H$	-0.43	$0.930H$	$0.935H$	0.54
Width of a foot	$0.055H$	$0.055H$	0	$0.057H$	$0.055H$	-3.51
Width of hip	$0.200H$	$0.199H$	-0.5	$0.219H$	$0.216H$	-1.36
Distance between shoulders	$0.259H$	$0.256H$	-1.16	$0.245H$	$0.238H$	-2.86
Length of foot	$0.152H$	-	-	$0.151H$	-	-

[1] Percent difference (male) = (2D model male dimension – Contini's (1972) American male dimension)/American male dimension*100%

[2] Percent difference (female) = (2D model female dimension – Contini's (1972) American female dimension)/American female dimension *100%

Similarly, the frontal area of the model female was 2.16% higher in the three-dimensional model than the 2D AutoCAD model. The male 3D model had a height of 175.58 cm, and the female 3D model has a height of 161.78 cm as compared to the height of the person in the AutoCAD model 175.8 cm height for a male and 162.1 cm for a female. The overall heights produced in the three-dimensional models did not exactly match the standard heights used in the two-dimensional model although the ratios of the body part lengths were maintained the same.

Next, the variation of the body's volume with distance measured from the bottom of the foot was determined using the 3D model for the male and female. The height of each 3D model was divided into intervals and the body's volume up to these different distances from the bottom of the foot was determined in SketchUp Pro 2021. The produced volumetric data are given in Appendix A. Then, plots for both male and females giving the volume of water displaced by the person if they were standing in water of a given depth Y were created. The volume submerged λ_s was made dimensionless with the cube of the height of the person H and the depth of flow was made dimensionless using H. Figure 3.6 gives these relationships for both male and females. It is

seen that the data for males and females fall close to one another. Regression to the data shown in Figure 3.6 gave the following equations for males and females, respectively

$$\frac{\lambda_s}{H^3} = 0.1499\left(\frac{Y}{H}\right)^6 - 0.4622\left(\frac{Y}{H}\right)^5 + 0.4543\left(\frac{Y}{H}\right)^4 - 0.1489\left(\frac{Y}{H}\right)^3 + 0.0166\left(\frac{Y}{H}\right)^2 + 0.0043\left(\frac{Y}{H}\right) \quad (3.7)$$

$$\frac{\lambda_s}{H^3} = 0.2442\left(\frac{Y}{H}\right)^6 - 0.6953\left(\frac{Y}{H}\right)^5 + 0.6386\left(\frac{Y}{H}\right)^4 - 0.1902\left(\frac{Y}{H}\right)^3 + 0.0118\left(\frac{Y}{H}\right)^2 + 0.0055\left(\frac{Y}{H}\right). \quad (3.8)$$

These equations had a very good fit to the data with correlation coefficients r^2 for Eqns. 3.7 and 3.8 of 0.9992 and 0.9988, respectively.

3.3.1.3 Determining the Forward and Backward Drag Forces

Calculating the drag forces (Eqn. 3.2) due to the forward flow (F_{DF}) and the backward flow (F_{DB}) within the submerged hydraulic jump is a critical part of this study, as they are key drivers of instability. The drag coefficient, forward and backward flow velocities, and a person's area normal to the flow (frontal area) are needed to calculate these drag forces.

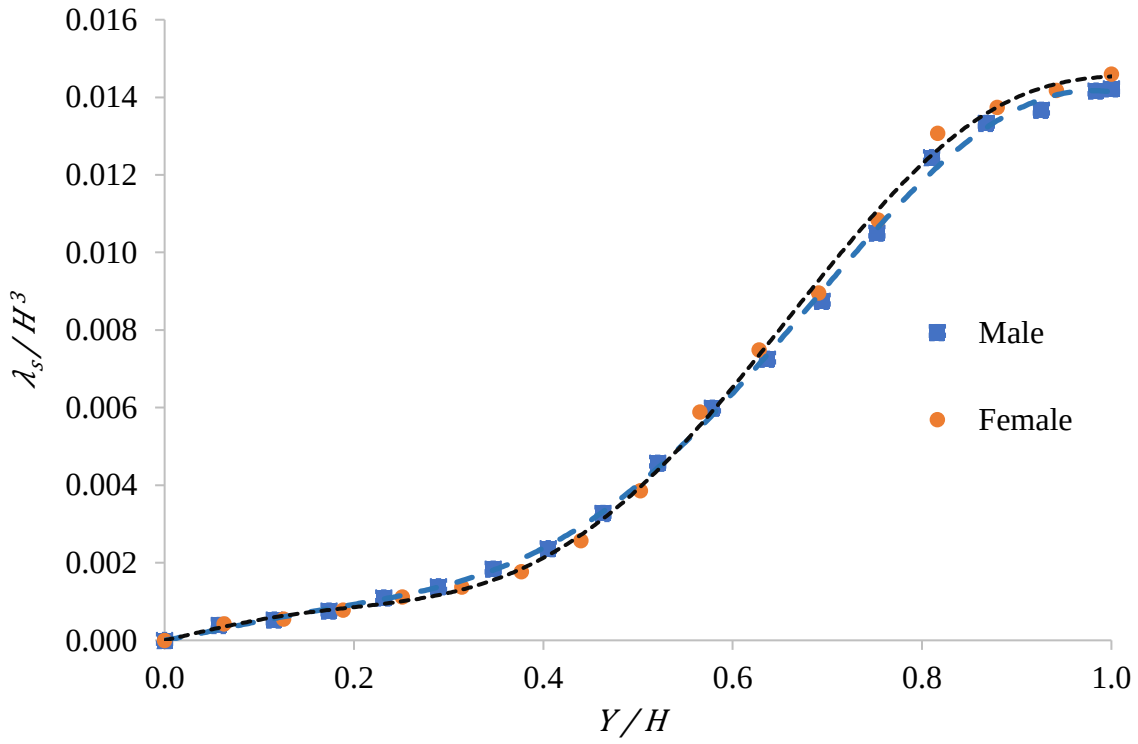

Figure 3.6. Volume displaced by male and female bodies for different water depths.

3.3.1.3.1 Drag Coefficient

The drag coefficient for humans in standing varies based on their position, shape, and the Reynolds number for the flow around the body (Hoerner 1965). For the flow around a person standing in a flood flow looking upstream, Shu *et al*. (2016) suggested that C_d is inversely proportional to the Reynolds number when the Reynolds number is <20,000, and C_d is approximately constant at 1.08 when the Reynolds number is >20,000 (Shu *et al*. 2016). However, the Reynolds number was not defined and there were no references for the drag coefficient estimates. Jonkman and Penning-Rowsell (2008) used C_d =1.1 while analyzing human instability in flood flows, but they did not justify the choice of this value. Based on experimental data from a wind tunnel, Hoerner (1965) estimated that the drag coefficient for a person standing facing the flow varies between 1.0 to 1.3. Without clothing, the drag coefficient is 5 to 10% less. For this study, the drag coefficient for a person standing perpendicular to the flow will be taken as 1.2 (the average of Hoerner's estimates).

3.3.1.3.2 Frontal Area

The area of a person's body normal to the flow (both for the forward and backward flow) changes with the velocity profile below the weir and the person's height. A person is divided into two portions to calculate the drag forces acting on his or her body; the lower portion is subjected to a forward flow, and the upper portion is subjected to a backward flow. Therefore, a relationship between the area of the body normal to the flow with the vertical distance measured upwards from the bottom of the foot are required. This work was done for both males and females using the AutoCAD 2018 2D human models described above (Figures 3.4b and 3.5b). These 2D models represent the front view of a person standing while keeping both legs together. Again, the male model has a height of 175.8 cm, and the female model has a height of 162.1 cm. The male model has a frontal area of 5384.96 cm^2, and the female model has a frontal area of 4399.13 cm^2. The male model was divided into 13 segments, while the female model was divided into 17 segments and the area of each segment was calculated using AutoCAD 2018. Then, the cumulative area was plotted against the vertical distance from the bottom of the foot. The cumulative area was then scaled with the square of the person's height H^2 and the vertical distance from the foot was scaled with H. The resulting dimensionless curves for male and females are given in Figure 3.7. Regression was used to develop the following equations

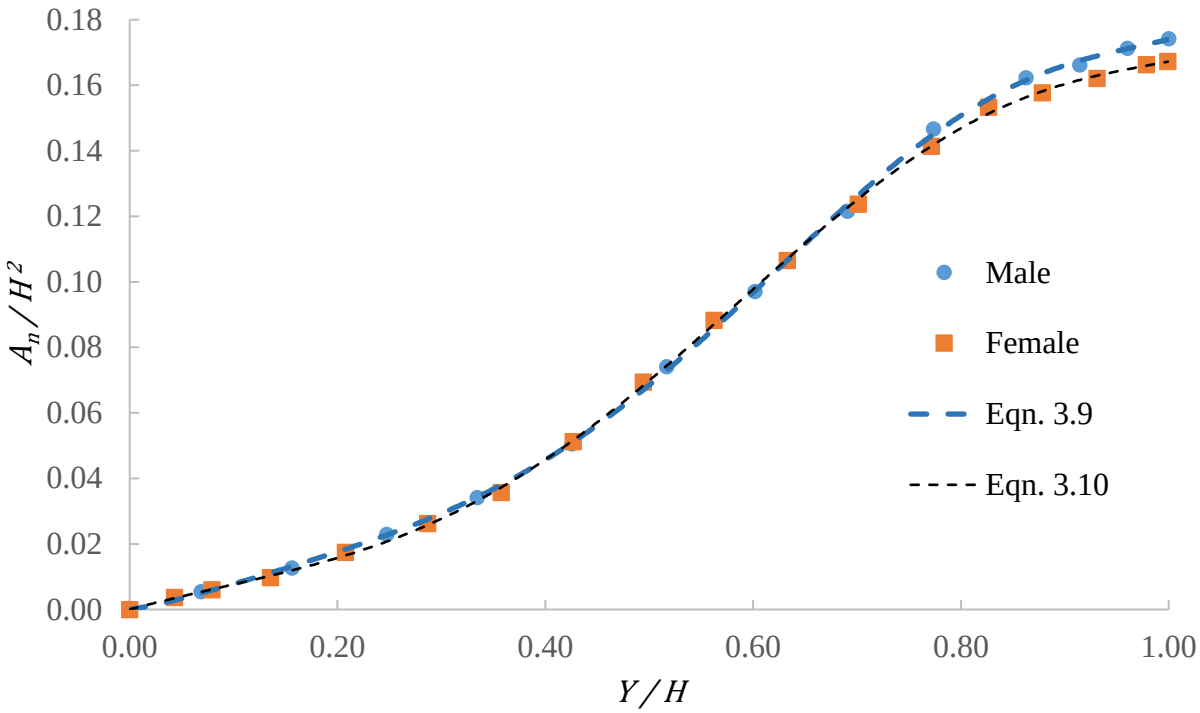

Figure 3.7. Dimensionless frontal area of male and female bodies with vertical distance measured from the bottom of the foot.

$$\frac{A_n}{H^2} = 2.3808\left(\frac{Y}{H}\right)^6 - 6.6519\left(\frac{Y}{H}\right)^5 + 6.2681\left(\frac{Y}{H}\right)^4 - 2.3246\left(\frac{Y}{H}\right)^3 + 0.4513\left(\frac{Y}{H}\right)^2 + 0.0504\left(\frac{Y}{H}\right) \quad (3.9)$$

$$\frac{A_n}{H^2} = 1.1468\left(\frac{Y}{H}\right)^6 - 2.6105\left(\frac{Y}{H}\right)^5 + 1.3854\left(\frac{Y}{H}\right)^4 + 0.2858\left(\frac{Y}{H}\right)^3 - 0.1253\left(\frac{Y}{H}\right)^2 + 0.0851\left(\frac{Y}{H}\right). \quad (3.10)$$

Both equations had correlation coefficient r^2 values of 0.9998.

3.3.1.3.3 Predicting the Velocity Profiles for the Flow Below the Weir

To calculate the drag force on the body, the velocity profile through the depth of flow is needed. Equations to estimate the velocity profile of the flow in the submerged hydraulic jump formed below a weir do not appear to exist. There are equations to assess the velocity profile in a submerged hydraulic jump formed below a gate (Wu and Rajaratnam 1995). Fan (1993) and Leutheusser and Fan (2001) provided equations to estimate the velocity of the flow just below

where the plunging flow over the weir impinges on the channel bed, and plots for the maximum backwards velocity in the roller of the submerged hydraulic jump and the roller length.

For a particular flow rate Q, one first needs to find the tailwater depth and the head on the weir (the depth of flow relative to the weir crest before the flow over the weir starts to contract). This is typically done using stage-discharge curves typically developed from flow and depth measurements at the site. Mazurek *et al.* (2008) developed stage-discharge curves from daily measurements of the upstream and downstream depths taken by the Department of Fisheries and Oceans Canada (now Fisheries and Oceans Canada) at the Wolf River barrier from September 14, 2004, to August 17, 2005. The relationship between the flow rate Q and head on the weir h was found to be (Mazurek *et al.* 2008)

$$h = 0.00002Q^3 - 0.001Q^2 + 0.0286Q + 0.173. \quad (3.11)$$

The equation gave a correlation r^2 of 0.805 and valid for $1.0 \leq Q \leq 44.0$ m^3/s. The depth on the downstream side of the weir was not the tailwater depth, which is usually taken as the depth at downstream end of the hydraulic jump, but instead the depth below the weir close to where the nappe impinges on the water surface. This is called by y_d. The location of the measurement is shown in Figure 3.8. In Figure 3.8, US and DS refer to upstream and downstream, respectively.

Figure 3.8. Location of upstream and downstream depth measurements (reproduced with permission from Fisheries and Oceans Canada).

For this depth downstream of the weir y_d, as measured from bed level, Mazurek *et al*. (2008) determined the depth-discharge relationship was

$$y_d = 0.374Q^{0.332} - 1 + P \tag{3.12}$$

with a correlation coefficient r^2 of 0.805 and again only valid for $1.0 \leq Q \leq 44.0$ m^3/s. For the work herein, it is assumed that y_d and y_t are the same.

The velocity of flow along the channel bed just downstream of where the plunging nappe impinges on the bed and then is turned around to become parallel with the bed needs to be determined. Herein, this velocity is called U_1. Following Leutheusser and Fan (2001) to find this velocity, the depth of this forward flow formed just downstream of the point of nappe impingement, called Y_1, the energy equation is applied (see Figure 3.9 for a definition sketch)

$$z_o + (h + P) + \frac{U_o^2}{2g} = z_1 + Y_1 + \frac{U_1^2}{2g} + C_L \frac{U_1^2}{2g}, \tag{3.13}$$

where z_o and z_1 are the bed elevations at sections upstream and downstream of the weir (see Figure 3.9); U_o is the velocity of flow upstream of the weir; and C_L is the coefficient of head loss, which was estimated to be equal to $0.1P/h$ by Leutheusser and Fan (2001). The velocity U_1 is found by using conservation of mass assuming a steady, incompressible flow,

$$U_1 = \frac{Q}{BY_1}, \tag{3.14}$$

for a rectangular channel of width B. The Froude number at this section 1, F_1, is defined as

$$F_1 = \frac{U_1}{\sqrt{gY_1}}. \tag{3.15}$$

Third, the subcritical sequent depth, Y_2, to form a free hydraulic jump (one that is not submerged) is calculated using conservation of momentum expressed in the form of the Belanger equation,

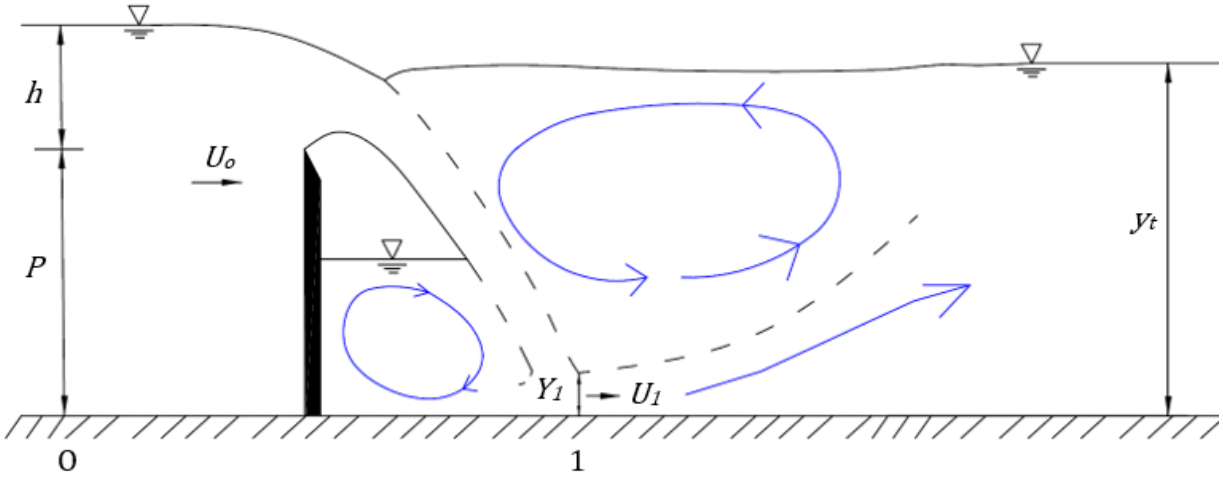

Figure 3.9. Definition sketch for the application of the energy equation.

$$\frac{Y_2}{Y_1} = \frac{1}{2}\left(-1 + \sqrt{1 + 8F_1^2}\right). \tag{3.16}$$

After Y_2 is found, the submergence S of the jump is calculated using Eqn. 2.2.

Fourth, for the case when the submergence of the jump $S > 0$ and the jump is submerged, which is the condition of concern here, the location of point 1 (see Figure 3.9) needs to be determined. This location was determined from the equations that describe the shape of the upper nappe for the flow over a sharp-crested weir. Let the horizontal distance from the upstream weir face to point 1 be X_j (see Figure 3.10 for a definition sketch). One can use the dimensionless upper nappe profile developed by Rajaratnam *et al.* (1968) to find the location of the hydraulic jump. To create their dimensionless profile, Rajaratnam *et al.* (1968) scaled the distance in the direction of flow from the weir crest, X, by $\overline{X_u}$, the horizontal distance travelled by the upper nappe from the weir crest to where the upper nappe crosses the level of the crest. The vertical distance from the weir crest Y_u was scaled with $\overline{Y_u}$, which is the vertical distance from the crest to the energy grade line just upstream of the weir. They developed equations for the scales $\overline{X_u}$ and $\overline{Y_u}$, given as

$$\frac{\overline{X_u}}{h + \frac{U_o^2}{2g}} = 1.34 - 0.3\,\frac{\frac{U_o^2}{2g}}{h + \frac{U_o^2}{2g}} \quad \text{and} \tag{3.17}$$

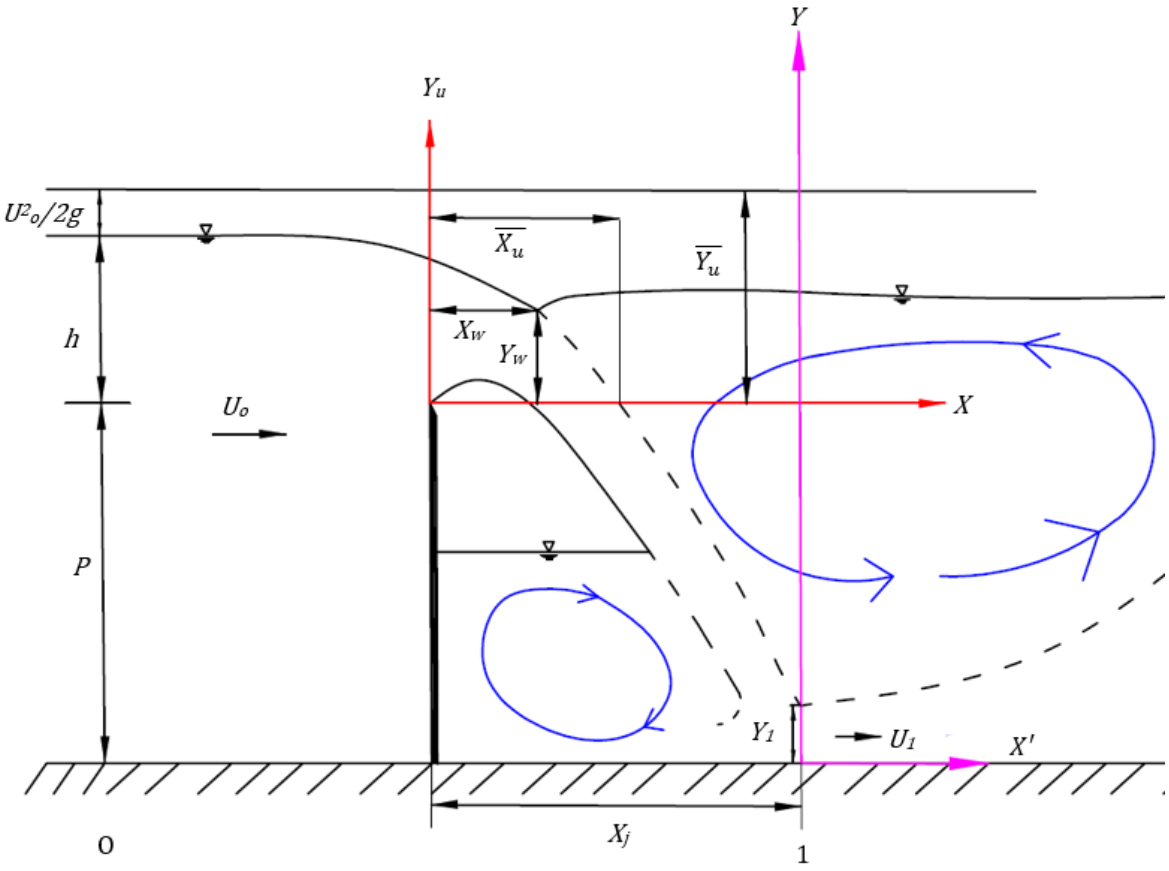

Figure 3.10. Definition sketch for upper nappe profile.

$$\frac{\overline{Y_u}}{h+\frac{U_o^2}{2g}} = 0.85 - 0.83\,\frac{\frac{U_o^2}{2g}}{h+\frac{U_o^2}{2g}}. \tag{3.18}$$

No equations were developed for the upper nappe dimensionless profile. Instead, a dimensionless plot was given that describes the profile. The original curve by Rajaratnam *et al.* (1968) plots $Y_u/\overline{Y_u}$ *vs.* $X/\overline{X_u}$, but this study requires an equation to find $X/\overline{X_u}$ from $Y_u/\overline{Y_u}$. Therefore, data from Rajaratnam *et al.* (1968) to describe the profile were replotted as in Figure 3.11. These data were given in the paper, although it appears the complete data set used by Rajaratnam *et al.* (1968) was not provided there. Then, regression was used to find a curve fit to these data, with the best fit given by

$$\frac{X}{\overline{X_u}} = -0.0133\left(\frac{Y_u}{\overline{Y_u}}\right)^3 - 0.1406\left(\frac{Y_u}{\overline{Y_u}}\right)^2 - 0.6619\left(\frac{Y_u}{\overline{Y_u}}\right) + 1. \quad (3.19)$$

This equation gives a correlation coefficient of r^2 of 0.994. Equation 3.19 predicts the upper nappe profile between the portion of the nappe above the weir crest to the end of nappe near the bed of the channel.

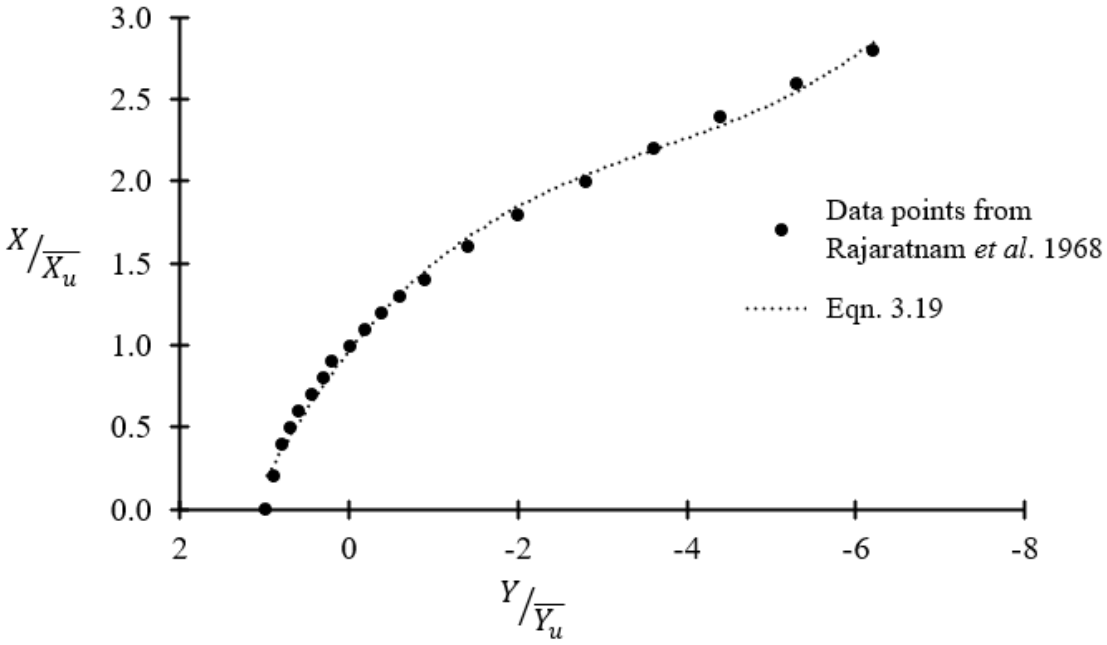

Figure 3.11. Upper nappe profile between top of weir crest and end of nappe.

Next, to calculate the position X_j (see Figure 3.10), this is taken as the position X where the upper profile intersects the depth above the bed Y_1. If one sets $Y_u = Y_1 - P$, one can solve Eqn. 3.19 for the value of X that is equal to X_j. It is assumed here that the submerged hydraulic jump starts at X_j.

Then, the forward velocity profile at some location, X', from the start of the jump (downstream of point 1) in the direction of flow (again refer to Figure 3.10) can be predicted, where

$$X' = X - X_j. \quad (3.20)$$

Two length scales L and b are required to determine this velocity profile (Wu 1994). L is the same for any X' location. It is the length scale for a distance along the direction of flow. It is the horizontal distance from the start of the jump to point on bed where $U_m/U_1 = 0.5$, where U_m is the maximum velocity of the flow along the bed at any X' and again U_1 is the velocity of flow at point 1. Assuming that a submerged hydraulic jump formed below a weir behaves similarly to a jump formed below a gate, L depends on the Froude number at section 1 and the submergence of the jump (Wu and Rajaratnam 1995),

$$\frac{L}{Y_1} = 7.26F_1^{0.64}(1+S)^{0.77} . \tag{3.21}$$

However, the length scale b changes with X'; b is the distance from the boundary (bed) where the local velocity is equal to $0.5U_m$ at that with X' location (Long *et al.* 1990). Wu (1994) found that the relationship between b and X' was linear for a submerged hydraulic jump formed below a sluice gate. However, no relationship was given. From Wu's (1994) study, 39 data points were used to develop the following relationship, here in terms of Y_1 instead of a gate opening as in Wu (1994).

$$\frac{b}{Y_1} = 0.0764\frac{X'}{Y_1} + 0.6532 \tag{3.22}$$

The correlation coefficient of r^2 value of 0.9755 was obtained for the fit to the chosen data points.

For the forward component of the velocity profile through the submerged jump, the dimensionless forward velocity profile for submerged jumps from Rajaratnam (1965a) was used (see Figure 3.12). This dimensionless profile is used to describe the velocity profile for $X' > 0.15L_{sj}$, where the fully developed region starts, and ends at around $0.85L_{sj}$ (Long *et al.* 1990). However, Rajaratnam (1965a) did not present an equation to fit the relationship between U/U_m and Y/b, where U is the velocity at height Y above the bed. To calculate this profile more easily, an equation was developed to describe Rajaratnam's (1965a) dimensionless velocity profile. Rajaratnam's (1965a) plot was "traced" in AutoCAD 2018. AutoCAD generated points that fall on this curve. This data was then fitted with two equations to describe the curve in Excel. Eqn. 3.23 predicts U/U_m up to $Y/b = 0.0365$ and Eqn. 3.24 predicts U/U_m if $Y/b > 0.0365$.

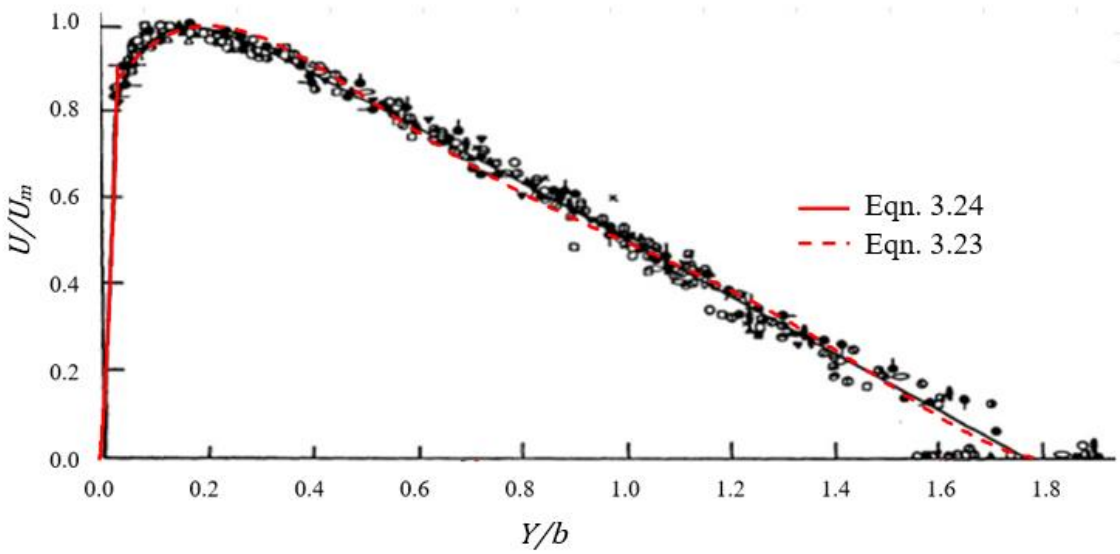

Figure 3.12. Dimensionless forward velocity profile for submerged jumps (adapted from Rajaratnam (1965a)).

$$\frac{U}{U_m} = 382.6\left(\frac{Y}{b}\right)^2 + 11.184\left(\frac{Y}{b}\right) - 0.0218 \tag{3.23}$$

$$\frac{U}{U_m} = 0.9378\left(\frac{Y}{b}\right)^5 - 4.7477\left(\frac{Y}{b}\right)^4 + 8.8848\left(\frac{Y}{b}\right)^3 - 7.5124\left(\frac{Y}{b}\right)^2 + 2.1378\left(\frac{Y}{b}\right) + 0.8 \tag{3.24}$$

Equation 3.23 gives a correlation coefficient of r^2 of 0.973, while Eqn. 3.24 gives a correlation coefficient of r^2 of 0.973. For Eqn. 3.24, a fifth order polynomial equation was needed to properly fit its shape. Here, U is the velocity at along the flow depth Y and b is length scale. The velocity scale U_m is the maximum velocity of the flow along the bed at any X'. Long *et al.* (1990) gave a dimensionless relationship between U_m/U_1 and X'/L (see Figure 3.13). Long *et al.* (1990) did not present any equation to fit this relationship. Again, for this study, Long's *et al.* (1990) dimensionless curve was traced in AutoCAD 2018 to determine data points to fit the following equation:

$$\frac{U_m}{U_1} = -0.0321\left(\frac{X'}{L}\right)^6 + 0.3838\left(\frac{X'}{L}\right)^5 - 1.7059\left(\frac{X'}{L}\right)^4 + 3.5399\left(\frac{X'}{L}\right)^3 - 3.3334\left(\frac{X'}{L}\right)^2 + 0.6431\left(\frac{X'}{L}\right) + 1. \tag{3.25}$$

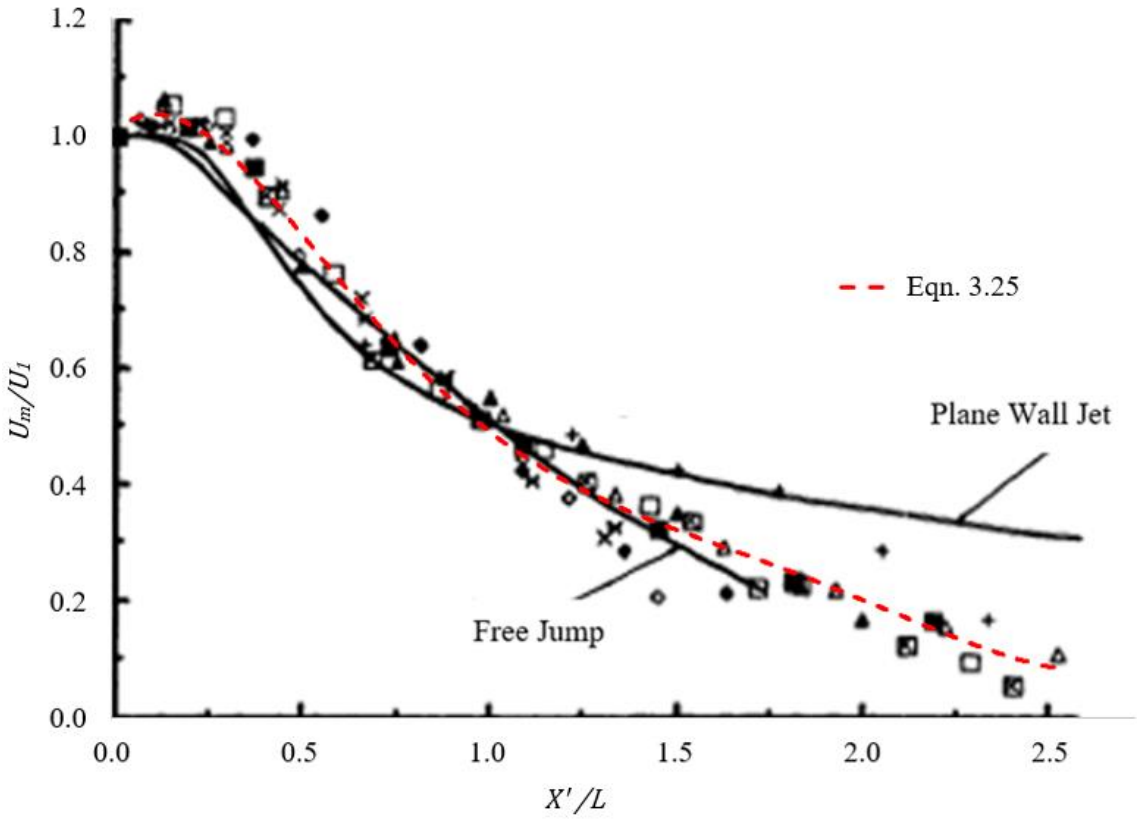

Figure 3.13. Long's *et al*. (1990) variation of the maximum velocity at a section with distance from the origin of the jump. The data points represent measurements of a submerged jump.

Equation 3.25 gives a correlation coefficient of r^2 of 0.977. For this work, 68 data points were used. It is noticeable in Figure 3.12 that the forward velocity profile ends when Y/b is about 1.77. This means that above Y/b of about 1.77 there is backward flow ($Y/b \approx 1.77$ is the start of the backward flow region).

For predicting the reverse velocity profile in the upper portion of the overall velocity profile, the velocity scale, U_s, and length scale, b_r are required. The scale U_s is the local reverse surface velocity (the velocity at the water surface at a particular X' location). The scale b_r is the distance from the water surface to the point where local reverse velocity is 75% of the local surface reverse velocity. Wu and Rajaratnam (1995) plotted b_r scaled with the tailwater depth y_t against the position along the jump, here X'/L_{sj}. Again, L_{sj} is the length of the submerged jump, which can be predicted by Eqn. 2.2. Wu and Rajaratnam (1995) suggested that b_r is approximately constant at $0.2y_t$ (see Figure 3.14), although there was a lot of variability in their data.

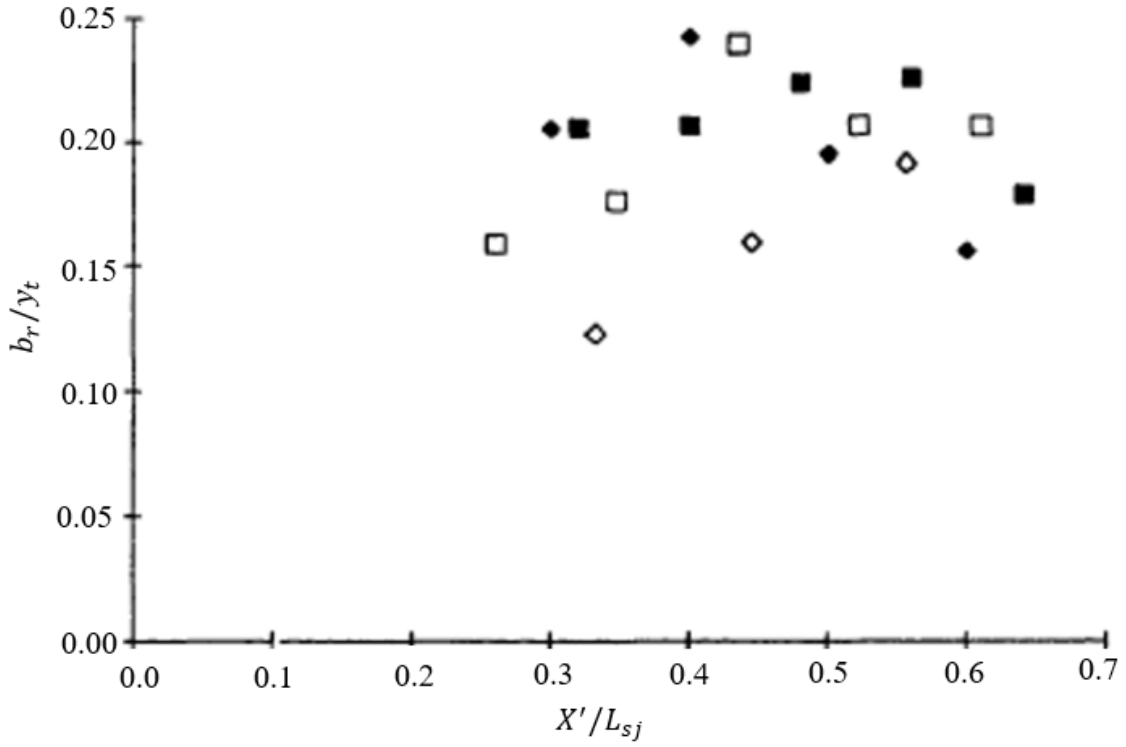

Figure 3.14. Variation of length scale, b_r (adapted from Wu (1994)).

To find the local reverse surface velocity, U_s, Wu and Rajaratnam (1995) gave a dimensionless relationship for a submerged hydraulic jump formed below a gate, which applies for X'/L_{sj} for 0.2 to 0.9,

$$\frac{U_s}{v^*} = 0.215 - 4.049\frac{X'}{L_{sj}} - 3.425\left(\frac{X'}{L_{sj}}\right)^2, \tag{3.26}$$

where v^* is the maximum reverse velocity through the jump. This maximum reverse velocity can again be found using the relationships developed Wu and Rajaratnam (1995),

$$\frac{v^*}{U_1} = -0.342F_1^{-0.263}\, e^{0.165\sin(S)}. \tag{3.27}$$

Wu (1994) suggested that the X' location where this maximum backward velocity occurs is at $0.6L_{sj}$. This was for a submerged hydraulic jump formed below a gate. However, from Fan's (1993) work for submerged hydraulic jumps formed below a weir, it is noticeable that the location of maximum backward velocity is sometimes close to the plunging nappe but sometimes near to the

middle of countercurrent region (the roller length of the jump). Fan (1993) made no comment on this behavior.

To find reverse velocity profile in the upper region of flow, using the scales b_r and U_s, an equation was again developed this time from the data of Wu (1994). The data points shown in his dimensionless profile were estimated using AutoCAD. For this work, all his presented data points were used (92 points). Then, a dimensionless profile was curve fitted with a polynomial using Excel,

$$\frac{U}{U_s} = -0.0353\left(\frac{Y_s}{b_r}\right)^2 - 0.2148\left(\frac{Y_s}{b_r}\right) + 1, \tag{3.28}$$

where again U is the velocity at a particular depth within the flow at some X' location and

$$Y_s = y - Y. \tag{3.29}$$

In Eqn. 3.29, y is the depth of flow at a particular X' location. Eqn. 3.28 had an r^2 value of 0.915. The developed curve is shown in Figure 3.15.

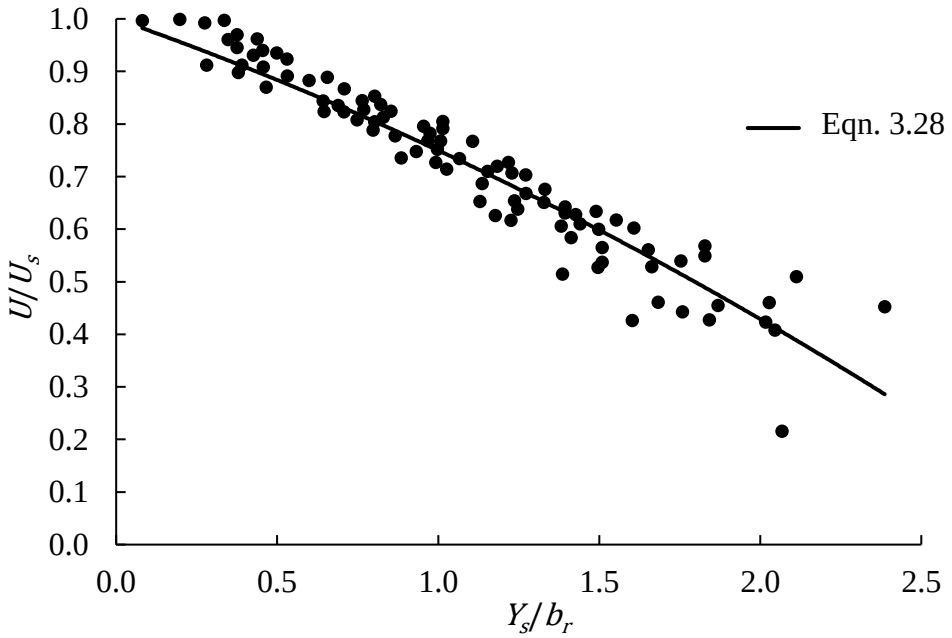

Figure 3.15. Dimensionless backward velocity profile for submerged jumps (adapted from Wu (1994)).

The above procedure will generate a complete velocity profile at different bed locations for a particular flow.

3.3.1.3.4 Using the Velocity Profiles to Calculate Drag

A complete velocity profile has two parts: the bottom is the forward flow, and the upper portion is the backward flow. To find the height above the bed where the velocity transitions from a forward flow to a backward flow (where there is zero velocity), interpolation was used between the highest point of the predicted forward velocity profile and the lowest point of the predicted backward velocity profile.

For both the forward and backward regions, the velocity profiles were divided up into intervals. For an interval, the velocity representing that interval was taken as the average of the velocities found at the top and bottom of that interval. The area normal to flow for a specific interval was determined from the variation of the projected area with height above the channel bed for the different bodies (Eqns. 3.9 and 3.10). The area was first determined for the height above the bed at the top of the interval and then determined for the height above the bed at the bottom of the interval. The difference in areas gave the projected area of the person's body over that interval. For each interval, the component of drag was then

$$F_{Di} = C_d A_{ni} \frac{\rho_w U_i^2}{2}, \tag{3.29}$$

where, F_{Di} represents the drag force on that particular segment of the velocity profile, and U_i and A_{ni} are the average velocity and projected area of the body for that interval. The drag coefficient C_d was taken as a constant with a value of 1.2. To find the drag force on the body for the forward flow, the components of drag acting over the height of the body from the channel bed to point of transition to a backward flow were summed. To find the drag force due to the backward flow on the body, the components of drag from the point of transition to a backward flow to the water surface were summed.

3.3.2 Determining the Moment Arms for the Forces acting on a Body

3.3.2.1 Moment Arm for Weight

Determining the moment arm for the weight of the body requires estimating the horizontal distance from the point of balance (heel or toe) to the center of mass of the person's body. Several studies have been done to examine the distance from heel to center of mass as a percentage of foot length (L_{foot}). Table 3.2 summarizes the findings. This study assumes that the horizontal distance to the center of mass from the heel (L_W) is 44.9 % of the foot length (L_{foot}). This means that the horizontal distance to the center of mass from the person's toe is ($L_{foot} - L_W$) or 55.1 % of L_{foot}.

Table 3.2. Horizontal distance to the center of mass from the heel from different studies.

Study	**Horizontal distance to center of mass from the heel**
Harless (1860)	43.6-46 % of L_{foot}
Braune and Fischer (1985)	40.4-45.3 % of L_{foot}
Duggar (1962)	43.8 % of L_{foot}
Dempster (1955)	42.9 % of L_{foot}
Clauser *et al*. (1969)	44.9 % of L_{foot}

For determining the typical length of the foot (L_{foot}), Contini (1972)'s suggested the male foot length is $0.152H$ while the female foot is $0.151H$, where again H represents the person's height.

3.3.2.2 Moment Arm for Buoyancy Force

The moment arm for the buoyancy force changes with the submergence level of the body. In general, it is considered that the buoyancy force and human weight act along the same line (Abt *et al.* 1989; Xia *et al.* 2014). However, this assumption is not valid, as the human body does not have a constant density (Drillis *et al.* 1964, Clauser *et al.*1969). This means that the center of its volume is not the same as the center of its mass.

Therefore, to find the center of buoyancy for the work herein, the 3D human model made in SketchUp Pro was cropped at the flow depth above the feet. Then, the location of center of buoyancy for that portion of the volume of the body was found using SketchUp Pro's CofG tool (version 3.1 was used). In the model, it was assumed that the body has a constant density so that the center of gravity would be the same as the center of volume. From this work, the variation of

the center of buoyancy with depth of flow for each male and female body were determined. The data were plotted in dimensionless form, using H as a length scale as in Figure 3.16. The curves shown in Figure 3.16 give the horizontal distance from the heel to the line of action of the buoyancy force (L_B) for different dimensionless flow depth (y/H). The horizontal distance from the toe to the line of action of the buoyancy force is calculated just by simply deducting L_B from L_{foot}. In Figure 3.16, the moment arm for the weight as compared to the heel, L_W, is also given for comparison to L_B.

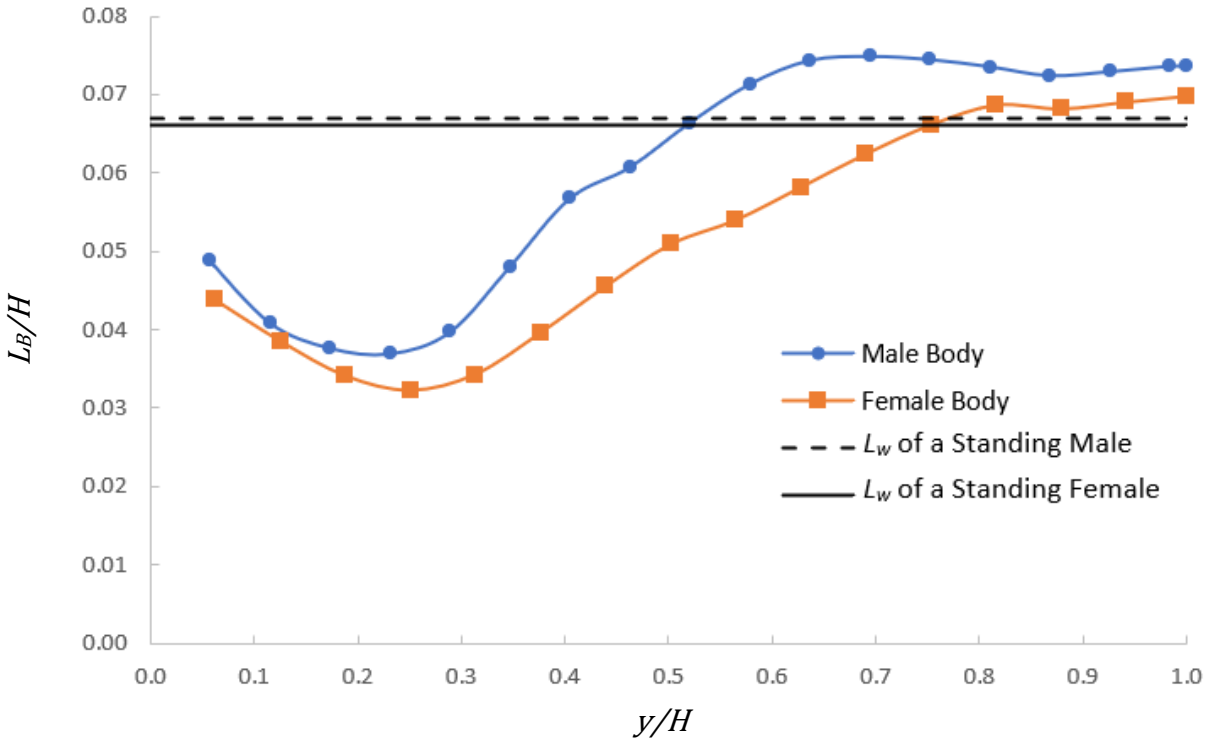

Figure 3.16. Horizontal distance from the heel to the line of action of the buoyancy force (L_B) with depth of flow.

3.3.2.3 Moment Arm for the Drag Force

For determining the moment arm for the forward drag force, moments with respect to the balance point are calculated for each interval used above to calculate the component of drag for that interval. The moment arm is taken to occur at the mid-point of the interval. All the moments due to the forward flow are summed. All the moments due to the reverse flow are summed separately from the forward flow. To find the equivalent moment arm for the total moment for the

forward flow, the total moment was divided by the total forward drag force. A similar method was applied for calculating the equivalent moment arm for the moment due to the backward flow velocities. Such a calculation can be expressed as

$$\bar{Y}\sum_{i=1}^{N} F_{Di} = \sum_{i=1}^{N} \bar{y}_i F_{Di}. \tag{3.30}$$

In Eqn. 3.30, $\bar{Y}$ will be either H_{DF} and H_{DB} as defined in Figure 3.2 (depending on whether one is considering a forward or backward flow), $\bar{y}_i$ represents the vertical axis coordinate of the center of the particular interval considered in the velocity profile, and F_{Di} represents the drag force on an interval.

3.3.3 Moments about the Point of Balance

Table 3.3 summarizes the moments acting on the body. A flow is classified as hazardous if Equations 3.4 and 3.5 are not satisfied.

Table 3.3. Moment arms and moments for forces with respect to different points of balance.

Force	**Moment Arm**		**Moment (clockwise +ve)**	
	Point of balance		Point of balance	
	Heel	Toe	Heel	Toe
Weight (W)	L_W	$L_{foot} - L_W$	$-W L_W$	$+W (L_{foot} - L_W)$
Buoyancy (B)	L_B	$L_{foot} - L_B$	$+F_B L_B$	$-F_B (L_{foot} - L_B)$
Forward Drag Force (F_{DF})	H_{DF}	H_{DF}	$+ F_{DF} H_{DF}$	$+ F_{DF} H_{DF}$
Backward Drag Force (F_{DB})	H_{DB}	H_{DB}	$- F_{DB} H_{DB}$	$- F_{DB} H_{DB}$

3.4 Application of the Framework to the Wolf River Sea Lamprey Barrier

3.4.1 Site Characteristics

The Wolf River Barrier is located on the Wolf River in Northern Ontario and was constructed in 1987 (Mazurek *et al.* 2008). The barrier is located at approximately 48°49’20” N and 88°32’65” W, east of Highway 17 and 79 km northeast of Thunder Bay. A satellite photo of the site is given in Figure 3.17, and a drawing of the barrier is given in Figure 3.18. The barrier is built into the rock bed of the channel. The upstream side of the barrier has a high bed level, resulting in the flow over the barrier acting as a fast, shallow (supercritical) flow instead of a slow, deep (subcritical) flow typical of other barriers and weirs. The weir is 13.72 m wide, and the crest

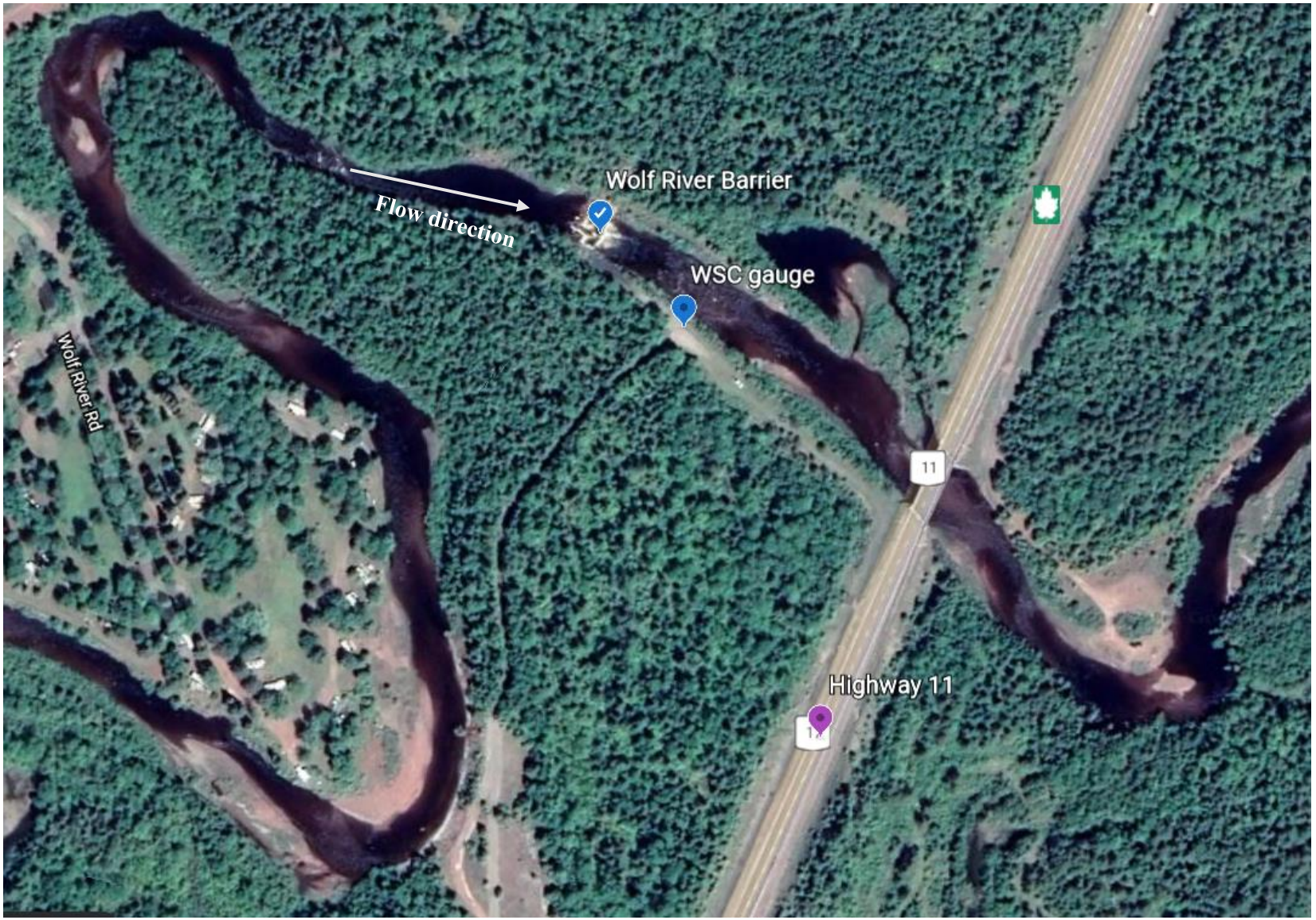

Figure 3.17. Satellite photo of the Wolf River barrier (from Google Earth May 2021).

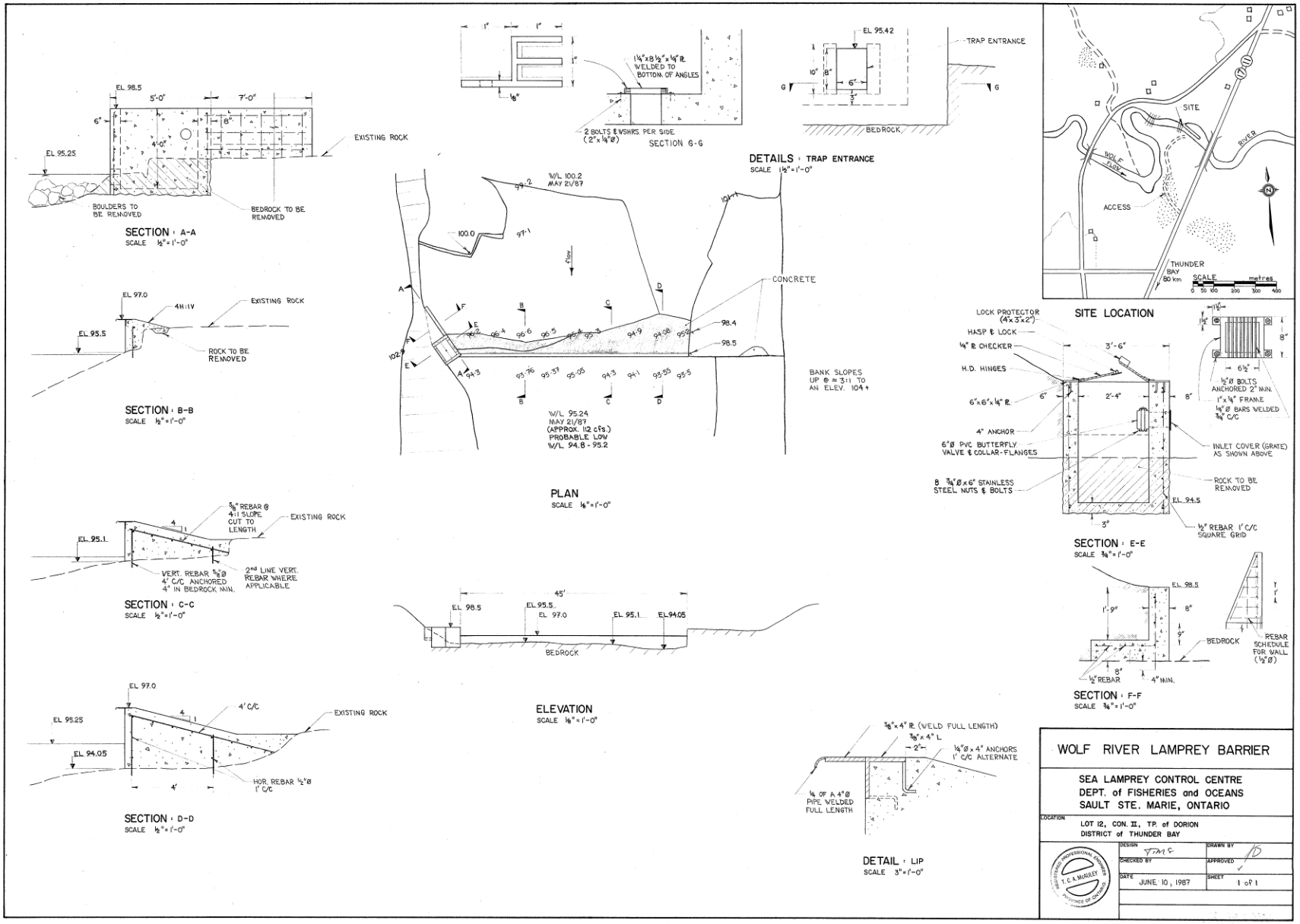

Figure 3.18. Wolf River barrier site plans (figure provided by Fisheries and Oceans Canada (DFO)).

of the barrier has a constant elevation (no notches). The maximum height of the barrier above the channel bed is 0.9 m. The barrier has a curved lip with 4-in (101 mm) length and ¼ of 4-in (101 mm) diameter arc attached to its downstream face.

The Wolf River Barrier is a weir or low head dam used as a sea lamprey barrier. The barrier creates a difference in height between the weir crest and downstream water surface to block the migration of sea lamprey from the Great Lakes into the stream in the spring, where they like to spawn (Mazurek *et al.* 2008). The Wolf River barrier is of interest to study because of past concerns by the dam owner, Fisheries and Oceans Canada, about drownings at its barrier sites.

The hydrologic information available for the site includes data from the Water Survey of Canada Station 02AC001 (called "Wolf River at Highway 17"). The station is located at 48°49'18" N and 88°32'4" W, which is approximately 90 m downstream of the barrier (Figure 3.17). The station provides daily average and peak instantaneous annual maximum and minimum flows for 1971-2020 (minimum flow 0.14 m^3/s and maximum flow 184 m^3/s). Also available were water surface elevations measurements taken by Fisheries and Oceans Canada for the periods September 14, 2004, to August 17, 2005. The measurements were taken just upstream of the weir and immediately below the weir as shown in Figure 3.8.

3.4.2 Model Testing

Experimental data of velocity profiles formed below the barrier were also available to validate the proposed framework based on model studies performed by Mazurek *et al.* (2008). Mazurek *et al.* (2008) created two experimental models for the Wolf River Barrier based on Froude number similarity; one had a length scale (ratio of the prototype to model lengths) of 3, and the flows in the laboratory flume used were equivalent to flow rates at the site of about 0.89 to 7.2 m^3/s. The other model had a length scale of 6, which could test up to a flow rate of about 20.2 m^3/s. Figure 3.19 gives the dimensions of each model of the Wolf River barrier created by Mazurek *et al.* (2008).

Mazurek *et al.* (2008) used a 50 MHz Sontek Micro-Acoustic Doppler Velocimeter (ADV) with three-dimensional down-looking or two-dimensional side-looking probes to take the detailed velocity measurements below the model weirs, that were set in a laboratory flume of 80 cm width.

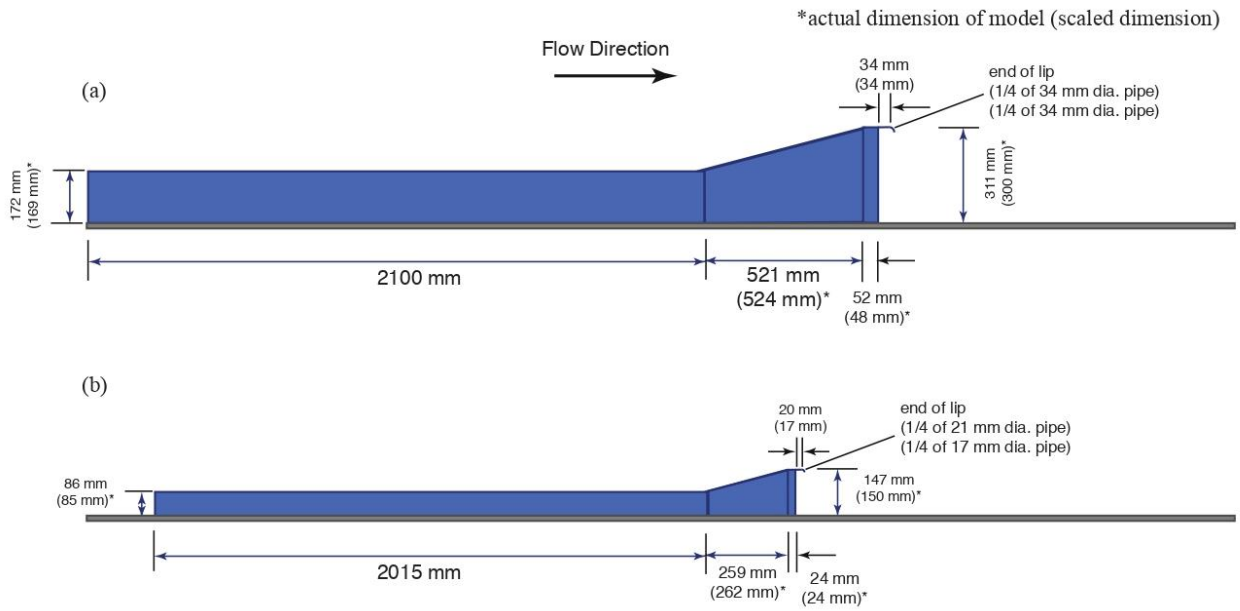

Figure 3.19. Model dimensions used for the Wolf River Barrier by Mazurek *et al*. (2008) (a) side-view of model with length scale of 3 (b) side-view of model with a length scale of 6.

The velocity measurements in the model tests covered the equivalent three flow rates at the site of 2.41, 7.0, and 20.20 m^3/s. Mazurek *et al.* (2008) estimated that these corresponded to probability of exceedances at the site of 73.76% to 11.34%. A submerged hydraulic jump was observed at all flow rates tested. Measurements were taken of the velocity profiles along the direction of flow along the center-plane of the flume.

3.4.3 Application of Framework

To apply the develop framework to the Wolf River barrier site, the predicted velocity profiles will first be compared to measurements in the model at three sections for three of the flows tested by Mazurek *et al.* (2008). The moments were then calculated for all the produced velocity profiles to decide whether those particular flows were hazardous or not. The developed framework is applied to the Wolf River Sea Lamprey Barrier in the next chapter, and the results are discussed.

CHAPTER 4. RESULTS AND DISCUSSION

4.1 Introduction

In this chapter, the developed methodology is applied to predict the stability of a person in standing in the flow below the Wolf River Sea Lamprey Barrier on the Wolf River in Ontario, Canada. First, measurements of the velocity profiles seen along the flow centreline in a model study of the barrier by Mazurek *et al.* (2008) for three flow rates are compared to the velocities predicted by the method developed in Chapter 3. Then, the full methodology is applied to predict the range of flows at the site for which standing in the flow below the barrier would not be possible. Moments generated both about a point of balance about the heel and the toe are considered.

4.2 Velocity Profile Prediction

To test the ability of the methodology proposed in Chapter 3 to predict the velocity profile in the flow below the Wolf River Barrier, predicted velocity profiles were compared to those measured in the flow below a scale model of the Wolf River Barrier for flow rates equivalent to flows at the site of 2.41, 7.0, and 20.2 m^3/s. Three velocity profiles were predicted for each flow rate at locations close to the middle of the countercurrent region where experimental velocity profile data was available from Mazurek *et al.* (2008). "Middle" here is where the horizontal distance from the weir's upstream face is about $X_w + 0.5L_{cr}$, where X_w is the horizontal distance from the weir crest to the location where the upper nappe touches the water surface below the weir (see Figure 3.10) and L_{cr} is the length of the countercurrent region at the water surface. For all the velocity profiles predicted in this study, it is assumed that the weir height and width are constant at 0.9 m and 13.72 m, respectively.

First, the head on the weir h for each flow rate was calculated from Eqn. 3.11. Results are given in Table 4.1. The tailwater depths for the studied flow rates could be predicted by the stage-discharge curve given in Eqn. 3.12. However, Eqn. 3.12 predicts the depth immediately downstream of the weir y_d (as measured by the Department of Fisheries and Oceans), but this is somewhat different than the depth at the downstream end of a submerged hydraulic jump or the

tailwater depth, y_t. The tailwater depth used in the calculations instead was the scaled-to-prototype value from the experimental data of Mazurek *et al*. (2008) so that the predicted velocity profile could be compared to the specific flow conditions in the scale model. Table 4.1 provides a comparison between the predicted y_d for the test flow rates and the tailwater y_t (prototype scale) used for the calculations. It should be noted that there appears to be no means available to predict the depth profile through a submerged hydraulic jump in the flow below a weir. Therefore, for predicting the backward velocity profiles, rather than considering the flow depth to be the same as y_d or y_t, the water surface profile data from Mazurek *et al*. (2008) were used and scaled to prototype values. This meant there was a better estimate of the vertical distance from the water surface, Y_s, for the backwards velocity profile calculations. Table 4.1 also provides the predicted Y_1, Y_2, F_1, L_{cr}, L_{sj}, X_j, although these data are not available for Mazurek *et al.* (2008) for comparison.

Table 4.1. Details of predicted characteristics of flows (all values at prototype scale).

Q (m^3/sec)	U_o (m/s)	h (m)	y_d (m)	y_t (m)	Y_1 (m)	Y_2 (m)	F_1	S	L_{cr} (m)	L_{sj} (m)	X_j (m)
2.41	0.15	0.24	0.40	**0.51	0.045	0.35	5.96	0.44	2.97	2.92	0.86
7.0	0.40	0.33	0.61	**0.78	0.12	0.61	3.93	0.28	4.47	4.56	1.01
*15.0	0.82	0.44	0.82	1.06	0.26	0.86	2.70	0.24	5.52	5.84	1.06
*17.0	0.91	0.47	0.86	1.12	0.29	0.91	2.55	0.23	5.77	6.13	1.10
*18.0	0.95	0.48	0.88	1.14	0.30	0.93	2.49	0.22	5.89	6.27	1.11
20.2	1.05	0.51	0.91	**1.19	0.34	0.98	2.73	0.21	6.71	6.98	1.14

*Scaled-to-prototype value from the experimental data of Mazurek *et al*. (2008) are not available for that discharge.

**y_t is found from Mazurek *et al*. (2008) experimental data.

In the scale model testing, flow rates of 2.41 and 7.0 m^3/s were conducted at a scaling ratio of 3. This scaling ratio is $L_p/L_m = 3$, where L_p is a length in the prototype and L_m is a length in the model. A scaling ratio of 6 was used for the flow rate of 20.2 m^3/s. To convert a velocity in the model to a velocity at the full-scale barrier, the velocity in the model should be multiplied by the root of the length scale (Ettema *et al*. 2000) for Froude number similarity. So, for flow rates of 2.41 and 7.0 m^3/s the ratio of the velocities in the prototype to the model is 1.73 and for 20.2 m^3/s it is 2.45.

Figures 4.1 to 4.3 show the predicted velocity profiles in comparison to the measurements of Mazurek *et al.* (2008) for flows of 2.41, 7.0, and 20.2 m^3/s, respectively, near the middle of the countercurrent region. For the 2.41 m^3/s flow, the middle of the countercurrent region was about

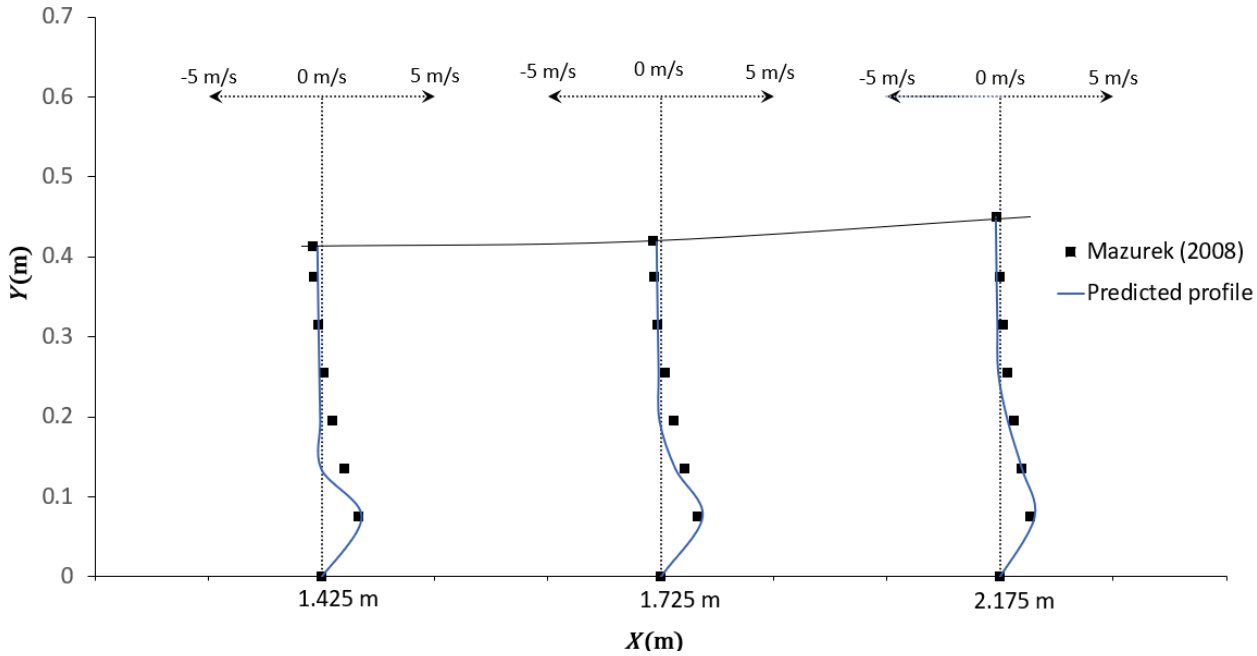

Figure 4.1. Predicted velocity profiles in comparison to the measurements of Mazurek *et al.* (2008) in a scale model for the Wolf River Barrier at a flow rate of 2.41 m^3/s.

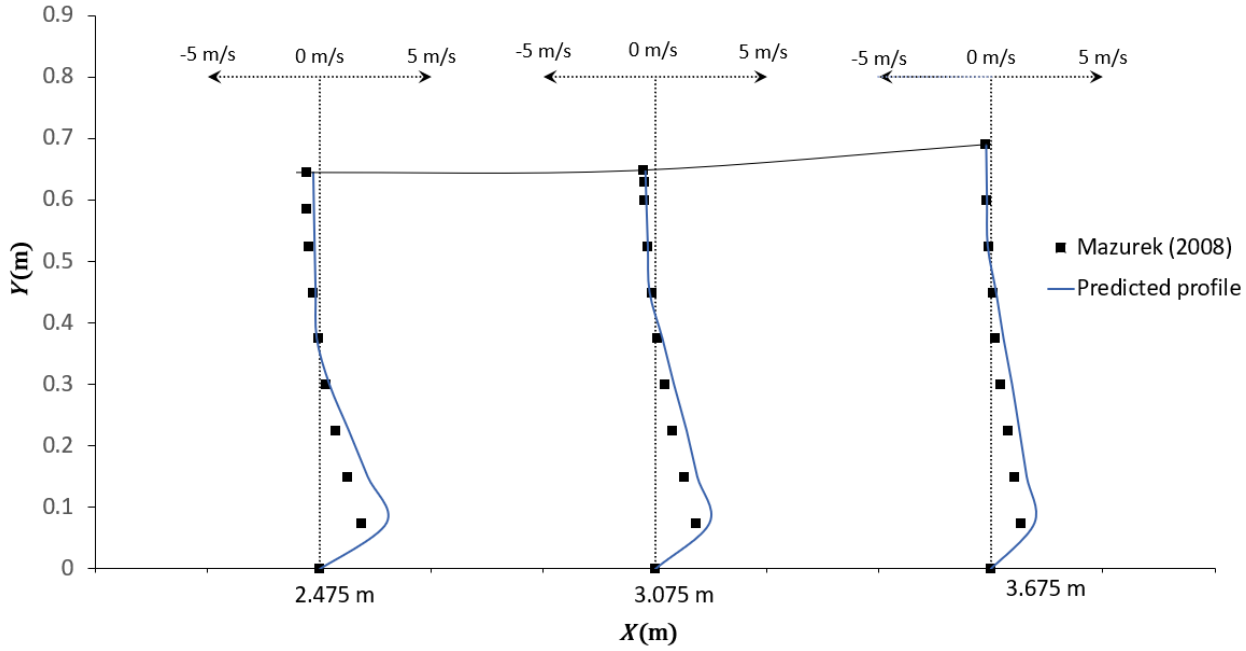

Figure 4.2. Predicted velocity profiles in comparison to the measurements of Mazurek *et al.* (2008) in a scale model for the Wolf River Barrier at a flow rate of 7.0 m^3/s.

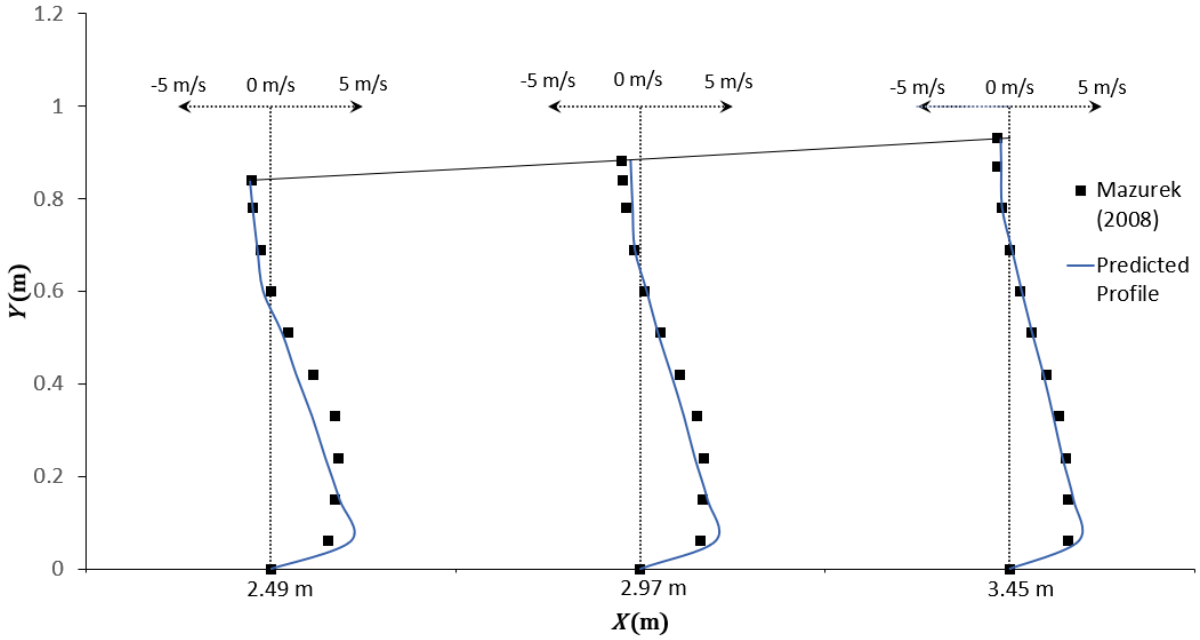

Figure 4.3. Predicted velocity profiles in comparison to the measurements of Mazurek *et al.* (2008) in a scale model for the Wolf River Barrier at a flow rate of 20.2 m^3/s.

2 m from the upstream face of the weir. Three velocity profiles at X = 1.425, 1.725 and 2.175 m were predicted where Mazurek *et al*. (2008) also measured the centreline velocity profiles in the scale model (Figure 4.1). The center of the countercurrent area for the flow rate of 7.0 m^3/s was about 2.5 m away from the upstream surface of the weir, and for a flow of 20.2 m^3/s, it was 3.5 m. Three velocity profiles were predicted at X= 2.475, 3.075 and 3.675 m (Figure 4.2) for the flow of 7.0 m^3/s; for the flow of 20.2 m^3/s, velocity profiles were predicted at X = 2.49, 2.97 and 3.45 m (Figure 4.3).

In Figure 4.1, it is noticeable that forward velocity profiles close to the nappe (X = 1.425 m) are not as well-predicted as those away from the nappe (X= 1.725 and 2.175 m). However, the prediction of maximum forward velocity was close to the experimental value (Mazurek *et al*. 2008) for all three locations. Predictions for the flows of 7.0 m^3/s (Figure 4.2) and 20.2 m^3/s (Figure 4.3) show similar characteristics to the predictions for the 2.41 m^3/s flow: velocity profiles close to nappe are less well-predicted than the velocity profile further into the submerged jump. This is most likely because the velocity profiles used were for a submerged hydraulic jump created by an underflow structure (*i.e.*, flow under a gate), whereas the measured flows are for an overflow structure where a nappe flow over the structure is created. The depths of the forward flow for the higher discharges (7.0 and 20.2 m^3/s) were better predicted as compared to the low discharge (2.41

m^3/s). Although for the 7.0 and 20.2 m^3/s flows the forward maximum velocity is overestimated, the overall velocity profiles show good agreement with the measured velocity profiles. All predictions for the velocities in the given profiles are shown in Appendix B.

Because of the relatively good agreement with the velocity profiles predicted by the technique outlined in Chapter 3 and the measurements in a scale model of the structure, there is some confidence in the velocity profile estimates.

4.3 Prediction of Velocity Profiles for Flows not Measured in the Model

To evaluate when the flow might cause instability if one were standing in that flow, velocity profiles for additional flows of 15, 17, and 18 m^3/s were developed. Details of predictions for the characteristics of these flows are given in Table 4.1. For these predictions, the depth of flow at a particular location along the length of the jump was unknown, since there were no scale model values to assess this depth and it appears that there are no predictive relationships for the water surface profile for a submerged hydraulic jump formed below a weir. Therefore, Eqn. 3.12 was used to predict the depth just downstream of the weir (y_d). In the scale model tests of Mazurek *et al.* (2008), the tailwater depth at the end of the jump y_t was 27.5 to 30.8 % higher than y_d (see Table 4.1). Depths at the middle of the submerged hydraulic jump (where the velocity profiles were predicted) was calculated by linear interpolation, considering the depth at the start of the jump as y_d and the tailwater depth $yt = 1.3y_d$.

Figures 4.4 to 4.6 shows the predicted velocity profiles for flows of 15, 17, and 18 m^3/s. The depth of the zone of forward velocity was determined by interpolating between the highest point of the predicted forward velocity profile and the lowest point of the predicted backward velocity profile.

4.4 Moments About the Point of Balance

To check whether a flow is safe or hazardous, moments about the point of balance (heel or toe) are required. For those calculations, the values of g, ρ_w, and C_d were taken as 9.81 m/s^2, 1000 kg/m^3 and 1.2, respectively. The height and BMI for males and females, respectively, were assumed to be 1.758 m and 26.4 and 1.618 m and 25.4. These assumptions mean that the male

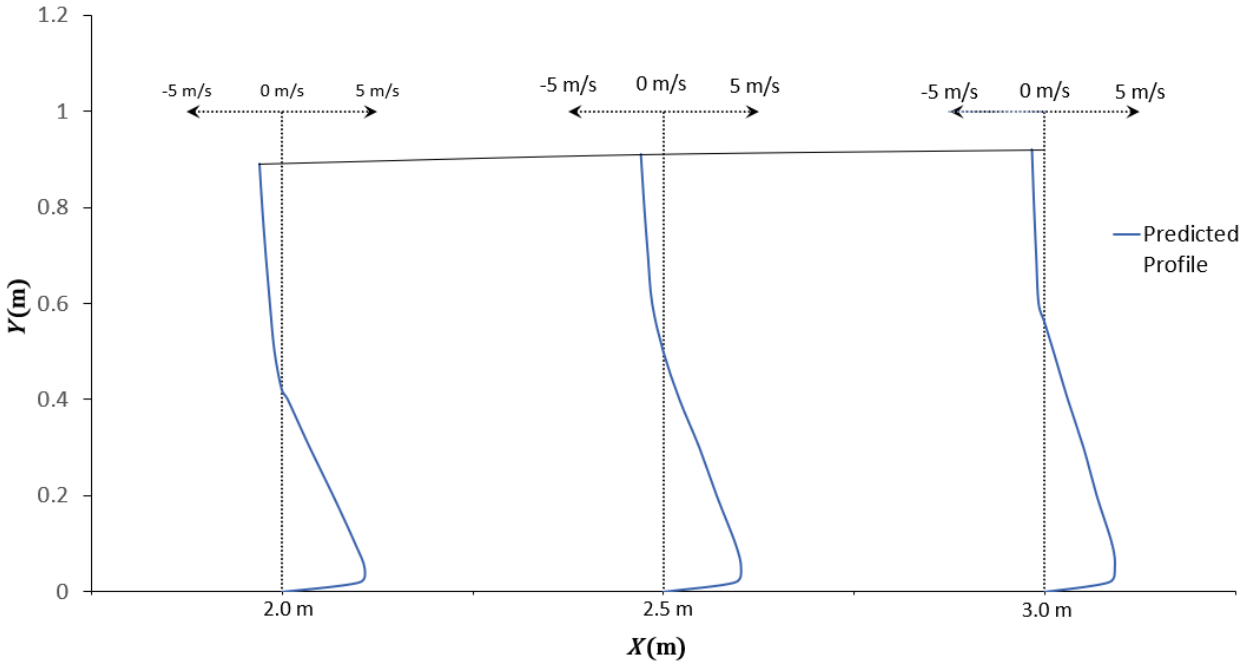

Figure 4.4. Predicted velocity profiles for the flow below the Wolf River Barrier at a flow rate of 15.0 m^3/s.

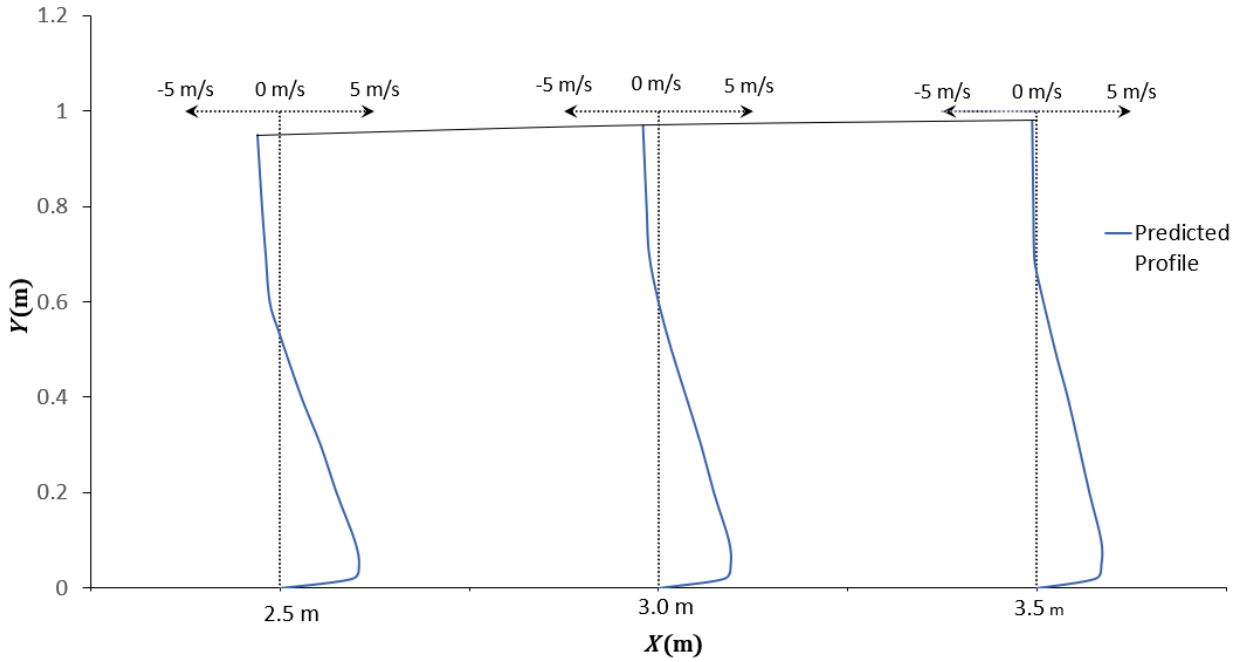

Figure 4.5. Predicted velocity profiles for the flow below the Wolf River Barrier at a flow rate of 17.0 m^3/s.

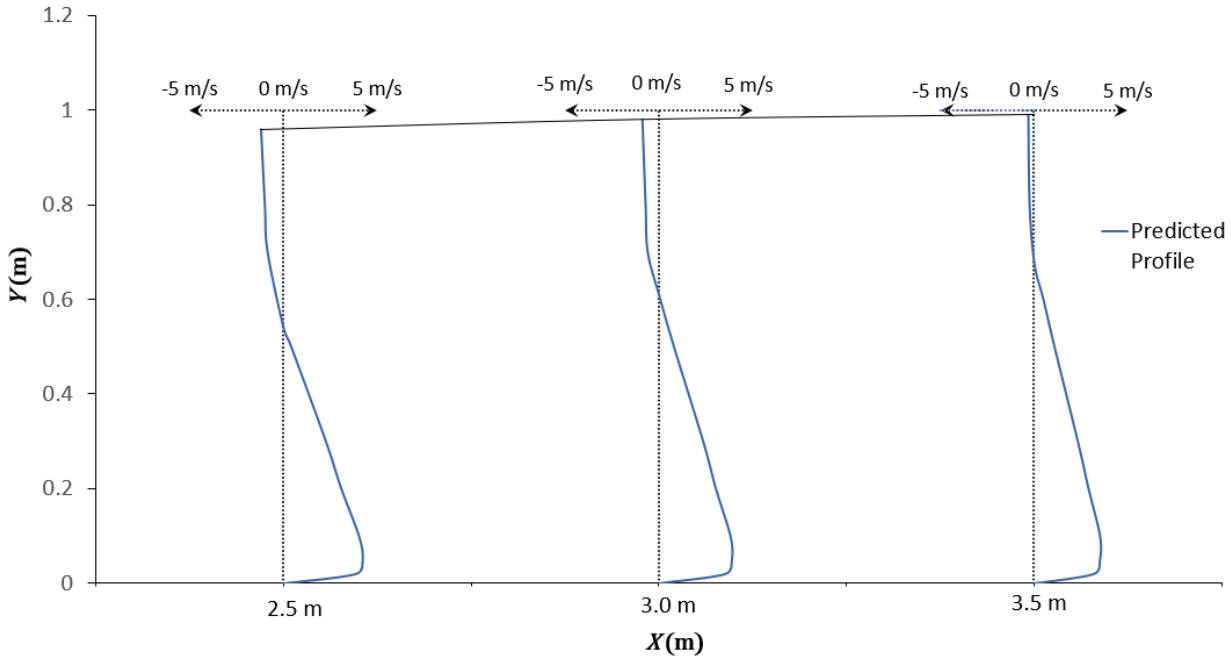

Figure 4.6. Predicted velocity profiles for the flow below the Wolf River Barrier at a flow rate of 18.0 m^3/s

body considered in this study has a higher weight than the female body, as the male body is taller with a higher BMI. Similarly, the length of the foot L_{foot} and the horizontal distance from the center of mass and the heel L_W are also higher for the male body. The values used for weight, the length of the foot, and the distance to the heel from the centre of mass are given in Table 4.2. This study considers only persons standing perpendicular to the flow facing upstream towards the weir. Sample calculations showing all steps to find the moments about the point of balance for a male body are shown in Appendix C.

Table 4.2. Weight, foot length, and distance to the center of mass from the heel used for the male and female models.

Model	**Weight, W**	**Foot length, L_{foot}**	**Distance to Heel from Centre of Mass, L_W**
	(N)	**(m)**	**(m)**
Male	800.40	0.267	0.115
Female	652.16	0.244	0.105

Table 4.3 shows the forces calculated using both the predicted velocity profiles and the measured velocity profiles by Mazurek *et al.* (2008) in the scale model of the Wolf River Sea lamprey barrier. The calculations were done for the modelled prototype flow rates of 2.41, 7.0, and 20.2 m^3/s. As a reminder, F_B is the buoyant force acting on the body and L_B is the horizontal

Table 4.3. Forces and moment arms for Q = 2.41, 7.0, and 20.2 m^3/s, with a comparison of the results produced using the predicted velocity profile and the velocity profile measured by Mazurek *et al.* (2008).

					Calculated from Measured Velocity Profile				**Calculated from Predicted Velocity Profile**				**Percent Difference in Forces and Moment Arms between Measured and Predicted Velocity Profiles**			
Type of Body	**Flow Q**	**Location X**	F_B	L_B	F_{DF}	H_{DF}	F_{DB}	H_{DB}	F_{DF}	H_{DF}	F_{DB}	H_{DB}	F_{DF}	H_{DF}	F_{DB}	H_{DB}
	(m^3/s)	(m)	(N)	(m)	(N)	(m)	(N)	(m)	(N)	(m)	(N)	(m)	(%)	(%)	(%)	(%)
Male	2.41	1.425	57.38	0.066	15.90	0.10	1.19	0.37	8.15	0.07	0.45	0.33	48.74	30.00	62.18	10.81
		1.725	58.23	0.066	16.94	0.11	0.38	0.37	13.25	0.09	0.15	0.34	21.78	18.18	60.53	8.11
		2.175	62.66	0.067	14.11	0.12	0.06	0.43	14.00	0.10	0.27	0.58	0.78	16.67	-350.00	-34.88
	7.00	2.475	105.70	0.090	28.96	0.13	8.41	0.56	83.62	0.13	2.09	0.55	-188.74	0.00	75.15	1.79
		3.075	106.63	0.091	30.31	0.14	4.97	0.58	71.27	0.15	4.02	0.57	-135.14	-7.14	19.11	1.72
		3.675	120.78	0.097	21.06	0.15	1.28	0.62	57.87	0.18	0.86	0.62	-174.79	-20.00	32.81	0.00
	20.20	2.490	189.41	0.111	418.51	0.25	27.54	0.77	349.51	0.20	38.38	0.75	16.49	20.00	-39.36	2.60
		2.970	213.95	0.114	447.97	0.25	40.00	0.80	361.24	0.22	9.15	0.80	19.36	12.00	77.13	0.00
		3.450	244.76	0.118	349.48	0.25	15.07	0.86	351.94	0.24	9.22	0.85	-0.70	4.00	38.82	1.16
Female	2.41	1.425	43.07	0.053	13.66	0.10	0.42	0.37	7.86	0.07	0.13	0.34	42.46	30.00	69.05	8.11
		1.725	43.65	0.053	14.44	0.10	0.36	0.38	12.05	0.08	0.13	0.35	16.55	20.00	63.89	7.89
		2.175	46.84	0.053	11.81	0.12	0.03	0.43	12.08	0.10	0.15	0.53	-2.29	16.67	-400.00	-23.26
	7.00	2.475	88.33	0.068	24.10	0.12	9.37	0.56	68.95	0.13	2.30	0.55	-186.10	-8.33	75.45	1.79
		3.075	89.34	0.068	24.99	0.13	5.58	0.58	58.03	0.15	4.49	0.57	-132.21	-15.38	19.53	1.72
		3.675	104.85	0.073	17.15	0.15	1.44	0.62	47.25	0.18	0.97	0.62	-175.51	-20.00	32.64	0.00
	20.20	2.490	181.63	0.084	352.25	0.26	29.24	0.77	290.24	0.20	41.08	0.75	17.60	23.08	-40.49	2.60
		2.970	208.75	0.086	377.79	0.26	41.77	0.80	304.05	0.22	9.54	0.80	19.52	15.38	77.16	0.00
		3.450	242.21	0.089	299.09	0.26	15.09	0.86	300.83	0.25	9.29	0.85	-0.58	3.85	38.44	1.16

distance from where the buoyant force acts to the heel of the body; F_{DF} and H_{DF} are the drag force due to the forward flow and its point of application above the bottom of the foot; and F_{DB} and H_{DB} are the drag force due to the backward flow and its point of application above the bottom of the foot. It is seen that the predicted profile gives closer results to what is given by the measured profile further downstream from the point of nappe impingement on the bed. Very large differences between the forces developed using the predicted and measured velocity profiles tend to occur for very small values of backward drag forces. Therefore, predictions are better for the forward flow drag forces as compared to the drag force due to the backwards velocity. The values of the point of application of the forces are more similar to that produced from the measured velocity profile than for the forces. It is also seen that the forces developed on the male body are always greater than the female body. This is because the males have a larger frontal area and submerged volume.

Tables 4.4 and 4.5 give the moments about the heel and toe, respectively. Again, this is for a person that is facing upstream towards the weir and whose body is perpendicular to the flow. In these tables, M_p is the net moment about the point of balance (the heel or toe respectively). For the moments about the heel as seen in Table 4.4, for the lower discharges, the moment created by the body's weight is dominating the overall moment balance *i.e.*, the moment due to the weight dominates over the moments created by the velocities and buoyancy. The net moment therefore is almost the same for the measured and predicted velocity profiles. For the higher discharges, the percent difference in the net moment between the measured and predicted velocity profiles is greater near the nappe than further downstream of the weir because the velocity profile was not as well-predicted there.

For Table 4.4, which gives the moment taken about the heel, a negative net moment, M_P, implies the person is "safer". The male body has a more negative net moment for all flow situations, which therefore implies that he is safer than the female. In addition, any person gets "less safe" as he or she moves downstream from the barrier. The net moment tends to the positive as the person moves downstream. This is because the depth increases as the person moves downstream and because the zone of backwards velocity takes up a smaller portion of the flow depth there. When taking a moment about the heel, the backward flow aids stability.

Table 4.4. Moments about the heel for Q = 2.41, 7.0, 20.2 m^3/s, with a comparison of the results produced using the predicted velocity profile and the velocity profile measured by Mazurek *et al.* (2008), $M_P < 0$ indicates stable.

					Calculated Moment about heel from Measured Velocity Profile			**Calculated Moment about heel from Predicted Velocity Profile**			**Percent Difference in Moments about heel between Measured and Predicted Velocity Profiles**		
Type of Body	**Flow Q**	**Location X**	$W L_W$	$F_B L_B$	$F_{DF} H_{DF}$	$F_{BF} H_{BF}$	M_P	$F_{DF} H_{DF}$	$F_{BF} H_{BF}$	M_P	$F_{DF} H_{DF}$	$F_{BF} H_{BF}$	M_P
	(m^3/s)	(m)	(N·m)	(N·m)	(N·m)	(N·m)	(N·m)	(N·m)	(N·m)	(N·m)	(%)	(%)	(%)
Male	2.41	1.425	-91.76	3.78	1.67	-0.44	-86.75	0.58	-0.15	-87.54	65.27	65.91	-0.91
		1.725		3.84	1.85	-0.38	-86.45	1.12	-0.15	-86.94	39.46	60.53	-0.57
		2.175		4.30	1.73	-0.03	-85.76	1.45	-0.16	-86.17	16.18	-433.33	-0.48
	7.00	2.475		9.48	3.73	-4.72	-83.26	11.10	-1.14	-72.32	-197.59	75.85	13.14
		3.075		9.75	4.13	-2.88	-80.75	11.04	-2.28	-73.25	-167.31	20.83	9.29
		3.675		11.68	3.26	-0.79	-77.62	10.28	-0.59	-70.33	-215.34	25.32	9.39
	20.20	2.490		20.98	103.80	-21.25	11.75	68.00	-28.97	-31.75	34.49	-36.33	370.21
		2.970		24.45	112.90	-32.00	14.11	79.47	-7.32	3.13	29.61	77.13	77.82
		3.450		28.83	88.73	-12.95	12.85	83.19	-7.83	12.43	6.24	39.54	3.27
Female	2.41	1.425	-68.35	2.30	1.35	-0.42	-65.12	0.52	-0.13	-65.66	61.48	69.05	-0.83
		1.725		2.33	1.48	-0.36	-64.89	0.95	-0.13	-65.20	35.81	63.89	-0.48
		2.175		2.50	1.36	-0.03	-64.51	1.17	-0.15	-64.82	13.97	-400.00	-0.48
	7.00	2.475		6.00	2.96	-5.27	-64.65	8.74	-1.27	-54.87	-195.27	75.90	15.13
		3.075		6.07	3.25	-3.23	-62.25	8.69	-2.55	-56.14	-167.38	21.05	9.82
		3.675		7.63	2.57	-0.89	-59.04	8.29	-0.60	-53.02	-222.57	32.58	10.20
	20.20	2.490		15.28	90.10	-22.54	14.50	56.82	-30.94	-27.18	36.94	-37.27	287.45
		2.970		17.90	98.48	-33.26	14.77	67.11	-7.62	9.05	31.85	77.09	38.73
		3.450		21.55	79.09	-12.95	19.35	74.06	-7.88	19.39	6.36	39.15	-0.21

Table 4.5. Moments about the toe for Q = 2.41, 7.0, 20.2 m^3/s, with a comparison of the results produced using the predicted velocity profile and the velocity profile measured by Mazurek *et al.* (2008), $M_P > 0$ indicates stable.

					Calculated Moment about Toe from Measured Velocity Profile			**Calculated Moment about Toe from Predicted Velocity Profile**			**Percent Difference in Moments about Toe between Measured and Predicted Velocity Profiles**		
Type of Body	**Flow Q**	**Location X**	$W\ (L_{foot}\text{-}L_W)$	$F_B\ (L_{foot}\text{-}L_B)$	$F_{DF}H_{DF}$	$F_{BF}H_{BF}$	M_P	$F_{DF}H_{DF}$	$F_{BF}H_{BF}$	M_P	$F_{DF}H_{DF}$	$F_{BF}H_{BF}$	M_P
	(m^3/s)	(m)	(N·m)	(N·m)	(N·m)	(N·m)	(N·m)	(N·m)	(N·m)	(N·m)	(%)	(%)	(%)
Male	2.41	1.425	122.13	-11.55	1.67	-0.44	110.80	0.58	-0.15	111.01	65.27	65.91	-0.19
		1.725		-11.72	1.85	-0.38	111.87	1.12	-0.15	111.38	39.46	60.53	0.44
		2.175		-12.45	1.73	-0.03	111.38	1.45	-0.16	110.97	16.18	-433.33	0.37
	7.00	2.475		-18.77	3.73	-4.72	102.37	11.10	-1.14	113.31	-197.59	75.85	-10.69
		3.075		-18.75	4.13	-2.88	104.63	11.04	-2.28	112.13	-167.31	20.83	-7.17
		3.675		-20.60	3.26	-0.79	103.99	10.28	-0.59	111.28	-215.34	25.32	-7.01
	20.20	2.490		-29.64	103.80	-21.25	175.02	68.00	-28.97	131.51	34.49	-36.33	24.86
		2.970		-32.72	112.90	-32.00	170.82	79.47	-7.32	159.85	29.61	77.13	6.42
		3.450		-36.57	88.73	-12.95	161.33	83.19	-7.83	160.91	6.24	39.54	0.26
Female	2.41	1.425	90.97	-8.22	1.35	-0.42	83.68	0.52	-0.13	83.13	61.48	69.05	0.66
		1.725		-8.33	1.48	-0.36	83.76	0.95	-0.13	83.46	35.81	63.89	0.36
		2.175		-8.94	1.36	-0.03	83.36	1.17	-0.15	83.05	13.97	-400.00	0.37
	7.00	2.475		-15.58	2.96	-5.27	73.09	8.74	-1.27	82.87	-195.27	75.90	-13.38
		3.075		-15.75	3.25	-3.23	75.23	8.69	-2.55	81.35	-167.38	21.05	-8.14
		3.675		-17.98	2.57	-0.89	74.66	8.29	-0.60	80.68	-222.57	32.58	-8.06
	20.20	2.490		-29.09	90.10	-22.54	127.44	56.82	-30.94	87.76	36.94	-37.27	31.14
		2.970		-33.10	98.48	-33.26	123.09	67.11	-7.62	117.37	31.85	77.09	4.65
		3.450		-37.62	79.09	-12.95	119.49	74.06	-7.88	119.53	6.36	39.15	-0.03

For the moments about the toe shown in Table 4.5, the percentage differences between the values calculated using the measured velocity profile and the predicted velocity profile for the net moment about the toe are smaller than those for the moment about the heel. For the moment about the toe, a positive moment implies stability. None of the flows created a negative moment. All flows are safe against toppling about the toe.

Tables 4.6-4.8, respectively, give the forces and moment arms, the net moment about the heel, and the net moment about the toe for the flow rates of 15, 17 and 18 m^3/s. For these flows, measured values of the velocity profile are not given. These flow rates were chosen for analysis because the lower flows of 2.41 and 7.0 m^3/s showed that a person would be stable in the flow. However, the flow rate of 20.2 m^3/s showed that a person could be unstable standing in that flow (for the moment about the heel). Therefore, the flow rate at which a person would start to be unstable in standing appears to be in the range of 15 to 18 m^3/s.

Table 4.6. Predicted forces and moment arms for the flow rates Q =15, 17, and 18 m^3/s.

Type of Body	**Flow** Q	**Location** X	F_B	L_B	F_{DF}	H_{DF}	F_{DB}	H_{DB}
	(m^3/s)	(m)	(N)	(m)	(N)	(m)	(N)	(m)
Male	15.00	2.00	218.88	0.114	261.11	0.13	62.46	0.76
		2.50	231.54	0.114	282.39	0.16	62.49	0.79
		3.00	238.10	0.115	272.53	0.18	18.74	0.81
	17.00	2.50	258.43	0.120	321.90	0.17	71.93	0.82
		3.00	272.56	0.121	318.40	0.19	32.51	0.85
		3.50	279.79	0.121	294.64	0.21	2.91	0.86
	18.00	2.50	265.44	0.120	341.62	0.17	77.30	0.83
		3.00	279.79	0.123	338.65	0.19	43.24	0.85
		3.50	287.13	0.124	318.16	0.22	5.01	0.88
Female	15.00	2.00	214.15	0.086	224.61	0.13	66.05	0.76
		2.50	227.97	0.087	240.69	0.15	65.28	0.79
		3.00	235.04	0.089	232.37	0.17	19.33	0.81
	17.00	2.50	256.81	0.091	274.07	0.16	73.74	0.81
		3.00	271.74	0.092	272.16	0.18	32.72	0.84
		3.50	279.31	0.092	253.89	0.21	2.90	0.86
	18.00	2.50	264.23	0.091	292.89	0.17	78.61	0.78
		3.00	279.31	0.092	291.63	0.19	43.43	0.85
		3.50	286.94	0.094	276.04	0.22	6.79	0.84

Table 4.7. Predicted moment about the heel for the flow rates of 15, 17, and 18 m^3/s; $M_P < 0$ indicates stable.

			Calculated Moment About the Heel				
Type of Body	**Flow** Q	**Location** X	WL_W	F_BL_B	$F_{DF}H_{DF}$	$F_{BF}H_{BF}$	M_P
	(m^3/s)	(m)	(N·m)	(N·m)	(N·m)	(N·m)	(N·m)
Male	15.00	2.00	-91.76	25.01	35.08	-47.68	-79.34
		2.50		26.46	43.82	-49.32	-70.79
		3.00		27.42	47.94	-15.22	-31.62
	17.00	2.50		30.89	53.12	-58.88	-66.62
		3.00		33.06	59.33	-27.56	-26.93
		3.50		33.94	61.09	-2.50	0.78
	18.00	2.50		31.73	59.28	-64.21	-64.94
		3.00		34.43	65.49	-36.75	-28.59
		3.50		35.59	68.54	-4.41	7.96
Female	15.00	2.00	-68.35	18.36	28.20	-50.18	-71.96
		2.50		19.92	35.69	-51.30	-64.04
		3.00		20.91	40.00	-15.65	-23.08
	17.00	2.50		23.27	43.73	-60.05	-61.40
		3.00		25.06	50.20	-27.64	-20.72
		3.50		25.76	53.22	-2.49	8.15
	18.00	2.50		23.94	49.90	-61.47	-55.98
		3.00		25.76	56.41	-36.77	-22.95
		3.50		26.92	60.33	-6.79	12.11

Table 4.8. Predicted moment about the toe for the flow rates of 15, 17, and 18 m^3/s; $M_P > 0$ indicates stable.

			Calculated Moment About the Toe				
Type of Body	**Flow** Q	**Location** X	$W(L_{foot}-L_W)$	$F_B(L_{foot}-L_B)$	$F_{DF}H_{DF}$	$F_{BF}H_{BF}$	M_P
	(m^3/s)	(m)	(N·m)	(N·m)	(N·m)	(N·m)	(N·m)
Male	15.00	2.00	122.13	-33.48	35.08	-47.68	76.05
		2.50		-35.42	43.82	-49.32	81.21
		3.00		-36.21	47.94	-15.22	118.64
	17.00	2.50		-38.16	53.12	-58.88	78.21
		3.00		-39.77	59.33	-27.56	114.12
		3.50		-40.83	61.09	-2.50	139.89
	18.00	2.50		-39.20	59.28	-64.21	78.01
		3.00		-40.33	65.49	-36.75	110.53
		3.50		-41.14	68.54	-4.41	145.11
Female	15.00	2.00	90.97	-33.95	28.20	-50.18	35.04
		2.50		-35.77	35.69	-51.30	39.58
		3.00		-36.50	40.00	-15.65	78.82
	17.00	2.50		-39.47	43.73	-60.05	35.18
		3.00		-41.32	50.20	-27.64	72.21
		3.50		-42.48	53.22	-2.49	99.23
	18.00	2.50		-40.61	49.90	-61.47	38.78
		3.00		-42.48	56.41	-36.77	68.13
		3.50		-43.17	60.33	-6.79	101.33

4.5 Assessment of Stability

In this study, a person's stability when standing in the flow below a weir is taken to be dependent on the net moment, M_P, generated about the potential point of balance, which is either the heel or toe. Equations 3.4 and 3.5 represent the conditions for a person's stability against toppling about his or her heel and toe, respectively. A body's weight in either of these cases contributes to stability.

For the flows of 2.41 and 7.0 m^3/s, the net moment about the heel for both males and females were found to be negative at all locations considered through the length of the jump (Table 4.4). This implies both male and females would be safe to stand in these flows. Similarly, the net moment about the toe is positive at all positions through the flow for both male and females (Table 4.5), which also indicates both males and females are stable in standing. Hence, for the Wolf River Barrier, discharges of 2.41 and 7 m^3/s can be considered safe for adults in standing.

For the flow rate of 20.2 m^3/s, the net moments about the toe showed that the male and female would be safe to stand in this flow. However, the moment about the heel showed that the flow is unsafe for both males and females. If a person stands facing the Wolf River Barrier when it has a discharge of 20.2 m^3/s, he or she will be toppled backward. Hence, a discharge of 20.2 m^3/s at the Wolf River Barrier should be considered as hazardous for adults. Therefore, the transition between a safe and hazardous flow occurs at some discharge between 7.0 and 20.2 m^3/s.

The moments for discharges of 18, 17 and 15 m^3/s, were then assessed to attempt to determine the "critical" value of discharge at which standing below the barrier would not be possible. For the flow of 18 m^3/s, the net moment about the heel is negative for velocity profiles at $X = 2.5$ and 3.0 m (stable) and positive at $X = 3.5$ m (unstable) (Table 4.7). Net moments about the toe are positive at all X locations (Table 4.8), which indicates a person is stable. Therefore, a discharge of 18 m^3/s at the Wolf River Barrier would still be hazardous for adults.

Similarly, for a flow rate of 17 m^3/s, again it is seen that net moments about heel at $X = 2.5$ and 3.0 m are negative and at X = 3.5 m the net moment about heel is positive (Table 4.7). Again, the net moments about the toe are positive at all X locations (Table 4.8), which indicates stability in standing. Therefore, a discharge of 17 m^3/s should also be considered hazardous for adults.

For a discharge of 15 m^3/s, the net moments about the heel are negative for all predicted velocity profiles, which indicates a person is stable in standing (Table 4.7). The net moments about the toe are all positive, which also indicates stability in standing. A discharge of 15 m^3/s at the Wolf River Barrier can be considered safe for standing for adults. The net moments for 15 m^3/s are show the flow is safe, but the values for the net moment are small. This implies that the value for the transition to instability occurs in the range of 15 to 17 m^3/s.

As discussed in Chapter 2 (Section 2.2), there will be a higher flow at which the flow regime will shift from the impinging jet regime, which creates the submerged hydraulic jump, to the surface jet regime, where there is no backward flow near the weir to entrap a body. Therefore, this study also tried to identify after what maximum discharge, the flow regime below the Wolf River barrier becomes a surface jet. Discharges up to 184 m^3/s were checked and it was found the flows never result in a surface jet. A flow of 184 m^3/s was the maximum average daily flow observed at the site from the recorded average daily discharges seen at the site from 1971 to 2020 (Maki and Grinstead 2009).

It is recommended that if a person topples in a flow below the weir, he or she should try to crawl on the bed downstream to move out of the roller.

CHAPTER 5: SUMMARY, CONCLUSIONS, AND RECOMMENDATIONS

5.1 Summary and Conclusions

A framework to analyze the stability of a person trying to stand in a submerged hydraulic jump below a weir was developed. Later, the framework was applied to evaluate the flow below the Wolf River Barrier located in Ontario, Canada. The maximum safe discharge for standing in the flow by adults at the Wolf River Barrier site was predicted by evaluating the flows using the framework and shown to be in the range of 15 to 17 m^3/s.

The analysis is based on assessing the forces applied on a person standing below the weir for submerged hydraulic jump flow conditions. A person's stability is assessed based on the net moment generated by the applied force about points of balance (heel/toe). Four forces were considered in the framework for analyzing the person's stability: weight, buoyancy, and the drag forces due to the forward and backward flows with the jump. The framework calculates the four forces and their respective moment arms to calculate the moment created by each force about the points of balance.

Weight was calculated using the height and body mass index (BMI) of a person. The framework treats males and females separately as their body structures are different. Although this study only checks the stability of a person based on average adult Canadian males and females body structure, it is organized in a way that it can be extended to any males or females of known height and weight with a similar body-mass index (a BMI of 26.4 was assumed for males and 25.4 for females). If the body shape and composition is significantly different than these "normal" values, the developed relationships between volume and surface area with height would have to be adjusted.

Buoyancy force depends on the submerged volume of the human body in the flow, which means that it changes with the depth of the flow. Therefore, this study developed plots and equations to find the relation between the submerged volume of the body and flow depth. Three-dimensional models were used to find the dimensionless relations between the submerged volume and flow depth for males and females separately.

Drag forces depend on the coefficient of drag, projected area, and velocity. A coefficient of drag of 1.2 was chosen in this study to determine the drag forces. Next, the projected area of humans was required to calculate the forces. This study considered that the flow below the weir is in submerged flow conditions, so two-directional flows will be present. Therefore, it raises the need to develop a way to calculate the projected area of a specific portion of the human body. Two 2D male and female models were created to develop dimensionless plots and equations to determine the projected area for different flow depths. These equations and plots are serviceable to find the projected area for a particular portion of a velocity profile.

Another critical part of this study is to predict the velocity profile of a submerged hydraulic jump formed below the weir. Previous studies only considered predictions of velocity profiles for submerged hydraulic jumps formed below underflow structures such as a sluice gate. This study developed the framework to predict the submerged hydraulic jump's velocity profiles below a weir adjusting the jump location to the end of the nappe. Equations were developed to estimate both the forward and backward velocity portions of the velocity profiles through the length of a submerged hydraulic jump. The predicted velocity profiles showed a better match to the experimental velocity profiles further away from the weir.

The net moments about the toe or heel of a person generated by flow rates of 2.41, 7.0, 15.0, 17.0, 18.0, and 20.2 m^3/s at downstream of the Wolf River Barrier were evaluated. A net negative moment about the heel and a positive net moment about the toe of a person indicates stability. Among the six discharges, analyzing the flows of 2.41, 7.0, and 20.2 m^3/s, it was found that the highest flow created a positive moment about the heel for both males and females, indicating that, in a flow of 20.2 m^3/s, both males and females will not be able to stand. Then, net moments generated by flow rates of 15.0, 17,0 and 18.0 m^3/s were also calculated from predicted velocity profiles; only a flow of 15.0 m^3/s generated net negative moments about the heel and positive net moments about the toe for both males and females, which show that the flow is safe for standing. Therefore, it was concluded that the highest safest discharge at the Wolf River Barrier would be between 15 to 17 m^3/s.

The velocity profiles predicted by the framework in this study were sensitive to the tailwater depth. Therefore, it is recommended that a stage-discharge relationship for the barrier be

developed from measurements of the tailwater depth downstream of the weir instead of a depth near the barrier's downstream face.

5.2 Recommendations

Some recommendations for future research to apply the framework to analyze human stability at different flow conditions are as follows:

- It is recommended that relationships for the velocity profiles be developed specifically for submerged hydraulic jumps formed below weirs. In particular, better relationships are needed to predict the length scales associated with the velocity profiles.
- The water surface profile of a submerged hydraulic jump below a weir is required to accurately calculate the distance from the water surface while predicting the reverse velocity profile. Therefore, experiments should be carried out to develop predictive relationships for this water surface profile.
- A computer program could be developed to automatically perform the required calculations instead of performing the calculations within Excel if this is to be used by practicing engineers.
- The impinging nappe below the overflow structure can create a scour hole in the bed when the bed is not rigid. The scour hole might have considerable effects on velocity profiles below a weir in submerged hydraulic jump conditions. This was not the case for the Wolf River barrier as the bed is rock. However, the formation of the countercurrent region also might be affected by the scour hole. Future research is recommended to find the effects of a scour hole on the velocity profiles in a submerged hydraulic jump, and how the framework will work in such a case should be evaluated.
- It would be helpful to test the analysis framework with laboratory or field-based experiments with real persons, although safety would be a strong consideration in the experimental design and ethics approval will be necessary.
- The framework used in this study checked the human stability against toppling. A human can also be unstable due to sliding. As this framework can calculate the drag force generated on a person, it could also be modified to find instability due to sliding. To do that work, the sliding resistance a person can generate for different bed conditions need to

be calculated. Hence, future research is recommended to extend this framework to include an analysis of instability in sliding.

- This study has not considered the possibility of being unstable because of turbulence in a flow. Future research is recommended to find the effect of turbulence on stability.
- The models of humans considered in this study are based on an average body structure. A sensitivity analysis should be conducted to evaluate the impact of changes in body structure.
- The net moment about the points of balance (heel/toe) can be affected by the position of feet and body posture. Therefore, future research is recommended to analyze the sensitivity of stability due to changes in body position.

REFERENCES

Abt, S.R., Wittier, R.J., Taylor, A., and Love, D.J. 1989. Human Stability in a High Flood Hazard Zone 1. JAWRA Journal of the American Water Resources Association, 25(4): 881–890.

Association of State Dam Safety 2019. Reports of Public Safety Incidents in the News: 2019. Available from https://damsafety.org/PSAD-2019. [accessed 10 November 2021].

Azimi, A.H., Rajaratnam, N., and Zhu, D.Z. 2016. Water Surface Characteristics of Submerged Rectangular Sharp-Crested Weirs. Journal of Hydraulic Engineering, 142(5): 06016001.

Blalock, M.E., and Sturm, T.W. 1981. Minimum Specific Energy in Compound Open Channel. Journal of the Hydraulics Division, 107(6): 699–717.

Borland-Coogan Associates and Flimspace (Firm) Productions 1980. The Drowning Machine, (Video). State College, Pennsylvania, USA.

Braune, W., and Fischer, O. 1985. The Center of Gravity of the Human Body as Related to the German Infantryman (translated from 1889 German edition). Springer-Verlag, New York, New York, USA.

Bennett, T. 2018. Canadian Update to ICOLD Technical Committee I Public Safety Around Dams. International Commission on Large Dams (ICOLD), July 1-7, 2018, Vienna, Austria.

Chen, Q., Xia, J., Falconer, R. A., and Guo, P. 2019. Further Improvement in a Criterion for Human Stability in Floodwaters. Journal of Flood Risk Management, 12(3): e12486.

Clauser, C. E., McConville, J. T., and Young, J. W. 1969. Weight, Volume, and Center of Mass of Segments of the Human Body. Report No. AMRL-TR-69-70, Aerospace Medical Division, United States Air Force, Wright-Patterson Air Force Base, Ohio, USA.

Contini, R. 1972. Body Segment Parameters, Part II. Artificial Limbs, 16(1), 1–19.

Cox, R.J., Shand, T.D., and Blacka, M.J. 2010. Australian Rainfall and Runoff Revision Project 10: Appropriate Safety Criteria for People. AR&R Report No: P10/S1/006, Water Research Laboratory, The University of New South Wales, NSW, Australia.

Davies, A., Wellard-Cole, L., Rangan, A., and Allman-Farinelli, M. 2020. Validity of Self-reported Weight and Height for BMI Classification: A Cross-sectional Study Among Young Adults. Nutrition, 71: 110622.

Dempster, W. T. 1955. Space Requirements of the Seated Operator: Geometrical, Kinematic, and Mechanical Aspects of the Body, with Special Reference to the Limbs. WADC Technical Report 55-159, Aerospace Medical Division, United States Air Force, Wright-Patterson Air Force Base, Ohio, USA.

Drillis, R., Contini, R., and Bluestein, M. 1964. Body Segment Parameters. Artificial limbs, 8(1): 44-66.

Duggar, B.C. 1962. The Center of Gravity of the Human Body. Human Factors: The Journal of the Human Factors and Ergonomics Society, 4(3): 131–148.

Elverum, K. A., and Smalley, T., 2012. The Drowning Machine. Boat and Water Safety, Minnesota Department of Natural Resources, Saint Paul, Minnesota, USA.

Ettema, R., Arndt, R., Roberts, P., and Wahl, T. (eds). 2000. Hydraulic Modeling: Concepts and Practice. ASCE Manuals and Reports on Engineering Practice No. 97, American Society of Civil Engineers, Reston, Virginia, USA.

Evans, E. M., Rowe, D. A., Racette, S. B., Ross, K. M., and McAuley, E. 2006. Is the current BMI Obesity Classification Appropriate for Black and White Postmenopausal Women?. International Journal of Obesity, 30(5), 837-843.

Fan. J.J., 1993. Submerged Hydraulic Jumps at Overflow Structures. MASc. Thesis, Department of Mechanical Engineering, University of Toronto, Toronto, Ontario, Canada.

Foster, D.N., and Cox, R.J. 1973. Stability of Children on Roads Used as Floodways, Technical Report No. 73/13, Water Research Laboratory, The University of New South Wales, Manly Vale, New South Wales, Australia.

Freeman, J.W., and Garcia, M.H. 1996. Hydraulic Model Study for the Drown-proofing of Yorkville Dam, Illinois. Hydrosystems Laboratory, Department of Civil Engineering, University of Illinois at Urbana-Champaign, Urbana, Illinois, USA.

Giles, E., and Vallandigham, P. H. 1991. Height Estimation from Foot and Shoeprint Length. Journal of Forensic Science, 36(4), 1134-1151.

Government of Ontario. 2021. Available from: https://data.ontario.ca/dataset/provincial-stream-water-quality-monitoring-network, (Accessed on April 20, 2021)

Hager, W. H. 1992. Energy Dissapators and Hydraulic Jump, Kluwer Academic Publishers, Dordrecht, The Netherlands.

Harless, E. 1860. The Static Moments of the Component Masses of the Human Body. Trans. of the Math-Phys., Royal Bavarian Acad. of Sci, 8(1): 69-96.

Hoerner, S. F. (1965). Fluid Dynamic Drag. Midland Park, New Jersey, USA

Hotchkiss, R. H., and Comstock, M. 1992. Discussion of "Drownproofing of Low Overflow Structures" by H.J. Leutheusser and W.M. Birk (February 1991, Vol. 117, No. 2). Journal of Hydraulic Engineering, 118(11): 1586-1589

Janssen, I., Katzmarzyk, P. T., Srinivasan, S. R., Chen, W., Malina, R. M., Bouchard, C., and Berenson, G. S. 2005. Utility of Childhood BMI in the Prediction of Adulthood Disease: Comparison of National and International references. Obesity Research, 13(6): 1106-1115.

Jonkman, S.N., Kelman, I., and Bain, V. 2005. A Physical Interpretation of Human Stability in Flowing Water, In: Vrijling *et al*. (Editors.) Proceedings of the International Symposium on Stochastic Hydraulics, 23-24 May 2005, Nijmegen, the Netherlands.

Jonkman, S.N. 2007. Loss of Life Estimation in Flood Risk Assessment; Theory and Applications. Ph.D., Thesis, Delft University of Technology, Delft, the Netherlands.

Jonkman, S.N., and Penning-Rowsell, E. 2008. Human Instability in Flood Flows. Journal of the American Water Resources Association, 44 (4): 1 – 11.

Jonkman, S. N., Vrijling, J. K., and Vrouwenvelder, A. C. W. M. 2008. Methods for the Estimation of Loss of Life Due to Floods: A Literature Review and a Proposal for a New Method. Natural Hazards, 46(3), 353-389.

Karvonen, R. A., Hepojoki, A., Huhta, H. K., and Louhio, A. 2000. The Use of Physical Models in Dam-break Analysis. RESCDAM Final Report. Helsinki University of Technology, Helsinki, Finland.

Kern, E. W., Hotchkiss, R. H., and Ames, D. P. 2015. Introducing a Low-head Dam Fatality Database and Internet Information Portal. Journal of the American Water Resources Association, 51(5): 1453-1459.

Lakshmana Rao, N.S. 1975. Theory of Weirs. Advances in Hydro-science, V.T. Chow (ed.), Academic Press, New York, USA, 10: 309-406

Leutheusser, H.J. 1988. Dam Safety, Yes.; But What About Safety at Dams?. Proc., 1988 National Conf., Hydraulics Division, ASCE, Colorado Springs, Colorado, USA, 1091–1096.

Leutheusser, H.J., and Birk, W.M. 1991. Drownproofing of Low Overflow Structures. Journal of Hydraulic Engineering, 117(2): 205–213.

Leutheusser, H.J., and Fan, J.J. 2001. Backward Flow Velocities of Submerged Hydraulic Jumps. Journal of Hydraulic Engineering, 127(6): 514–517

Lind, N., Hartford, D., and Assaf, H. 2004. Hydrodynamic Models of Human Stability in a Flood[1]. Journal of the American Water Resources Association, 40(1): 89–96.

Long, D., Steffler, P. M., and Rajaratnam, N. 1990. LDA Study of Flow Structure in Submerged Hydraulic Jump. Journal of Hydraulic Research, 28(4): 437-460.

Maki, C., and Grinstead, J. 2009. Wolf River Watershed Assessment Report. Lakehead Region Conservation Authority, Thunder Bay, Ontario, Canada.

Mazurek, K.A., Hallett, A., Aktar, A., Thomson, J., Amos, M., and Katapodis, C. 2008. Phase I Development of an Improved Sea Lamprey Barrier. Great Lakes Fishery Commission, Canada.

McCardle, W.D., Katch, F.I., and Katch, V.L. 2007. Exercise Physiology: Energy, Nutrition, and Human Performance. Lipponcott, Willians, and Wilkins, Conshocken, Pennsylvania.

Mossa, M., Yasuda, Y., and Chanson, H. (*Editors*). 2004. Fluvial, Environmental and Coastal Developments in Hydraulic Engineering: Proceedings of the International Workshop on

State-of-the-Art Hydraulic Engineering, Bari, Italy, 16-19 February 2004. CRC Press, Florida, USA.

National Heart, Lung, Blood Institute., and National Institute of Diabetes, Digestive, and Kidney Diseases.1998. Clinical Guidelines on the Identification, Evaluation, and Treatment of Overweight and Obesity in Adults: The Evidence Report. Report No. 98-4083, National Institutes of Health Publication, Bethesda, Maryland, USA.

Ohtsu, I., and Yasuda, Y. 1991. Hydraulic Jump in Sloping Channels. Journal of Hydraulic Engineering, 117(7), 905-921.

Ontario Ministry of Natural Resources. 1988. Flood Plain Planning Policy Statement: Implementation Guidelines. October 1988, Ministry of Natural Resources, Province of Ontario, Toronto, Ontario.

Olsen, R.J., Johnson, M.C., and Barfuss, S.L. 2013. Risk of Entrapment at Low Head Dams. Journal of Hydraulic Engineering, 139(6): 675-678.

Rajaratnam, N. 1965a. The hydraulic jump as a well jet. Journal of the Hydraulics Division (ASCE), 91(5), 107-132.

Rajaratnam, N., 1965b. Submerged Hydraulic Jump. Journal of the Hydraulics Division (ASCE), 91(4): 71–96.

Rajaratnam, N. 1965c. Flow Below a Submerged Sluice Gate as a Wall Jet Problem. In Proc., 2nd Australasian Conf. on Hydraulics and Fluid Mechanics, 6-11 December 1965, Auckland, New Zealand, B131-146.

Rajaratnam, N., 1967. Hydraulic Jumps. In Advances in Hydroscience. vol. 4. Edited by V. T. Chow. Academic Press, New York, USA. pp.197–280.

Rajaratnam, N., and Muralidhar, D. 1969. Flow Below Deeply Submerged Rectangular Weirs. Journal of Hydraulic Research, 7(3), 355-374.

Rajaratnam, N., Subramanya, K., and Muralidhar, D. 1968. Flow Profiles Over Sharp-Crested Weirs. Journal of the Hydraulics Division (ASCE), 94(3), 843-848.

Rao, N.S.G., and Rajaratnam, N. 1963. The Submerged Hydraulic Jump. Journal of the Hydraulics Division (ASCE), 89(1), 139–162.

Sendroy Jr, J., and Collison, H. A. 1966. Determination of Human Body Volume from Height and Weight. Journal of Applied Physiology, 21(1): 167-172.

Shields, M., Gorber, S. C., Janssen, I., and Tremblay, M. S. 2011. Bias in Self-reported Estimates of Obesity in Canadian Health Surveys: An Update on Correction Equations for Adults. Health Reports, 22(3): 35 - 45.

Shu, C.W., Han, S.S., Kong, W.N., and Dong, B.L. 2016. Mechanism of Toppling Instability of the Human Body in Floodwaters. IOP Conference Series: Earth and Environmental Science, 39: 012038.

Takahashi, S., Endoh, K., & Muro, Z. I. 1992. Experimental Study on People's Safety Against Overtopping Waves on Breakwaters. Report of The Port and Harbour Research Institute, 34 (4), 4-31, Ministry of Transport, Nagase, Yokosuka, Japan. (in Japanese).

United States Bureau of Reclamation 1988. Downstream Hazard Classification Guidelines. ACER Technical Memorandum No. 11, Assistant Commissioner – Engineering and Research, United States Department of Interior, Bureau of Reclamation, December 1988, Denver, Colorado, USA.

World Health Organization 2000. The Asian-Pacific Perspective: Redefining Obesity and Its Treatment, International Obesity Task Force, WHO Western Pacific Region, Geneva, Switzerland.

Wu, S., 1994. Four Contributions to the Application of Turbulent Jet Theory in Hydraulic Engineering. Ph.D., Thesis, Department of Civil Engineering, University of Alberta, Edmonton, Alberta, Canada.

Wu, S., and Rajaratnam, N. 1995. Free Jumps, Submerged Jumps and Wall Jets. Journal of Hydraulic Research, 33(2): 197–212.

Wu, S., and Rajaratnam, N. 1996. Submerged Flow Regimes of Rectangular Sharp-Crested Weirs. Journal of Hydraulic Engineering, 122(7): 412–414.

Xia, J., Falconer, R.A., Wang, Y., and Xiao, X. 2014. New Criterion for the Stability of a Human Body in Floodwaters. Journal of Hydraulic Research, 52(1): 93–104.

Yasuda, Y. 2004. Characteristics of Plunging Flows in Stepped-Channel Chutes. In Fluvial, Environmental and Coastal Developments in Hydraulic Engineering (pp. 17-26). CRC Press, USA.

Yee, M. 2003. Human Stability in Floodways, Bachelor thesis, School of Civil and Environmental Engineering, University of New South Wales, Sydney, Australia.

Zachoval, Z., Böhm, P., Parílková, J., Safár, R., and Sulc, J. 2013. Shape of the Nappe During Free Overfall from a Rectangular Channel with Zero Bed Slope. Journal of Hydrology and Hydromechanics, 61(3): 222-231.

APPENDIX A: 2D and 3D Human Model Data

This appendix provides the data generated from the 2D model in AutoCAD 2018 and 3D models in Sketchup Pro 2021.

Table A-1. Data found from Male 2D Model in AutoCAD 2018, Height, H = 175.80 cm.

y (cm)	A_n	y/H	A_n/H^2
0	0	0	0
12.07	167.31	0.0687	0.0054
27.45	392.00	0.1561	0.0127
43.49	709.43	0.2474	0.0230
58.78	1055.08	0.3344	0.0341
74.82	1562.98	0.4256	0.0506
90.86	2290.84	0.5169	0.0741
105.78	2999.92	0.6017	0.0971
121.45	3758.10	0.6909	0.1216
136.00	4531.39	0.7736	0.1466
151.67	5016.64	0.8627	0.1623
160.74	5136.57	0.9144	0.1662
168.83	5292.83	0.9604	0.1713
175.80	5384.96	1.0000	0.1742

Table A-2. Data found from Female 2D Model in AutoCAD 2018, Height, H = 162.10 cm.

y (cm)	A_n	y/H	A_n/H^2
0	0	0	0
7.15	100.55	0.0431	0.0037
12.99	161.02	0.0792	0.0060
22.13	260.08	0.1356	0.0097
33.80	462.63	0.2076	0.0174
46.65	694.24	0.2868	0.0263
58.11	943.25	0.3576	0.0357
69.33	1351.29	0.4267	0.0513
80.28	1828.27	0.4943	0.0694
91.33	2322.26	0.5625	0.0882
102.75	2803.25	0.6329	0.1065
113.81	3254.23	0.7011	0.1237
125.22	3719.60	0.7716	0.1414
134.14	4032.01	0.8266	0.1533
142.52	4148.63	0.8783	0.1577
151.08	4262.10	0.9311	0.1620
158.75	4373.94	0.9784	0.1663
162.10	4399.13	1.0000	0.1674

Table A-3. Data found from 3D male human model in SketchUp Pro 2021, Height, H = 175.58 cm.

y (cm)	λ_s (cm^3)	y/H	λ_s/H^3	L_W (cm)	L_W/H	L_B (cm)	L_B/H
0	0	0	0			-	-
10.16	2081.82	0.0579	0.0004			8.57	0.0488
20.32	2829.3	0.1157	0.0005			7.18	0.0409
30.48	4088.03	0.1736	0.0008			6.62	0.0377
40.64	5930.91	0.2315	0.0011			6.49	0.0370
50.8	7478.13	0.2893	0.0014			6.98	0.0397
60.96	9958.69	0.3472	0.0018			8.44	0.0480
71.12	12814.35	0.4051	0.0024			9.96	0.0567
81.28	17722.11	0.4629	0.0033			10.66	0.0607
91.44	24713.86	0.5208	0.0046	11.83	0.067	11.66	0.0664
101.6	32419.21	0.5787	0.0060			12.52	0.0713
111.76	39243.22	0.6365	0.0073			13.05	0.0743
121.92	47306.38	0.6944	0.0087			13.14	0.0748
132.08	56839.9	0.7522	0.0105			13.07	0.0744
142.24	67349.55	0.8101	0.0124			12.91	0.0735
152.4	72138.44	0.8680	0.0133			12.71	0.0724
162.56	73966.15	0.9258	0.0137			12.80	0.0729
172.72	76662.83	0.9837	0.0142			12.92	0.0736
175.58	76955.45	1.0000	0.0142			12.92	0.0736

Table A-4. Data found from 3D female human model in SketchUp Pro 2021, Height, H = 161.78 cm.

y (cm)	λ_s (cm^3)	y/H	λ_s/H^3	L_W (cm)	L_W/H	L_B (cm)	L_B/H
0	0	0	0			-	-
10.16	1794.30	0.0628	0.0004			7.09	0.044
20.32	2309.75	0.1256	0.0005			6.24	0.039
30.48	3302.24	0.1884	0.0008			5.52	0.034
40.64	4751.14	0.2512	0.0011			5.22	0.032
50.8	5805.12	0.3140	0.0014			5.55	0.034
60.96	7502.45	0.3768	0.0018			6.41	0.040
71.12	10889.07	0.4396	0.0026			7.37	0.046
81.28	16350.63	0.5024	0.0039	10.69	0.066	8.24	0.051
91.44	24936.49	0.5652	0.0059			8.74	0.054
101.6	31688.35	0.6280	0.0075			9.42	0.058
111.76	37925.63	0.6908	0.0090			10.11	0.062
121.92	45886.35	0.7536	0.0108			10.71	0.066
132.08	55356.03	0.8164	0.0131			11.12	0.069
142.24	58186.11	0.8792	0.0137			11.04	0.068
152.4	60030.64	0.9420	0.0142			11.18	0.069
161.78	61815.73	1.0000	0.0146			11.32	0.070

APPENDIX B: Predicted Velocity Profile Data and Calculated Drag Forces and Submerged Volumes

This appendix provides the velocity values at different predicted velocity profiles at different downstream locations for all discharges considered in this study. It also provides the data used in this study to calculate the drag forces developed on male and female bodies for different velocity profiles and submerge volumes of human models at each profile's location.

Table B-1. Predicted velocity profile data for Q = 2.41 m^3/s.

$X = 1.425$ m		$X = 1.725$ m		$X = 2.175$ m	
Y	U	Y	U	Y	U
(m)	(m/s)	(m)	(m/s)	(m)	(m/s)
0	0	0	0	0	0
0.075	1.77	0.075	1.844	0.075	1.533
0.134	0	0.135	0.648	0.135	0.979
0.135	-0.019	0.190	0	0.195	0.345
0.195	-0.064	0.195	-0.056	0.244	0
0.255	-0.105	0.255	-0.097	0.255	-0.075
0.272	-0.110	0.283	-0.114	0.315	-0.114
0.315	-0.140	0.315	-0.134	0.364	-0.142
0.375	-0.171	0.375	-0.166	0.375	-0.149
0.414	-0.189	0.420	-0.187	0.450	-0.185

Table B-2. Predicted velocity profile data for Q = 7.0 m^3/s.

$X = 2.475$ m		$X = 3.075$ m		$X = 3.675$ m	
Y	U	Y	U	Y	U
(m)	(m/s)	(m)	(m/s)	(m)	(m/s)
0	0	0	0	0	0
0.075	2.983	0.075	2.427	0.075	1.960
0.150	2.139	0.150	1.877	0.150	1.608
0.225	1.293	0.225	1.401	0.225	1.284
0.300	0.429	0.300	0.835	0.300	0.954
0.358	0	0.375	0.317	0.375	0.570
0.375	-0.142	0.400	0.160	0.450	0.240
0.450	-0.191	0.420	0	0.475	0.120
0.525	-0.235	0.450	-0.258	0.500	0
0.585	-0.267	0.525	-0.335	0.525	-0.136
0.645	-0.296	0.600	-0.403	0.600	-0.169
		0.630	-0.429	0.690	-0.205
		0.648	-0.443		

Table B-3. Predicted velocity profile data for Q = 20.20 m^3/s.

$X = 2.490$ m		$X = 2.970$ m		$X = 3.450$ m	
Y	U	Y	U	Y	U
(m)	(m/s)	(m)	(m/s)	(m)	(m/s)
0	0	0	0	0	0
0.060	4.320	0.060	4.059	0.060	3.723
0.150	3.698	0.150	3.623	0.150	3.441
0.240	2.927	0.240	2.937	0.240	2.850
0.330	2.208	0.330	2.347	0.330	2.349
0.420	1.350	0.420	1.664	0.420	1.819
0.510	0.584	0.510	0.941	0.510	1.206
0.550	0	0.600	0.336	0.600	0.644
0.600	-0.437	0.610	0.230	0.690	0.114
0.610	-0.440	0.630	0	0.700	0
0.690	-0.745	0.690	-0.311	0.780	-0.419
0.780	-1.006	0.780	-0.428	0.870	-0.467
0.840	-1.154	0.840	-0.496	0.930	-0.500
		0.882	-0.537		

Table B-4. Predicted velocity profile data for Q = 18.0 m^3/s.

$X = 2.500$ m		$X = 3.000$ m		$X = 3.500$ m	
Y	U	Y	U	Y	U
(m)	(m/s)	(m)	(m/s)	(m)	(m/s)
0	0	0	0	0	0
0.020	3.861	0.020	3.532	0.020	3.162
0.050	4.215	0.050	3.882	0.050	3.488
0.100	4.017	0.100	3.806	0.100	3.495
0.200	3.075	0.200	3.030	0.200	2.883
0.300	2.255	0.300	2.353	0.300	2.310
0.500	0.409	0.500	0.795	0.500	1.068
0.540	0	0.610	0	0.600	0.478
0.700	-0.852	0.700	-0.605	0.675	0
0.800	-0.999	0.800	-0.716	0.800	-0.260
0.960	-1.201	0.980	-0.885	0.990	-0.327

Table B-5. Predicted velocity profile data for Q = 17.0 m^3/s

$X = 2.500$ m		$X = 3.000$ m		$X = 3.500$ m	
Y	U	Y	U	Y	U
(m)	(m/s)	(m)	(m/s)	(m)	(m/s)
0	0	0	0	0	0
0.020	3.834	0.020	3.481	0.02	3.094
0.050	4.176	0.050	3.821	0.05	3.411
0.100	3.947	0.100	3.723	0.1	3.401
0.200	2.990	0.200	2.936	0.2	2.782
0.300	2.145	0.300	2.256	0.3	2.215
0.400	1.135	0.400	1.475	0.4	1.634
0.530	0	0.500	0.686	0.5	0.961
0.600	-0.542	0.600	0	0.66	0
0.700	-0.759	0.700	-0.492	0.7	-0.143
0.800	-0.952	0.800	-0.627	0.8	-0.183
0.950	-1.192	0.970	-0.817	0.98	-0.244

Table B-6. Predicted velocity profile data for Q = 15.0 m^3/s.

$X = 2.000$ m		$X = 2.500$ m		$X = 3.000$ m	
Y	U	Y	U	Y	U
(m)	(m/s)	(m)	(m/s)	(m)	(m/s)
0	0	0	0	0	0
0.020	4.059	0.020	3.770	0.020	3.365
0.050	4.319	0.050	4.082	0.050	3.680
0.100	3.832	0.100	3.788	0.100	3.535
0.200	2.681	0.200	2.805	0.200	2.734
0.300	1.461	0.300	1.896	0.300	2.041
0.420	0	0.400	0.852	0.400	1.218
0.500	-0.385	0.500	0	0.500	0.464
0.600	-0.628	0.600	-0.582	0.560	0
0.700	-0.842	0.700	-0.802	0.700	-0.444
0.800	-1.029	0.800	-0.994	0.800	-0.554
0.890	-1.172	0.910	-1.172	0.920	-0.666

Table B-7. Data for calculating drag force (F_D) and submerged volume (λ_s) calculation for Q = 2.41 m^3/s at X = 1.425 m.

Male										
Y	U	U	H	Y/H	λ_s	U_i	U_i	A_{ni}	F_{Di}	F_{Di}
(m)	(m/s)	(m/s)	(m)		(m^3)	(m/s)	(m/s)	(m^2)	(N)	(N)
	Mazurek	Predicted				Mazurek	Predicted		Mazurek	Predicted
0	0	0		0		-	-	-	-	-
0.075	1.611	1.768		0.043		0.806	0.884	0.0087	3.383	4.072
0.134	1.010	0.000		0.076		1.311	0.884	0.0087	8.976	4.082
0.135	1.003	-0.019		0.077		1.007	-0.009	0.0002	0.095	0.000
0.195	0.444	-0.064	1.758	0.111	0.0058	0.723	-0.041	0.0097	3.039	-0.010
0.255	0.071	-0.104		0.145		0.257	-0.084	0.0101	0.401	-0.043
0.272	0.000	-0.110		0.155		0.035	-0.107	0.0029	0.002	-0.020
0.315	-0.173	-0.140		0.179		-0.086	-0.125	0.0075	-0.034	-0.071
0.375	-0.370	-0.171		0.213		-0.272	-0.156	0.0109	-0.483	-0.159
0.414	-0.406	-0.189		0.235		-0.388	-0.180	0.0075	-0.675	-0.145
Female										
Y	U	U	H	Y/H	λ_s	U_i	U_i	A_{ni}	F_{Di}	F_{Di}
(m)	(m/s)	(m/s)	(m)		(m^3)	(m/s)	(m/s)	(m^2)	(N)	(N)
	Mazurek	Predicted				Mazurek	Predicted		Mazurek	Predicted
0	0	0		0		-	-	-	-	-
0.075	1.611	1.768		0.046		0.806	0.884	0.0097	3.781	4.551
0.134	1.010	0		0.083		1.311	0.884	0.0071	7.274	3.308
0.135	1.003	-0.019		0.083		1.007	-0.009	0.0001	0.072	0.000
0.195	0.444	-0.064	1.618	0.121	0.0044	0.723	-0.041	0.0071	2.231	-0.007
0.255	0.071	-0.104		0.158		0.257	-0.084	0.0075	0.298	-0.032
0.272	0	-0.110		0.168		0.035	-0.107	0.0023	0.002	-0.016
0.315	-0.173	-0.140		0.195		-0.086	-0.125	0.0061	-0.028	-0.058
0.375	-0.370	-0.171		0.232		-0.272	-0.156	0.0098	-0.432	-0.142
0.414	-0.406	-0.189		0.256		-0.388	-0.180	0.0073	-0.657	-0.142

Table B-8. Data for calculating drag force (F_D) and submerged volume (λ_s) calculation for Q = 2.41 m^3/s at X = 1.725 m.

Male										
Y	U	U	H	Y/H	λ_s	U_i	U_i	A_{ni}	F_{Di}	F_{Di}
(m)	(m/s)	(m/s)	(m)		(m^3)	(m/s)	(m/s)	(m^2)	(N)	(N)
	Mazurek	Predicted				Mazurek	Predicted		Mazurek	Predicted
0	0	0		0		-	-	-	-	-
0.075	1.611	1.844		0.043		0.805	0.922	0.0087	3.380	4.431
0.135	1.026	0.648		0.077		1.318	1.246	0.0089	9.244	8.259
0.190	0.581	0		0.108		0.803	0.324	0.0089	3.430	0.558
0.195	0.541	-0.056	1.758	0.111	0.0059	0.561	-0.028	0.0008	0.156	0.000
0.255	0.147	-0.097		0.145		0.344	-0.077	0.0101	0.716	-0.036
0.283	0	-0.114		0.161		0.073	-0.106	0.0048	0.016	-0.032
0.315	-0.172	-0.134		0.179		-0.086	-0.124	0.0056	-0.025	-0.052
0.375	-0.315	-0.166		0.213		-0.243	-0.150	0.0109	-0.388	-0.147
0.420	-0.366	-0.187		0.239		-0.340	-0.176	0.0087	-0.602	-0.162
Female										
Y	U	U	H	Y/H	λ_s	U_i	U_i	A_{ni}	F_{Di}	F_{Di}
(m)	(m/s)	(m/s)	(m)		(m^3)	(m/s)	(m/s)	(m^2)	(N)	(N)
	Mazurek	Predicted				Mazurek	Predicted		Mazurek	Predicted
0	0	0		0		-	-	-	-	-
0.075	1.611	1.844		0.046		0.805	0.922	0.0097	3.779	4.953
0.135	1.026	0.648		0.083		1.318	1.246	0.0072	7.482	6.684
0.190	0.581	0		0.117		0.803	0.324	0.0065	2.520	0.410
0.195	0.541	-0.056	1.618	0.121	0.0044	0.561	-0.028	0.0006	0.113	0.000
0.255	0.147	-0.097		0.158		0.344	-0.077	0.0075	0.533	-0.027
0.283	0	-0.114		0.175		0.073	-0.106	0.0038	0.012	-0.025
0.315	-0.172	-0.134		0.195		-0.086	-0.124	0.0046	-0.021	-0.043
0.375	-0.315	-0.166		0.232		-0.243	-0.150	0.0098	-0.347	-0.132
0.420	-0.366	-0.187		0.260		-0.340	-0.176	0.0085	-0.588	-0.158

Table B-9. Data for calculating drag force (F_D) and submerged volume (λ_s) calculation for Q = 2.41 m^3/s at X = 2.175 m.

Male										
Y	U	U	H	Y/H	λ_s	U_i	U_i	A_{ni}	F_{Di}	F_{Di}
(m)	(m/s)	(m/s)	(m)		(m^3)	(m/s)	(m/s)	(m^2)	(N)	(N)
	Mazurek	Predicted				Mazurek	Predicted		Mazurek	Predicted
0	0	0		0		-	-	-	-	-
0.075	1.341	1.533		0.043		0.670	0.767	0.0087	2.343	3.063
0.135	0.937	0.979		0.077		1.139	1.256	0.0089	6.904	8.390
0.195	0.586	0.345		0.111		0.762	0.662	0.0097	3.370	2.544
0.244	0.357	0	1.758	0.139	0.0064	0.471	0.173	0.0082	1.097	0.147
0.255	0.305	-0.075		0.145		0.331	-0.037	0.0019	0.123	-0.002
0.315	0.115	-0.114		0.179		0.210	-0.094	0.0104	0.276	-0.056
0.364	0	-0.142		0.207		0.057	-0.128	0.0089	0.018	-0.087
0.375	-0.032	-0.149		0.213		-0.016	-0.145	0.0020	0.000	-0.026
0.450	-0.155	-0.185		0.256		-0.094	-0.167	0.0147	-0.077	-0.246
Female										
Y	U	U	H	Y/H	λ_s	U_i	U_i	A_{ni}	F_{Di}	F_{Di}
(m)	(m/s)	(m/s)	(m)		(m^3)	(m/s)	(m/s)	(m^2)	(N)	(N)
	Mazurek	Predicted				Mazurek	Predicted		Mazurek	Predicted
0	0	0		0		-	-	-	-	-
0.075	1.341	1.533		0.046		0.670	0.767	0.0097	2.619	3.424
0.135	0.937	0.979		0.083		1.139	1.256	0.0072	5.588	6.790
0.195	0.586	0.345		0.121		0.762	0.662	0.0071	2.474	1.868
0.244	0.357	0	1.618	0.151	0.0048	0.471	0.173	0.0061	0.812	0.109
0.255	0.305	-0.075		0.158		0.331	-0.037	0.0014	0.094	-0.001
0.315	0.115	-0.114		0.195		0.210	-0.094	0.0084	0.223	-0.045
0.364	0	-0.142		0.225		0.057	-0.128	0.0079	0.016	-0.077
0.375	-0.032	-0.149		0.232		-0.016	-0.145	0.0019	0.000	-0.024
0.450	-0.155	-0.185		0.278		-0.094	-0.167	0.0147	-0.077	-0.246

Table B-10. Data for calculating drag force (F_D) and submerged volume (λ_s) calculation for Q = 7.0 m^3/s at X = 2.475 m.

Male										
Y	U	U	H	Y/H	λ_s	U_i	U_i	A_{ni}	F_{Di}	F_{Di}
(m)	(m/s)	(m/s)	(m)		(m^3)	(m/s)	(m/s)	(m^2)	(N)	(N)
	Mazurek	Predicted				Mazurek	Predicted		Mazurek	Predicted
0	0	0		0		-	-	-	-	-
0.075	1.847	2.983		0.043		0.924	1.492	0.0087	4.446	11.598
0.150	1.217	2.139		0.085		1.532	2.561	0.0112	15.816	44.208
0.225	0.694	1.293		0.128		0.955	1.716	0.0123	6.748	21.786
0.300	0.279	0.429	1.758	0.171	0.0108	0.486	0.861	0.0129	1.829	5.731
0.358	0	0		0.204		0.140	0.214	0.0104	0.122	0.287
0.375	-0.083	-0.142		0.213		-0.041	-0.071	0.0032	0.003	0.009
0.450	-0.333	-0.191		0.256		-0.208	-0.166	0.0147	-0.382	-0.244
0.525	-0.497	-0.235		0.299		-0.415	-0.213	0.0166	-1.717	-0.453
0.585	-0.579	-0.267		0.333		-0.538	-0.251	0.0152	-2.631	-0.573
0.645	-0.616	-0.296		0.367		-0.598	-0.281	0.0172	-3.682	-0.815
Female										
Y	U	U	H	Y/H	λ_s	U_i	U_i	A_{ni}	F_{Di}	F_{Di}
(m)	(m/s)	(m/s)	(m)		(m^3)	(m/s)	(m/s)	(m^2)	(N)	(N)
	Mazurek	Predicted				Mazurek	Predicted		Mazurek	Predicted
0	0	0		0		-	-	-	-	-
0.075	1.847	2.983		0.046		0.924	1.492	0.0097	4.970	12.964
0.150	1.217	2.139		0.093		1.532	2.561	0.0089	12.590	35.192
0.225	0.694	1.293		0.139		0.955	1.716	0.0090	4.937	15.937
0.300	0.279	0.429	1.618	0.185	0.0090	0.486	0.861	0.0100	1.425	4.464
0.358	0	0		0.221		0.140	0.214	0.0090	0.106	0.249
0.375	-0.083	-0.142		0.232		0.098	0.144	0.0120	0.069	0.148
0.450	-0.333	-0.191		0.278		-0.208	-0.166	0.0147	-0.382	-0.244
0.525	-0.497	-0.235		0.325		-0.415	-0.213	0.0180	-1.863	-0.491
0.585	-0.579	-0.267		0.362		-0.538	-0.251	0.0171	-2.959	-0.645
0.645	-0.616	-0.296		0.399		-0.598	-0.281	0.0194	-4.163	-0.922

Table B-11. Data for calculating drag force (F_D) and submerged volume (λ_s) calculation for Q = 7.0 m^3/s at X = 3.075 m.

Male										
Y	U	U	H	Y/H	λ_s	U_i	U_i	A_{ni}	F_{Di}	F_{Di}
(m)	(m/s)	(m/s)	(m)		(m^3)	(m/s)	(m/s)	(m^2)	(N)	(N)
	Mazurek	Predicted				Mazurek	Predicted		Mazurek	Predicted
0	0	0		0		-	-	-	-	-
0.075	1.796	2.427		0.043		0.898	1.214	0.0087	4.203	7.678
0.150	1.255	1.877		0.085		1.526	2.152	0.0112	15.682	31.207
0.225	0.750	1.401		0.128		1.003	1.639	0.0123	7.437	19.861
0.300	0.399	0.835		0.171		0.575	1.118	0.0129	2.552	9.657
0.375	0.060	0.317	1.758	0.213	0.0109	0.229	0.576	0.0136	0.428	2.694
0.400	0	0.160		0.228		0.030	0.238	0.0047	0.003	0.162
0.420	-0.060	0		0.239		-0.030	0.080	0.0039	-0.002	0.015
0.450	-0.163	-0.258		0.256		-0.112	-0.129	0.0061	-0.045	-0.061
0.525	-0.356	-0.335		0.299		-0.260	-0.296	0.0166	-0.672	-0.875
0.600	-0.493	-0.403		0.341		-0.424	-0.369	0.0193	-2.080	-1.573
0.630	-0.510	-0.429		0.358		-0.501	-0.416	0.0086	-1.295	-0.892
0.648	-0.531	-0.443		0.369		-0.520	-0.436	0.0054	-0.880	-0.618
Female										
Y	U	U	H	Y/H	λ_s	U_i	U_i	A_{ni}	F_{Di}	F_{Di}
(m)	(m/s)	(m/s)	(m)		(m^3)	(m/s)	(m/s)	(m^2)	(N)	(N)
	Mazurek	Predicted				Mazurek	Predicted		Mazurek	Predicted
0	0	0		0		-	-	-	-	-
0.075	1.796	2.427		0.046		0.898	1.214	0.0097	4.698	8.582
0.150	1.255	1.877		0.093		1.526	2.152	0.0089	12.484	24.842
0.225	0.750	1.401		0.139		1.003	1.639	0.0090	5.441	14.529
0.300	0.399	0.835		0.185		0.575	1.118	0.0100	1.988	7.523
0.375	0.060	0.317	1.618	0.232	0.0091	0.229	0.576	0.0120	0.378	2.382
0.400	0	0.160		0.247		0.030	0.238	0.0046	0.002	0.156
0.420	-0.060	0		0.260		-0.030	0.080	0.0039	-0.002	0.015
0.450	-0.163	-0.258		0.278		-0.112	-0.129	0.0063	-0.047	-0.062
0.525	-0.356	-0.335		0.325		-0.260	-0.296	0.0180	-0.729	-0.949
0.600	-0.493	-0.403		0.371		-0.424	-0.369	0.0217	-2.343	-1.772
0.630	-0.510	-0.429		0.389		-0.501	-0.416	0.0097	-1.465	-1.009
0.648	-0.531	-0.443		0.401		-0.520	-0.436	0.0061	-0.993	-0.697

Table B-12. Data for calculating drag force (F_D) and submerged volume (λ_s) calculation for Q = 7.0 m^3/s at X = 3.675 m.

Male										
Y	U	U	H	Y/H	λ_s	U_i	U_i	A_{ni}	F_{Di}	F_{Di}
(m)	(m/s)	(m/s)	(m)		(m^3)	(m/s)	(m/s)	(m^2)	(N)	(N)
	Mazurek	Predicted				Mazurek	Predicted		Mazurek	Predicted
0	0	0		0		-	-	-	-	-
0.075	1.307	1.960		0.043		0.653	0.980	0.0087	2.225	5.005
0.150	1.052	1.608		0.085		1.179	1.784	0.0112	9.371	21.446
0.225	0.740	1.284		0.128		0.896	1.446	0.0123	5.933	15.460
0.300	0.426	0.954		0.171		0.583	1.119	0.0129	2.626	9.677
0.375	0.192	0.570	1.758	0.213	0.0123	0.309	0.762	0.0136	0.775	4.723
0.450	0.053	0.240		0.256		0.122	0.405	0.0147	0.132	1.452
0.475	0	0.120		0.270		0.026	0.180	0.0053	0.002	0.103
0.500	-0.059	0		0.284		-0.029	0.060	0.0055	-0.003	0.012
0.525	-0.117	-0.136		0.299		-0.088	-0.068	0.0058	-0.027	-0.016
0.600	-0.215	-0.169		0.341		-0.166	-0.153	0.0193	-0.319	-0.269
0.690	-0.260	-0.205		0.392		-0.237	-0.187	0.0275	-0.929	-0.576
Female										
Y	U	U	H	Y/H	λ_s	U_i	U_i	A_{ni}	F_{Di}	F_{Di}
(m)	(m/s)	(m/s)	(m)		(m^3)	(m/s)	(m/s)	(m^2)	(N)	(N)
	Mazurek	Predicted				Mazurek	Predicted		Mazurek	Predicted
0	0	0		0		-	-	-	-	-
0.075	1.307	1.960		0.046		0.653	0.980	0.0097	2.488	5.595
0.150	1.052	1.608		0.093		1.179	1.784	0.0089	7.460	17.072
0.225	0.740	1.284		0.139		0.896	1.446	0.0090	4.340	11.309
0.300	0.426	0.954		0.185		0.583	1.119	0.0100	2.046	7.538
0.375	0.192	0.570	1.618	0.232	0.0107	0.309	0.762	0.0120	0.685	4.175
0.450	0.053	0.240		0.278		0.122	0.405	0.0147	0.132	1.450
0.475	0	0.120		0.294		0.026	0.180	0.0056	0.002	0.110
0.500	-0.059	0		0.309		-0.029	0.060	0.0060	-0.003	0.013
0.525	-0.117	-0.136		0.325		-0.088	-0.068	0.0064	-0.030	-0.018
0.600	-0.215	-0.169		0.371		-0.166	-0.153	0.0217	-0.359	-0.303
0.690	-0.260	-0.205		0.427		-0.237	-0.187	0.0309	-1.044	-0.647

Table B-13. Data for calculating drag force (F_D) and submerged volume (λ_s) calculation for Q = 20.2 m^3/s at X = 2.49 m.

Male										
Y	U	U	H	Y/H	λ_s	U_i	U_i	A_{ni}	F_{Di}	F_{Di}
(m)	(m/s)	(m/s)	(m)		(m^3)	(m/s)	(m/s)	(m^2)	(N)	(N)
	Mazurek	Predicted				Mazurek	Predicted		Mazurek	Predicted
0	0	0		0		-	-	-	-	-
0.060	3.118	4.320		0.034		1.559	2.160	0.0067	9.740	18.701
0.150	3.453	3.698		0.085		3.285	4.009	0.0132	85.717	127.663
0.240	3.687	2.927		0.137		3.570	3.313	0.0149	113.652	97.869
0.330	3.000	2.208		0.188		3.344	2.567	0.0157	105.093	61.965
0.420	2.295	1.350		0.239		2.648	1.779	0.0169	71.020	32.056
0.510	0.918	0.584	1.758	0.290	0.0193	1.607	0.967	0.0192	29.712	10.766
0.550	0.520	0		0.313		0.719	0.292	0.0096	2.978	0.492
0.600	0.030	-0.437		0.341		0.275	-0.218	0.0132	0.597	-0.377
0.610	0	-0.440		0.347		0.015	-0.438	0.0028	0.000	-0.323
0.690	-0.563	-0.745		0.392		-0.282	-0.592	0.0247	-1.172	-5.189
0.780	-0.969	-1.006		0.444		-0.766	-0.875	0.0328	-11.549	-15.077
0.840	-1.024	-1.154		0.478		-0.996	-1.080	0.0249	-14.815	-17.416

Female										
Y	U	U	H	Y/H	λ_s	U_i	U_i	A_{ni}	F_{Di}	F_{Di}
(m)	(m/s)	(m/s)	(m)		(m^3)	(m/s)	(m/s)	(m^2)	(N)	(N)
	Mazurek	Predicted				Mazurek	Predicted		Mazurek	Predicted
0	0	0		0		-	-	-	-	-
0.060	3.118	4.320		0.037		1.559	2.160	0.0079	11.451	21.986
0.150	3.453	3.698		0.093		3.285	4.009	0.0108	69.913	104.126
0.240	3.687	2.927		0.148		3.570	3.313	0.0109	83.445	71.857
0.330	3.000	2.208		0.204		3.344	2.567	0.0127	84.874	50.044
0.420	2.295	1.350		0.260		2.648	1.779	0.0159	66.982	30.233
0.510	0.918	0.584	1.618	0.315	0.0185	1.607	0.967	0.0204	31.594	11.448
0.550	0.520	0		0.340		0.719	0.292	0.0107	3.321	0.548
0.600	0.030	-0.437		0.371		0.275	-0.218	0.0149	0.675	-0.426
0.610	0	-0.440		0.377		0.015	-0.438	0.0032	0.000	-0.366
0.690	-0.563	-0.745		0.427		-0.282	-0.592	0.0277	-1.317	-5.829
0.780	-0.969	-1.006		0.482		-0.766	-0.875	0.0356	-12.540	-16.371
0.840	-1.024	-1.154		0.519		-0.996	-1.080	0.0258	-15.386	-18.087

Table B-14. Data for calculating drag force (F_D) and submerged volume (λ_s) calculation for Q = 20.2 m^3/s at X = 2.97 m.

Male										
Y	U	U	H	Y/H	λ_s	U_i	U_i	A_{ni}	F_{Di}	F_{Di}
(m)	(m/s)	(m/s)	(m)		(m^3)	(m/s)	(m/s)	(m^2)	(N)	(N)
	Mazurek	Predicted				Mazurek	Predicted		Mazurek	Predicted
0	0	0		0		-	-	-	-	-
0.060	3.118	4.059		0.034		1.559	2.029	0.0067	9.740	16.510
0.150	3.453	3.623		0.085		3.285	3.841	0.0132	85.717	117.167
0.240	3.687	2.937		0.137		3.570	3.280	0.0149	113.652	95.942
0.330	3.494	2.347		0.188		3.591	2.642	0.0157	121.191	65.618
0.420	2.295	1.664		0.239		2.895	2.005	0.0169	84.887	40.735
0.510	0.918	0.941	1.758	0.290	0.0218	1.607	1.302	0.0192	29.712	19.520
0.600	0.030	0.336		0.341		0.474	0.639	0.0228	3.067	5.571
0.610	0	0.230		0.347		0.015	0.283	0.0028	0.000	0.135
0.630	-0.160	0		0.358		-0.080	0.115	0.0058	-0.022	0.046
0.690	-0.563	-0.311		0.392		-0.362	-0.155	0.0189	-1.480	-0.273
0.780	-0.969	-0.428		0.444		-0.766	-0.370	0.0328	-11.549	-2.688
0.840	-1.024	-0.496		0.478		-0.996	-0.462	0.0249	-14.815	-3.186
0.882	-1.054	-0.537		0.502		-1.039	-0.516	0.0188	-12.136	-3.001
Female										
Y	U	U	H	Y/H	λ_s	U_i	U_i	A_{ni}	F_{Di}	F_{Di}
(m)	(m/s)	(m/s)	(m)		(m^3)	(m/s)	(m/s)	(m^2)	(N)	(N)
	Mazurek	Predicted				Mazurek	Predicted		Mazurek	Predicted
0	0	0		0		-	-	-	-	-
0.060	3.118	4.059		0.037		1.559	2.029	0.0079	11.451	19.409
0.150	3.453	3.623		0.093		3.285	3.841	0.0108	69.913	95.565
0.240	3.687	2.937		0.148		3.570	3.280	0.0109	83.445	70.442
0.330	3.494	2.347		0.204		3.591	2.642	0.0127	97.876	52.994
0.420	2.295	1.664		0.260		2.895	2.005	0.0159	80.060	38.419
0.510	0.918	0.941	1.618	0.315	0.0213	1.607	1.302	0.0204	31.594	20.757
0.600	0.030	0.336		0.371		0.474	0.639	0.0256	3.446	6.259
0.610	0	0.230		0.377		0.015	0.283	0.0032	0.000	0.153
0.630	-0.160	0		0.389		-0.080	0.115	0.0065	-0.025	0.052
0.690	-0.563	-0.311		0.427		-0.362	-0.155	0.0212	-1.659	-0.306
0.780	-0.969	-0.428		0.482		-0.766	-0.370	0.0356	-12.540	-2.919
0.840	-1.024	-0.496		0.519		-0.996	-0.462	0.0258	-15.386	-3.309
0.882	-1.054	-0.537		0.545		-1.039	-0.516	0.0188	-12.157	-3.006

Table B-15. Data for calculating drag force (F_D) and submerged volume (λ_s) calculation for Q = 20.2 m^3/s at X = 3.45 m.

Male										
Y	U	U	H	Y/H	λ_s	U_i	U_i	A_{ni}	F_{Di}	F_{Di}
(m)	(m/s)	(m/s)	(m)		(m^3)	(m/s)	(m/s)	(m^2)	(N)	(N)
	Mazurek	Predicted				Mazurek	Predicted		Mazurek	Predicted
0	0	0		0		-	-	-	-	-
0.060	3.161	3.723		0.034		1.580	1.862	0.0067	10.011	13.891
0.150	3.155	3.441		0.085		3.158	3.582	0.0132	79.203	101.912
0.240	3.060	2.850		0.137		3.107	3.145	0.0149	86.101	88.221
0.330	2.682	2.349		0.188		2.871	2.599	0.0157	77.471	63.514
0.420	1.985	1.819		0.239		2.334	2.084	0.0169	55.164	44.002
0.510	1.199	1.206	1.758	0.290	0.0249	1.592	1.513	0.0192	29.171	26.338
0.600	0.585	0.644		0.341		0.892	0.925	0.0228	10.868	11.692
0.690	0.016	0.114		0.392		0.301	0.379	0.0275	1.489	2.365
0.700	0	0		0.398		0.008	0.057	0.0034	0.000	0.007
0.780	-0.407	-0.419		0.444		-0.204	-0.210	0.0294	-0.733	-0.775
0.870	-0.663	-0.467		0.495		-0.535	-0.443	0.0382	-6.565	-4.499
0.930	-0.694	-0.500		0.529		-0.679	-0.484	0.0281	-7.768	-3.942
Female										
Y	U	U	H	Y/H	λ_s	U_i	U_i	A_{ni}	F_{Di}	F_{Di}
(m)	(m/s)	(m/s)	(m)		(m^3)	(m/s)	(m/s)	(m^2)	(N)	(N)
	Mazurek	Predicted				Mazurek	Predicted		Mazurek	Predicted
0	0	0		0		-	-	-	-	-
0.060	3.161	3.723		0.037		1.580	1.862	0.0079	11.770	16.331
0.150	3.155	3.441		0.093		3.158	3.582	0.0108	64.601	83.123
0.240	3.060	2.850		0.148		3.107	3.145	0.0109	63.216	64.773
0.330	2.682	2.349		0.204		2.871	2.599	0.0127	62.567	51.295
0.420	1.985	1.819		0.260		2.334	2.084	0.0159	52.028	41.500
0.510	1.199	1.206	1.618	0.315	0.0247	1.592	1.513	0.0204	31.018	28.006
0.600	0.585	0.644		0.371		0.892	0.925	0.0256	12.212	13.137
0.690	0.016	0.114		0.427		0.301	0.379	0.0309	1.674	2.659
0.700	0	0		0.433		0.008	0.057	0.0037	0.000	0.007
0.780	-0.407	-0.419		0.482		-0.204	-0.210	0.0319	-0.794	-0.840
0.870	-0.663	-0.467		0.538		-0.535	-0.443	0.0392	-6.744	-4.622
0.930	-0.694	-0.500		0.575		-0.679	-0.484	0.0273	-7.549	-3.831

Table B-16. Data for calculating drag force (F_D) and submerged volume (λ_s) calculation for Q = 18.0 m^3/s at X = 2.5 m.

Male							
Y	U	H	Y/H	λ_s	U_i	A_{ni}	F_{Di}
(m)	(m/s)	(m)		(m^3)	(m/s)	(m^2)	(N)
	Predicted				Predicted		Predicted
0	0		0		-	-	-
0.020	3.861		0.011		1.931	0.0019	4.344
0.050	4.215		0.028		4.038	0.0035	33.879
0.100	4.017		0.057		4.116	0.0068	69.486
0.200	3.075	1.758	0.114	0.0271	3.546	0.0158	119.366
0.300	2.255		0.171		2.665	0.0171	72.713
0.500	0.409		0.284		1.332	0.0391	41.596
0.540	0		0.307		0.204	0.0094	0.236
0.700	-0.852		0.398		-0.426	0.0465	-5.057
0.800	-0.999		0.455		-0.925	0.0375	-19.252
0.960	-1.201		0.546		-1.100	0.0729	-52.989
Female							
Y	U	H	Y/H	λ_s	U_i	A_{ni}	F_{Di}
(m)	(m/s)	(m)		(m^3)	(m/s)	(m^2)	(N)
	Predicted				Predicted		Predicted
0	0		0		-	-	-
0.020	3.861		0.012		1.931	0.0027	6.049
0.050	4.215		0.031		4.038	0.0039	38.063
0.100	4.017		0.062		4.116	0.0061	62.431
0.200	3.075	1.618	0.124	0.0269	3.546	0.0119	89.466
0.300	2.255		0.185		2.665	0.0131	55.855
0.500	0.409		0.309		1.332	0.0383	40.764
0.540	0		0.334		0.204	0.0104	0.262
0.700	-0.852		0.433		-0.426	0.0523	-5.687
0.800	-0.999		0.494		-0.925	0.0403	-20.729
0.960	-1.201		0.593		-1.100	0.0718	-52.190

Table B-17. Data for calculating drag force (F_D) and submerged volume (λ_s) calculation for Q = 18.0 m^3/s at X = 3.0 m.

Male							
Y	U	H	Y/H	λ_s	U_i	A_{ni}	F_{Di}
(m)	(m/s)	(m)		(m^3)	(m/s)	(m^2)	(N)
	Predicted				Predicted		Predicted
0	0		0		-	-	-
0.020	3.532		0.011		1.766	0.0019	3.634
0.050	3.882		0.028		3.707	0.0035	28.549
0.100	3.806		0.057		3.844	0.0068	60.599
0.200	3.030	1.758	0.114	0.0285	3.418	0.0158	110.889
0.300	2.353		0.171		2.691	0.0171	74.182
0.500	0.795		0.284		1.574	0.0391	58.149
0.610	0		0.347		0.398	0.0279	2.644
0.700	-0.605		0.398		-0.302	0.0280	-1.537
0.800	-0.716		0.455		-0.660	0.0375	-9.796
0.980	-0.885		0.557		-0.801	0.0830	-31.905
Female							
Y	U	H	Y/H	λ_s	U_i	A_{ni}	F_{Di}
(m)	(m/s)	(m)		(m^3)	(m/s)	(m^2)	(N)
	Predicted				Predicted		Predicted
0	0		0		-	-	-
0.020	3.532		0.012		1.766	0.0027	5.061
0.050	3.882		0.031		3.707	0.0039	32.075
0.100	3.806		0.062		3.844	0.0061	54.447
0.200	3.030	1.618	0.124	0.0285	3.418	0.0119	83.113
0.300	2.353		0.185		2.691	0.0131	56.983
0.500	0.795		0.309		1.574	0.0383	56.986
0.610	0		0.377		0.398	0.0313	2.968
0.700	-0.605		0.433		-0.302	0.0314	-1.724
0.800	-0.716		0.494		-0.660	0.0403	-10.547
0.980	-0.885		0.606		-0.801	0.0810	-31.163

Table B-18. Data for calculating drag force (F_D) and submerged volume (λ_s) calculation for Q = 18.0 m^3/s at X = 3.5 m.

Male							
Y	U	H	Y/H	λ_s	U_i	A_{ni}	F_{Di}
(m)	(m/s)	(m)		(m^3)	(m/s)	(m^2)	(N)
	Predicted				Predicted		Predicted
0	0		0		-	-	-
0.020	3.162		0.011		1.581	0.0019	2.913
0.050	3.488		0.028		3.325	0.0035	22.969
0.100	3.495		0.057		3.491	0.0068	50.001
0.200	2.883	1.758	0.114	0.0293	3.189	0.0158	96.539
0.300	2.310		0.171		2.597	0.0171	69.042
0.500	1.068		0.284		1.689	0.0391	66.943
0.600	0.478		0.341		0.773	0.0251	8.986
0.675	0		0.384		0.239	0.0225	0.773
0.800	-0.260		0.455		-0.130	0.0458	-0.464
0.990	-0.327		0.563		-0.293	0.0880	-4.543
Female							
Y	U	H	Y/H	λ_s	U_i	A_{ni}	F_{Di}
(m)	(m/s)	(m)		(m^3)	(m/s)	(m^2)	(N)
	Predicted				Predicted		Predicted
0	0		0		-	-	-
0.020	3.162		0.012		1.581	0.0027	4.056
0.050	3.488		0.031		3.325	0.0039	25.805
0.100	3.495		0.062		3.491	0.0061	44.925
0.200	2.883	1.618	0.124	0.0292	3.189	0.0119	72.357
0.300	2.310		0.185		2.597	0.0131	53.035
0.500	1.068		0.309		1.689	0.0383	65.604
0.600	0.478		0.371		0.773	0.0281	10.078
0.675	0		0.417		0.239	0.0254	0.871
0.800	-0.260		0.494		-0.130	0.0496	-0.503
0.990	-0.327		0.612		-0.293	0.0856	-4.418

Table B-19. Data for calculating drag force (F_D) and submerged volume (λ_s) calculation for Q = 17.0 m^3/s at X = 2.5 m.

Male							
Y	U	H	Y/H	λ_s	U_i	A_{ni}	F_{Di}
(m)	(m/s)	(m)		(m^3)	(m/s)	(m^2)	(N)
	Predicted				Predicted		Predicted
0	0		0		-	-	-
0.020	3.834		0.011		1.917	0.0019	4.284
0.050	4.176		0.028		4.005	0.0035	33.329
0.100	3.947		0.057		4.061	0.0068	67.661
0.200	2.990		0.114		3.469	0.0158	114.221
0.300	2.145	1.758	0.171	0.0263	2.568	0.0171	67.513
0.400	1.135		0.228		1.640	0.0183	29.521
0.530	0		0.301		0.567	0.0278	5.367
0.600	-0.542		0.341		-0.271	0.0181	-0.795
0.700	-0.759		0.398		-0.650	0.0308	-7.829
0.800	-0.952		0.455		-0.855	0.0375	-16.449
0.950	-1.192		0.540		-1.072	0.0680	-46.861
Female							
Y	U	H	Y/H	λ_s	U_i	A_{ni}	F_{Di}
(m)	(m/s)	(m)		(m^3)	(m/s)	(m^2)	(N)
	Predicted				Predicted		Predicted
0	0		0		-	-	-
0.020	3.834		0.012		1.917	0.0027	5.966
0.050	4.176		0.031		4.005	0.0039	37.445
0.100	3.947		0.062		4.061	0.0061	60.792
0.200	2.990		0.124		3.469	0.0119	85.610
0.300	2.145	1.618	0.185	0.0262	2.568	0.0131	51.861
0.400	1.135		0.247		1.640	0.0165	26.695
0.530	0		0.328		0.567	0.0295	5.698
0.600	-0.542		0.371		-0.271	0.0204	-0.896
0.700	-0.759		0.433		-0.650	0.0346	-8.787
0.800	-0.952		0.494		-0.855	0.0403	-17.711
0.950	-1.192		0.587		-1.072	0.0672	-46.345

Table B-20. Data for calculating drag force (F_D) and submerged volume (λ_s) calculation for Q = 17.0 m^3/s at X = 3.0 m.

Male							
Y	U	H	Y/H	λ_s	U_i	A_{ni}	F_{Di}
(m)	(m/s)	(m)		(m^3)	(m/s)	(m^2)	(N)
	Predicted				Predicted		Predicted
0	0		0		-	-	-
0.020	3.481		0.011		1.741	0.0019	3.531
0.050	3.821		0.028		3.651	0.0035	27.701
0.100	3.723		0.057		3.772	0.0068	58.357
0.200	2.936		0.114		3.330	0.0158	105.237
0.300	2.256	1.758	0.171	0.0278	2.596	0.0171	69.017
0.400	1.475		0.228		1.866	0.0183	38.212
0.500	0.686		0.284		1.081	0.0208	14.576
0.600	0		0.341		0.343	0.0251	1.766
0.700	-0.492		0.398		-0.246	0.0308	-1.119
0.800	-0.627		0.455		-0.559	0.0375	-7.033
0.970	-0.817		0.552		-0.722	0.0779	-24.360
Female							
Y	U	H	Y/H	λ_s	U_i	A_{ni}	F_{Di}
(m)	(m/s)	(m)		(m^3)	(m/s)	(m^2)	(N)
	Predicted				Predicted		Predicted
0	0		0		-	-	-
0.020	3.481		0.012		1.741	0.0027	4.918
0.050	3.821		0.031		3.651	0.0039	31.122
0.100	3.723		0.062		3.772	0.0061	52.433
0.200	2.936		0.124		3.330	0.0119	78.877
0.300	2.256	1.618	0.185	0.0277	2.596	0.0131	53.016
0.400	1.475		0.247		1.866	0.0165	34.555
0.500	0.686		0.309		1.081	0.0218	15.255
0.600	0		0.371		0.343	0.0281	1.981
0.700	-0.492		0.433		-0.246	0.0346	-1.256
0.800	-0.627		0.494		-0.559	0.0403	-7.573
0.970	-0.817		0.600		-0.722	0.0764	-23.893

Table B-21. Data for calculating drag force (F_D) and submerged volume (λ_s) calculation for Q = 17.0 m^3/s at X = 3.5 m.

Male							
Y	U	H	Y/H	λ_s	U_i	A_{ni}	F_{Di}
(m)	(m/s)	(m)		(m^3)	(m/s)	(m^2)	(N)
	Predicted				Predicted		Predicted
0	0		0		-	-	-
0.020	3.094		0.011		1.547	0.0019	2.790
0.050	3.411		0.028		3.253	0.0035	21.982
0.100	3.401		0.057		3.406	0.0068	47.589
0.200	2.782		0.114		3.092	0.0158	90.743
0.300	2.215	1.758	0.171	0.0285	2.499	0.0171	63.938
0.400	1.634		0.228		1.925	0.0183	40.662
0.500	0.961		0.284		1.297	0.0208	21.013
0.660	0		0.375		0.480	0.0428	5.927
0.700	-0.143		0.398		-0.071	0.0131	-0.040
0.800	-0.183		0.455		-0.163	0.0375	-0.597
0.980	-0.244		0.557		-0.214	0.0830	-2.271
Female							
Y	U	H	Y/H	λ_s	U_i	A_{ni}	F_{Di}
(m)	(m/s)	(m)		(m^3)	(m/s)	(m^2)	(N)
	Predicted				Predicted		Predicted
0	0		0		-	-	-
0.020	3.094		0.012		1.547	0.0027	3.885
0.050	3.411		0.031		3.253	0.0039	24.697
0.100	3.401		0.062		3.406	0.0061	42.758
0.200	2.782		0.124		3.092	0.0119	68.013
0.300	2.215	1.618	0.185	0.0285	2.499	0.0131	49.114
0.400	1.634		0.247		1.925	0.0165	36.769
0.500	0.961		0.309		1.297	0.0218	21.991
0.660	0		0.408		0.480	0.0481	6.665
0.700	-0.143		0.433		-0.071	0.0146	-0.044
0.800	-0.183		0.494		-0.163	0.0403	-0.643
0.980	-0.244		0.606		-0.214	0.0810	-2.218

Table B-22. Data for calculating drag force (F_D) and submerged volume (λ_s) calculation for Q = 15.0 m^3/s at X = 2.0 m.

Male							
Y	U	H	Y/H	λ_s	U_i	A_{ni}	F_{Di}
(m)	(m/s)	(m)		(m^3)	(m/s)	(m^2)	(N)
	Predicted				Predicted		Predicted
0	0		0		-	-	-
0.020	4.059		0.011		2.029	0.0019	4.800
0.050	4.319		0.028		4.189	0.0035	36.457
0.100	3.832		0.057		4.075	0.0068	68.130
0.200	2.681		0.114		3.257	0.0158	100.691
0.300	1.461	1.758	0.171	0.0223	2.071	0.0171	43.922
0.420	0		0.239		0.730	0.0222	7.108
0.500	-0.385		0.284		-0.193	0.0169	-0.377
0.600	-0.628		0.341		-0.507	0.0251	-3.860
0.700	-0.842		0.398		-0.735	0.0308	-10.002
0.800	-1.029		0.455		-0.936	0.0375	-19.675
0.890	-1.172		0.506		-1.101	0.0393	-28.548
Female							
Y	U	H	Y/H	λ_s	U_i	A_{ni}	F_{Di}
(m)	(m/s)	(m)		(m^3)	(m/s)	(m^2)	(N)
	Predicted				Predicted		Predicted
0	0		0		-	-	-
0.020	4.059		0.012		2.029	0.0027	6.685
0.050	4.319		0.031		4.189	0.0039	40.960
0.100	3.832		0.062		4.075	0.0061	61.214
0.200	2.681		0.124		3.257	0.0119	75.469
0.300	1.461	1.618	0.185	0.0218	2.071	0.0131	33.739
0.420	0		0.260		0.730	0.0204	6.542
0.500	-0.385		0.309		-0.193	0.0179	-0.399
0.600	-0.628		0.371		-0.507	0.0281	-4.329
0.700	-0.842		0.433		-0.735	0.0346	-11.227
0.800	-1.029		0.494		-0.936	0.0403	-21.184
0.890	-1.172		0.550		-1.101	0.0398	-28.914

Table B-23. Data for calculating drag force (F_D) and submerged volume (λ_s) calculation for Q = 15.0 m^3/s at X = 2.5 m.

Male							
Y	U	H	Y/H	λ_s	U_i	A_{ni}	F_{Di}
(m)	(m/s)	(m)		(m^3)	(m/s)	(m^2)	(N)
	Predicted				Predicted		Predicted
0	0		0		-	-	-
0.020	3.770		0.011		1.885	0.0019	4.141
0.050	4.082		0.028		3.926	0.0035	32.025
0.100	3.788		0.057		3.935	0.0068	63.504
0.200	2.805		0.114		3.296	0.0158	103.144
0.300	1.896	1.758	0.171	0.0236	2.351	0.0171	56.576
0.400	0.852		0.228		1.374	0.0183	20.735
0.500	0		0.284		0.426	0.0208	2.268
0.600	-0.582		0.341		-0.291	0.0251	-1.272
0.700	-0.802		0.398		-0.692	0.0308	-8.855
0.800	-0.994		0.455		-0.898	0.0375	-18.117
0.910	-1.172		0.518		-1.083	0.0487	-34.242
Female							
Y	U	H	Y/H	λ_s	U_i	A_{ni}	F_{Di}
(m)	(m/s)	(m)		(m^3)	(m/s)	(m^2)	(N)
	Predicted				Predicted		Predicted
0	0		0		-	-	-
0.020	3.770		0.012		1.885	0.0027	5.767
0.050	4.082		0.031		3.926	0.0039	35.980
0.100	3.788		0.062		3.935	0.0061	57.057
0.200	2.805		0.124		3.296	0.0119	77.308
0.300	1.896	1.618	0.185	0.0232	2.351	0.0131	43.459
0.400	0.852		0.247		1.374	0.0165	18.750
0.500	0		0.309		0.426	0.0218	2.373
0.600	-0.582		0.371		-0.291	0.0281	-1.427
0.700	-0.802		0.433		-0.692	0.0346	-9.939
0.800	-0.994		0.494		-0.898	0.0403	-19.507
0.910	-1.172		0.562		-1.083	0.0489	-34.413

Table B-24. Data for calculating drag force (F_D) and submerged volume (λ_s) calculation for Q = 15.0 m^3/s at X = 3.0 m.

Male							
Y	U	H	Y/H	λ_s	U_i	A_{ni}	F_{Di}
(m)	(m/s)	(m)		(m^3)	(m/s)	(m^2)	(N)
	Predicted				Predicted		Predicted
0	0		0		-	-	-
0.020	3.365		0.011		1.682	0.0019	3.298
0.050	3.680		0.028		3.522	0.0035	25.782
0.100	3.535		0.057		3.608	0.0068	53.387
0.200	2.734		0.114		3.134	0.0158	93.262
0.300	2.041	1.758	0.171	0.0243	2.387	0.0171	58.370
0.400	1.218		0.228		1.629	0.0183	29.145
0.500	0.464		0.284		0.841	0.0208	8.820
0.560	0		0.319		0.232	0.0144	0.465
0.700	-0.444		0.398		-0.222	0.0415	-1.224
0.800	-0.554		0.455		-0.499	0.0375	-5.593
0.920	-0.666		0.523		-0.610	0.0534	-11.924
Female							
Y	U	H	Y/H	λ_s	U_i	A_{ni}	F_{Di}
(m)	(m/s)	(m)		(m^3)	(m/s)	(m^2)	(N)
	Predicted				Predicted		Predicted
0	0		0		-	-	-
0.020	3.365		0.012		1.682	0.0027	4.593
0.050	3.680		0.031		3.522	0.0039	28.966
0.100	3.535		0.062		3.608	0.0061	47.967
0.200	2.734		0.124		3.134	0.0119	69.901
0.300	2.041	1.618	0.185	0.0240	2.387	0.0131	44.837
0.400	1.218		0.247		1.629	0.0165	26.355
0.500	0.464		0.309		0.841	0.0218	9.231
0.560	0		0.346		0.232	0.0161	0.518
0.700	-0.444		0.433		-0.222	0.0466	-1.377
0.800	-0.554		0.494		-0.499	0.0403	-6.023
0.920	-0.666		0.569		-0.610	0.0535	-11.936

APPENDIX C: Sample Calculation

This appendix provides a sample calculation to determine whether a flow below the Wolf River Barrier is safe or hazardous for a male. Given data: weir height, $P = 0.9$ m, width, $B = 13.72$ m, discharge, $Q = 18.0$ m^3/s, human height, $H = 1.758$ m, and BMI = 26.4.

Step 1. Estimating the human weight *(W)*

$H = 1.758$ m and BMI = 26.4

$W = H^* (\text{BMI})^2 * g = 1.758\ \text{m} * (26.4)^2 * 9.81 \text{m/s}^2 = 800.4$ N

Step 2: Estimating buoyancy force, F_B

Consider water temperature is 5˚C

Specific weight of the water, $\gamma_w = g\rho_w = 9.81 \text{m/s}^2 * 1000\ \text{kgm}^{-3}$

Now submerged volume λ_s of a male body can be determined using Eqn. 3.7,

$$\frac{\lambda_s}{H^3} = 0.1499\left(\frac{Y}{H}\right)^6 - 0.4622\left(\frac{Y}{H}\right)^5 + 0.4543\left(\frac{Y}{H}\right)^4 - 0.1489\left(\frac{Y}{H}\right)^3 + 0.0166\left(\frac{Y}{H}\right)^2 + 0.0043\left(\frac{Y}{H}\right)$$

Depth downstream of the weir y_d can be calculated using Eqn. 3.12 for the Wolf River Barrier:

$$y_d = 0.374Q^{0.332} - 1 + P$$

$$=> y_d = 0.374 * (18.0)^{0.332} - 1 + 0.9$$

$$=> y_d = 0.88 \text{ m}$$

Consider $y_t = 1.3 y_d = 1.14$ m

Now considering at the beginning of the jump at $Xj = 1.1$ m (calculation shown in step 3) depth is y_d and end of the jump at $(Xj + L_{cr})$ =1.1 m + 6.72 m = 7.82 m, depth is y_t. If linear increment of flow depth is considered, at X = 3.5 m flow depth is 0.99 m. Similarly, depth of other X locations can be calculated.

Now, at X = 3.5 m

$$\frac{\lambda_s}{1.758^3} = 0.1499\left(\frac{0.99}{1.758}\right)^6 - 0.4622\left(\frac{0.99}{1.758}\right)^5 + 0.4543\left(\frac{0.99}{1.758}\right)^4 - 0.1489\left(\frac{0.99}{1.758}\right)^3 + 0.0166\left(\frac{0.99}{H}\right)^2 + 0.0043\left(\frac{0.99}{H}\right)$$

$$=> \lambda_s = 0.0293 \text{ m}^3$$

Now the buoyant force on the body is estimated from Eqn. 3.3

$F_B = \lambda_s \gamma_w$

$=> F_B = 9.81 \text{ms}^{-2} * 1000 \text{ kgm}^{-3} * 0.0293 m^3$

$=> F_B = 287.13 \text{ N}$

Step 3. Estimating the Forward (F_{DF}) and Backward (F_{DB}) Drag Forces

Consider that Coefficient of drag C_d =1.2

Now to determine the velocity profile several parameters and scales are required.

Here, weir height, P= 0.9 m, width, B = 13.72 m, discharge, Q = 18.0 m^3/s

Depth of flow over the crest at upstream h can be calculated using Eq. 3.11 for Wolf River Barrier.

$h = 0.00002Q^3 - 0.001Q^2 + 0.0286Q + 0.173$

$=> h = 0.00002 * (18.0)^3 - 0.001 * (18.0)^2 + 0.0286 * (18.0) + 0.173$

$=> h = 0.48 \text{ m}$

Depth downstream of the weir (calculated above in step 2)

$y_d = 0.88 \text{ m}$

Now the forward flow depth at section 1 Y_1 is calculated using energy equation (Eqn. 3.13) which eventually determines the forward velocity U_1 at section 1.

$$z_o + (h + P) + \frac{U_o^2}{2g} = z_1 + Y_1 + \frac{U_1^2}{2g} + C_L \frac{U_1^2}{2g}$$

$$=> (h + P) + \frac{U_o^2}{2g} = Y_1 + \frac{U_1^2}{2g} + C_L \frac{U_1^2}{2g} \quad [\text{ as } z_o = z_1]$$

$$=> (h + P) + \frac{\left(\frac{Q}{(h+P)*B}\right)^2}{2g} = Y_1 + \frac{\left(\frac{Q}{BY_1}\right)^2}{2g} + C_L \frac{\left(\frac{Q}{BY_1}\right)^2}{2g} \quad [\text{ as } U_0 = \frac{Q}{(h+P)*B} \text{ and } U_1 = \frac{Q}{BY_1}]$$

$$=> (h + P) + \frac{\left(\frac{Q}{(h+P)*B}\right)^2}{2g} = Y_1 + \frac{\left(\frac{Q}{BY_1}\right)^2}{2g} + \frac{0.1P}{h} * \frac{\left(\frac{Q}{BY_1}\right)^2}{2g} [\text{ as } C_L = 0.1\frac{\text{P}}{\text{h}}]$$

$$\Rightarrow (0.48 + 0.9) + \frac{\left(\frac{18.0}{(0.48+0.9)*13.72}\right)^2}{2*9.81} = Y_1 + \frac{\left(\frac{18.0}{13.72*Y_1}\right)^2}{2*9.81} + \frac{0.1*0.9}{0.48} * \frac{\left(\frac{18.0}{13.72*Y_1}\right)^2}{2*9.81}$$

$\Rightarrow Y_1 = 0.305$ m [only taking positive root]

Therefore, $U_1 = \frac{Q}{BY_1}$

$$\Rightarrow U_1 = \frac{18.0\ m^3 s^{-1}}{13.72\ \text{m} * 0.305\ \text{m}}$$

$\Rightarrow U_1 = 4.31\ \text{ms}^{-1}$

The Froude number at section 1

$$F_1 = \frac{U_1}{\sqrt{gY_1}}$$

$\Rightarrow F_1 = \frac{4.31}{\sqrt{9.81*0.305}}$

$\Rightarrow F_1 = 2.49$

The subcritical sequent depth, Y_2, to form a free hydraulic jump is calculated using Belanger equation (Eqn. 3.16)

$$\frac{Y_2}{Y_1} = \frac{1}{2}\left(-1 + \sqrt{1 + 8F_1^2}\right)$$

$$\Rightarrow \frac{Y_2}{0.305} = \frac{1}{2}\left(-1 + \sqrt{1 + 8 * 2.49^2}\right)$$

$\Rightarrow Y_2 = 0.93$ m

The submergence S of the jump is calculated using Eqn. 2.2

$$S = \frac{y_t - Y_2}{Y_2}$$

$$\Rightarrow S = \frac{1.14\ - 0.93}{0.93}$$

$\Rightarrow S = 0.23$

Length of countercurrent region can be calculated using Eqn. 2.1

$$\frac{L_{cr}}{Y_2} = 5.46 + 6.67S$$

$$=> \frac{L_{cr}}{0.93} = 5.46 + 6.67 * 0.23$$

$$=> L_{cr} = 6.5 \text{ m}$$

Length of countercurrent region can be calculated using Eqn. 2.3

$$\frac{L_{sj}}{Y_2} = 6.1 + 4.9S$$

$$=> \frac{L_{sj}}{0.93} = 6.1 + 4.9 * 0.23$$

$$=> L_{sj} = 6.72 \text{ m}$$

Now, From Eqn. 3.17

$$\frac{\overline{X_u}}{h + \frac{U_o^2}{2g}} = 1.34 - 0.3 \frac{\frac{U_o^2}{2g}}{h + \frac{U_o^2}{2g}}$$

$$=> \frac{\overline{X_u}}{0.48 + \frac{0.95^2}{2*9.81}} = 1.34 - 0.3 \frac{\frac{0.95^2}{2*9.81}}{h + \frac{0.95^2}{2*9.81}} \text{ [here, } U_o = \frac{Q}{(h+P)*B} = \frac{18.0}{(0.48+0.9)*13.72} = 0.95 \text{ ms}^{-1}]$$

$$=> \overline{X_u} = 0.69 \text{ m}$$

From Eqn. 3.18

$$\frac{\overline{Y_u}}{h + \frac{U_o^2}{2g}} = 0.85 - 0.83 \frac{\frac{U_o^2}{2g}}{h + \frac{U_o^2}{2g}}$$

$$=> \frac{\overline{Y_u}}{0.48 + \frac{0.95^2}{2 * 9.81}} = 0.85 - 0.83 \frac{\frac{0.95^2}{2 * 9.81}}{0.48 + \frac{0.95^2}{2 * 9.81}}$$

$=> \overline{Y_u} = 0.41$ m

Horizontal distance from weir crest to section 1, X_j can be calculated using Eqn. 3.19

$$\frac{X}{\overline{X_u}} = -0.0133\left(\frac{Y_u}{\overline{Y_u}}\right)^3 - 0.1406\left(\frac{Y_u}{\overline{Y_u}}\right)^2 - 0.6619\left(\frac{Y_u}{\overline{Y_u}}\right) + 1$$

$$=> \frac{X_j}{\overline{X_u}} = -0.0133\left(\frac{Y_1 - P}{\overline{Y_u}}\right)^3 - 0.1406\left(\frac{Y_1 - P}{\overline{Y_u}}\right)^2 - 0.6619\left(\frac{Y_1 - P}{\overline{Y_u}}\right) + 1$$ [if vertical distance from the weir crest to Y_1 depth at section 1 is $Y_1 - P$ and is then $X = X_j$]

$$=> \frac{X_j}{0.69} = -0.0133\left(\frac{Y_1 - P}{0.41}\right)^3 - 0.1406\left(\frac{Y_1 - P}{0.41}\right)^2 - 0.6619\left(\frac{Y_1 - P}{0.41}\right) + 1$$

$=> X_j = 1.1$ m

Therefore, the jump starts at a location 1.1 m away from the weir face.

L_{cr} is 6.5 m (calculated above) and according to the literature review the countercurrent region starts at a point where nappe touches the water surface. So, the mid of countercurrent region should be around at distance of 3m from section 1. So, consider several locations X= 2.5 m, 3.0 m, and 3.5 m near that region to predict the velocity profile.

Now if, X= 3.5 m

$X' = X - X_j$

$=> X' = 3.5 \text{ m} - 1.1 \text{ m}$

$=> X' = 2.4$ m

Length scale L is calculated from Eqn. 3.21

$$\frac{L}{Y_1} = 7.26F_1^{0.64}(1 + S)^{0.77}$$

$$=> \frac{L}{0.305} = 7.26 * 2.49^{0.64} * (1 + 0.23)^{0.77}$$

$=> L = 4.66$ m

Length scale b is calculated from Eqn. 3.22

$$\frac{b}{Y_1} = 0.0764\frac{X'}{Y_1} + 0.6532$$

$$=> \frac{b}{0.305} = 0.0764 * \frac{2.4}{0.305} + 0.6532$$

$$=> b = 0.38 \text{ m}$$

Velocity scale U_m is calculated using Eqn. 3.25

$$\frac{U_m}{U_1} = -0.0321\left(\frac{X'}{L}\right)^6 + 0.3838\left(\frac{X'}{L}\right)^5 - 1.7059\left(\frac{X'}{L}\right)^4 + 3.5399\left(\frac{X'}{L}\right)^3 - 3.3334\left(\frac{X'}{L}\right)^2 + 0.6431\left(\frac{X'}{L}\right) + 1$$

$$=> \frac{U_m}{4.31} = -0.0321\left(\frac{2.4}{4.33}\right)^6 + 0.3838\left(\frac{2.4}{4.33}\right)^5 - 1.7059\left(\frac{2.4}{4.33}\right)^4 + 3.5399\left(\frac{2.4}{4.33}\right)^3 - 3.3334\left(\frac{2.4}{4.33}\right)^2 + 0.6431\left(\frac{2.4}{4.33}\right) + 1$$

$$=> U_m = 3.55 \text{ m/s}$$

Now consider several points in between $Y = 0$ to $Y = 0.99$ m (flow depth at X=3.5 m)

Y (m)	Y/b
0	0.000
0.02	0.052
0.05	0.131
0.1	0.262
0.2	0.524
0.3	0.786
0.5	1.311
0.6	1.573
0.675	1.776
0.7	1.835
0.8	2.097
0.99	2.595

Here, up to $Y = 0.6$ m $Y/b < 1.77$. So up to $Y = 0.6$ m velocity will be in forward direction and rest will be in backward direction.

Here every $Y/b > 0.0365$, so using Eqn. 3.24 forward velocity profile can be estimated.

$$\frac{U}{U_m} = 0.9378\left(\frac{Y}{b}\right)^5 - 4.7477\left(\frac{Y}{b}\right)^4 + 8.8848\left(\frac{Y}{b}\right)^3 - 7.5124\left(\frac{Y}{b}\right)^2 + 2.1378\left(\frac{Y}{b}\right) + 0.8$$

$$\Rightarrow \frac{U}{3.84} = 0.9378\left(\frac{0.02}{0.34}\right)^5 - 4.7477\left(\frac{0.02}{0.34}\right)^4 + 8.8848\left(\frac{0.02}{0.34}\right)^3 - 7.5124\left(\frac{0.02}{0.34}\right)^2 + 2.1378\left(\frac{0.02}{0.34}\right) + 0.8 \quad \text{[for } Y\text{=0.02 m]}$$

$$\Rightarrow U = 3.455 \text{ ms}^{-1}$$

Similarly,

Y (m)	Y/b	U (m/s)
0	0.000	0.000
0.02	0.052	3.162
0.05	0.131	3.488
0.1	0.262	3.495
0.2	0.524	2.883
0.3	0.786	2.310
0.5	1.311	1.068
0.6	1.573	0.478
0.675	1.776	0

Now, for reverse velocity profile the velocity scale, U_s, and length scale, b_r are required.

From Eqn. 3.27

$$\frac{v^*}{U_1} = -0.342F_1^{-0.263}\, e^{0.165\sin(S)}$$

$$\Rightarrow \frac{v^*}{4.31} = -0.342 * (2.49)^{-0.263}\, e^{0.165\sin(0.23)}$$

$$\Rightarrow v^* = -1.2 \text{ ms}^{-1}$$

U_s can be estimated from Eqn. 3.26

$$\frac{U_s}{v^*} = 0.215 - 4.049\frac{X'}{L_{sj}} - 3.425\left(\frac{X'}{L_{sj}}\right)^2$$

$$\Rightarrow \frac{U_s}{1.2} = 0.215 - 4.049\frac{2.4}{6.27} - 3.425\left(\frac{2.4}{6.27}\right)^2$$

$\Rightarrow U_s$ =-0.326 m/s (acceptable, as $0 < \frac{U_s}{v^*} < 1$)

Now,

$b_r = 0.2 * y_t$

$=> b_r = 0.2 * 1.14 = 0.23$ m

Y (m)	$Y_s = 0.99 - Y$ (m)
0.7	0.29
0.8	0.19
0.99	0

Now, reverse velocity can be calculated from Eqn. 3.28

At $Y = 0.8$ m,

$$\frac{U}{U_s} = -0.0353 \left(\frac{Y_s}{b_r}\right)^2 - 0.2148\left(\frac{Y_s}{b_r}\right) + 1$$

$$=> \frac{U}{-0.734} = -0.0353 \left(\frac{0.19}{0.23}\right)^2 - 0.2148\left(\frac{0.19}{0.23}\right) + 1$$

$=> U = -0.26\ \text{ms}^{-1}$

Similarly,

Y (m)	U (m/s)
0.7	-0.22
0.8	-0.26
0.87	-0.33

Therefore, the total velocity profile at $X = 3.5$ m for Q = 18.0 m^3/s

Y (m)	U (m/s)
0	0.00
0.02	3.16
0.05	3.49
0.1	3.50
0.2	2.88
0.3	2.31
0.5	1.07
0.6	0.48
0.675	0.00
0.8	-0.26
0.99	-0.33

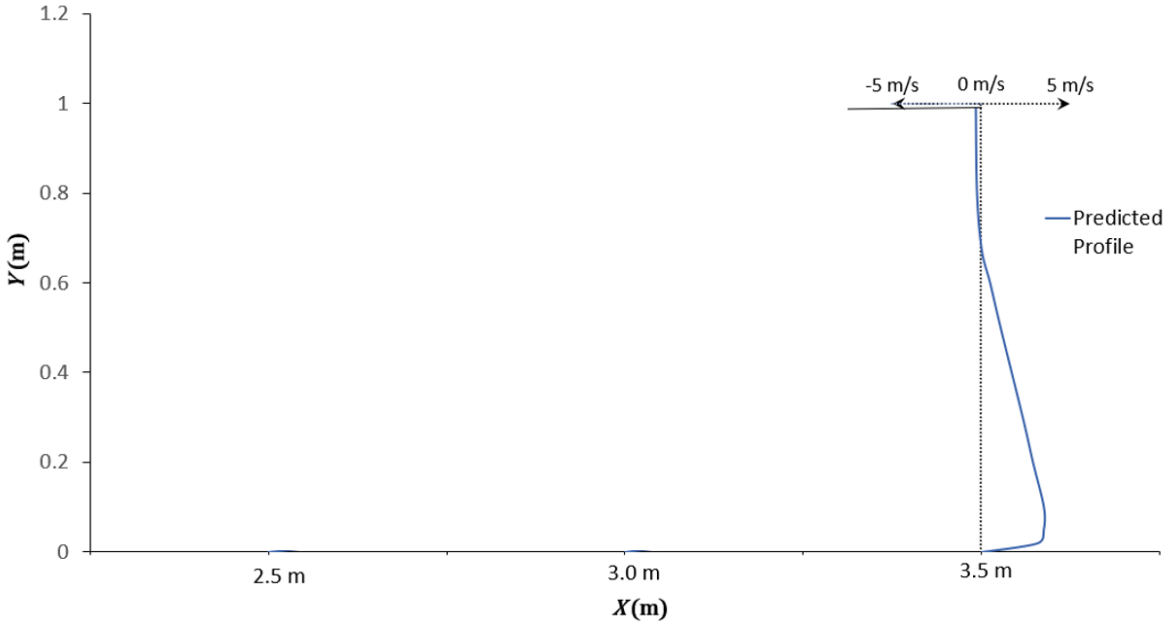

Figure C-1. Predicted velocity profile at X= 3.5 m for Q= 18.0 m^3/s.

Now to calculate the frontal area Eqn. 3.9 is used

$$\frac{A_n}{H^2} = 2.3808\left(\frac{Y}{H}\right)^6 - 6.6519\left(\frac{Y}{H}\right)^5 + 6.2681\left(\frac{Y}{H}\right)^4 - 2.3246\left(\frac{Y}{H}\right)^3 + 0.4513\left(\frac{Y}{H}\right)^2 + 0.0504\left(\frac{Y}{H}\right)$$

For, $Y = 0.020$ m

$$\frac{A_n}{0.020^2} = 2.3808\left(\frac{0.020}{1.758}\right)^6 - 6.6519\left(\frac{0.020}{1.758}\right)^5 + 6.2681\left(\frac{0.020}{1.758}\right)^4 - 2.3246\left(\frac{0.020}{1.758}\right)^3 + 0.4513\left(\frac{0.020}{1.758}\right)^2 + 0.0504\left(\frac{0.020}{1.758}\right)$$

$=> A_n = 0.0019\ \text{m}^2$

Similarly, for $Y = 0.050$ m

$A_n = 0.0054\ \text{m}^2$

So, frontal area in the interval between $Y = 0.020$ m and $Y = 0.050$ m is

$A_i = (0.0054 - 0.0019)\ \text{m}^2$

$=> A_i = 0.0035\ \text{m}^2$

Average flow velocity the interval between Y = 0.020 m and Y = 0.050 m is

$$U_i = \frac{3.16 + 3.49}{2}\ \text{ms}^{-1}$$

$$=> U_i = 3.325\text{ms}^{-1}$$

Drag force created by the flow within the interval between Y = 0.020 m and Y = 0.050 m is calculated using Eqn. 3.29

$$F_{Di} = C_d A_{ni} \frac{\rho_w U_i^2}{2}$$

$$=> F_{Di} = 1.2 * 0.0035 * \frac{1000 * 3.325^2}{2}\ \text{N}$$

$$=> F_{Di} = 22.97\ \text{N}$$

Vertical axes coordinate $\bar{y}_i$ of the center of the the interval between Y = 0.020 m and Y = 0.050 m is

$$\bar{y}_i = \frac{0.020+0.050}{2}\ \text{m}$$

$$=> \bar{y}_i = 0.035\ \text{m}$$

Similarly,

Y (m)	U (m/s)	Interval	U_i (m/s)	F_{Di} (N)	$\bar{y}_i$ (m)
0	0.00				
0.02	3.16	I	1.581	2.913	0.010
0.05	3.49	II	3.325	22.969	0.035
0.1	3.50	III	3.491	50.001	0.075
0.2	2.88	IV	3.189	96.539	0.150
0.3	2.31	V	2.597	69.042	0.250
0.5	1.07	VI	1.689	66.943	0.400
0.6	0.48	VII	0.773	8.986	0.550
0.675	0.00	VIII	0.239	0.773	0.638
0.8	-0.26	IX	-0.130	-0.464	0.738
0.99	-0.33	X	-0.293	-4.543	0.895

Now, Total forward drag force,

$F_{DF} = 2.91 + 22.97 + 50.00 + 96.54 + 69.04 + 66.94 + 8.97 + 0.77 = 318.16$ N

Similarly total backward drag force,

$F_{DF} =$ -5.01 N (here negative represents the opposite direction of forward drag)

Step 4. Estimating the moment arms about the points of balance

There are two points of balance. One is heel and another is toe.

Length of foot, L_{foot} = 0.152 $H = 0.152$* 1.758 m = 0.267 m

Moment arm for weight about heel, L_W = 0.55 * L_{foot} = 0.55 * 0.267 m = 0.115 m

Moment arm for weight about heel, (L_{foot} -L_W) = 0.267- 0.115 = 0.152 m

Moment arm for buoyancy about heel L_B can be estimated from the plot given Figure 3.16

At X=3.5m, flow depth, $y = 0.99$ m

So, $L_B = 0.124$ m

Moment arm for buoyancy about heel (L_{foot} -L_B) $= 0.267 - 0.124 = 0.143$ m

Moment arms for forward and backward drag do not changes with the change of points of balance, as those are vertical distances. These can be calculated using Eqn. 3.30.

$$\bar{Y}\sum_{i=1}^{N} F_{Di} = \sum_{i=1}^{N} \bar{y}_i F_{Di}$$

Now, for forward drag forces

$$\bar{Y} * 318.16 = (2.91 * 0.010 + 22.97 * 0.035 + 50.00 * 0.075 + 96.54 * 0.150 + 69.04 * 0.250 + 66.94 * 0.400 + 8.97 * 0.550 + 0.77 * 0.638)$$

$=> H_{DF} = 0.215$ m (As for forward drag force $\bar{Y} = H_{DF}$)

Similarly, for backward drag forces,

$H_{DB} = 0.88$ m

Step 5. Estimating the net moment about the points of balance and flow evaluation

This study considers clockwise moment as positive. To consider a flow as safe the M_P about heel must be less than or equal zero ($M_P \leq 0$) and M_P about toe must be more than or equal zero ($M_P \geq 0$). If any of these conditions is not satisfied at any location of downstream the flow will be considered hazardous.

Moment about the heel can be estimated using Eqn. 3.4

$$M_P = F_{DF}H_{DF} - F_{DB}H_{DB} + F_B L_B - W L_W$$

$$=> M_P = 318.16 * 0.215 - 5.01 * 0.880 + 287.13 * 0.124 - 800.4 * 0.115$$

$=> M_P = 7.96$ N

Moment about toe can be estimated using Eqn. 3.5

$$M_P = F_{DF}H_{DF} - F_{DB}H_{DB} - F_B(L_{foot} - L_B) + W(L_{foot} - L_W)$$

$$=> M_P = 318.16 * 0.215 - 5.01 * 0.880 - 287.13 * 0.124 + 800.4 * 0.152$$

$=> M_P = +145.11$ N·m

Here the net moment about the heel is positive, and it does not satisfy the stability condition ($M_P \leq 0$) about the heel.

Same procedure is applied for predicted velocity profiles at X= 2.5 and 3.0 m. M_P about heel were -64.94 N and -28.59 N, respectively. On the other hand, M_P about toe were +78.01 N and +110.53 N, respectively.

Hence, it can be concluded that as the net moment about the heel at X = 3.5 m is positive, the person is not safe against toppling at that location. Therefore, the downstream of the Wolf River Barrier is hazardous for a male of 1.758 m height and 26.4 BMI when the flow rate is 18.0 m^3/s.